LAPPEENRANTA UNIVERSITY OF TECHNOLOGY

LUT School of Engineering Science

Degree Program of Chemical Engineering

Master's Thesis

2018

Huhe Bao

# Methanol synthesis from $CO_2$ and $H_2$ by reactive distillation

Supervisors: Docent Arto Laari

Docent Esko Lahdenperä

Examiners: Professor Tuomas Koiranen

Docent Arto Laari

**Abstract**

LAPPEENRANTA UNIVERSITY OF TECHNOLOGY

LUT School of Engineering Science

Degree Program of Chemical Engineering

Huhe Bao

**Methanol synthesis from CO2 and H2 by reactive distillation**

Master's Thesis

2018

116 pages, 50 figures, 50 tables and 1 appendix

Examiners: Professor Tuomas Koiranen

Docent Arto Laari

Keyword: Methanol synthesis, $CO_2$ hydrogenation, Aspen Plus, Reactive distillation

The widely use of fossil fuel generates large amount of $CO_2$, which causes greenhouse effect. Since fossil fuel is nonrenewable, a potential energy crisis is no doubt coming. Thus, the reuse of $CO_2$ has generated a lot of attention. Among them, $CO_2$ hydrogenation is one of the most attractive ways to transform $CO_2$ into hydrocarbons, which can be used as an alternative for conventional fossil fuel.

Methanol is one of promising candidate, which has various applications in transport, chemical industry, pharmaceutical industry, and other fields. Recent years has seen a rapid growth in methanol production. The conventional methanol process uses fossil fuel, such as coal and natural gas, as the raw material. Due to the similarity to

conventional methanol process, there are lot of researches in $CO_2$ hydrogenation to methanol. There is already one industrial $CO_2$ to methanol plant operating in Iceland.

Most $CO_2$ to methanol studies consider gas–phase reaction, which has however relatively low conversion and severe conditions. In contrast, liquid phase $CO_2$ hydrogenation to methanol has in principle milder conditions and higher conversion and requires less equipment when implemented in pilot or industrial scale. Moreover, reactive distillation process, which combines liquid phase $CO_2$ hydrogenation and separation of products, can significantly improve conversion and overcome thermodynamic limitations.

In the thesis, reactive distillation technology is used to enhance the $CO_2$ hydrogenation. A simulation model is built to study the process using Aspen Plus. The process includes the main reactive distillation column and a downstream unit to purify methanol product and recover excess raw materials. Besides, a detailed solution is given to separate the azeotropic water–butanol solution, which is formed during the process. Moreover, the whole process is optimized to obtain the best operating parameters and suitable equipment variables.

In conclusion, the one–way methanol conversion is much higher and required conditions are much lower than in conventional gas–phase methanol process. The whole process does not contain any complex circulating lines and most unreacted raw materials can be recycled.

# Content

## Acronyms

| | |
|---|---|
| GHG | Greenhouse emission |
| ECBM | Enhanced coal bed methane recovery |
| DME | Dimethyl ether |
| $DMM_n$ | Polyoxymethylene dimethyl ethers |
| MTO | Methanol to olefin |
| MTG | Methanol to gasoline |
| MTA | Methanol to aromatics |
| DMC | Dimethyl carbonate |
| TPSR | Temperature-Programmed Surface Reaction |
| CSTR | Continuously stirred tank reactor |
| RD | Reactive distillation |
| RCM | Residual curve method |
| SA | Static analysis |
| AR | Attainable region method |
| MTBE | Methyl Tertiary Butyl Ether |
| CEM | Chemical equilibrium manifold |
| LMB | Line of mass balance |
| LCI | Line of chemical interaction |
| FTR | F-T reaction |
| MINLP | Mixed integer nonlinear programming |
| OCFE | Orthogonal collocation on finite element |
| MIDO | Mixed integer dynamic optimization |
| CPT | Chemical process technology |
| ANN | Artificial neural network |
| MPC | Model prediction control |
| PID | Proportional integral differential |
| ETBE | Ethyl Tertiary Butyl Ether |
| MIMO | Multiple Input, Multiple Output |
| SQP | Sequential Quadratic Programming |
| CFD | Computational Fluid Dynamics |
| ERD | Enzymatic reactive distillation |
| TAME | Tertiary Amyl Methyl Ether |
| TAEE | Tertiary Amyl Ethyl Ether |
| MIBK | Methyl Isobutyl Ketone |

| | |
|---|---|
| EO | Ethylene Oxide |
| EG | Ethylene Glycol |
| IB | Isobutylene |
| TBA | Tert-butylalcohol |
| PX | P-xylene |
| MX | Mixed xylene |
| OX | O-xylene |
| BG | β-glycosidases |

# 1. Introduction

Greenhouse emissions (GHG), as a side effect of modern industrialization, nowadays has caused many attentions worldwide due to its function in globe warming and other climate change issues. In 2016, the total GHG emissions were 49.3 gigatons in $CO_2$ equivalent, about 72% of the emission is $CO_2$, and the rest includes $CH_4$, $N_2O$ and fluorinated gases (19%, 6% and 3%, respectively) [1]. As for country/region contribution, as shown in Figure 1, although there is slight decrease comparing to 2015 (–0.3%), China still shares the largest contribution, namely 10.5 gigatons as $CO_2$ equivalent, followed closely by United States and European Union. According to the source of GHG, as shown in Figure 2, transportation, electricity and industry are the major sources, which take 80% share. The GHG emissions from transportation is mainly due to the fuels of different kinds, like gasoline, diesel etc. The GHG emission in electricity is from the coal–fired power plants. The GHG emissions from industry includes all different kinds of fossil fuel based chemicals and GHG related to specific processes.

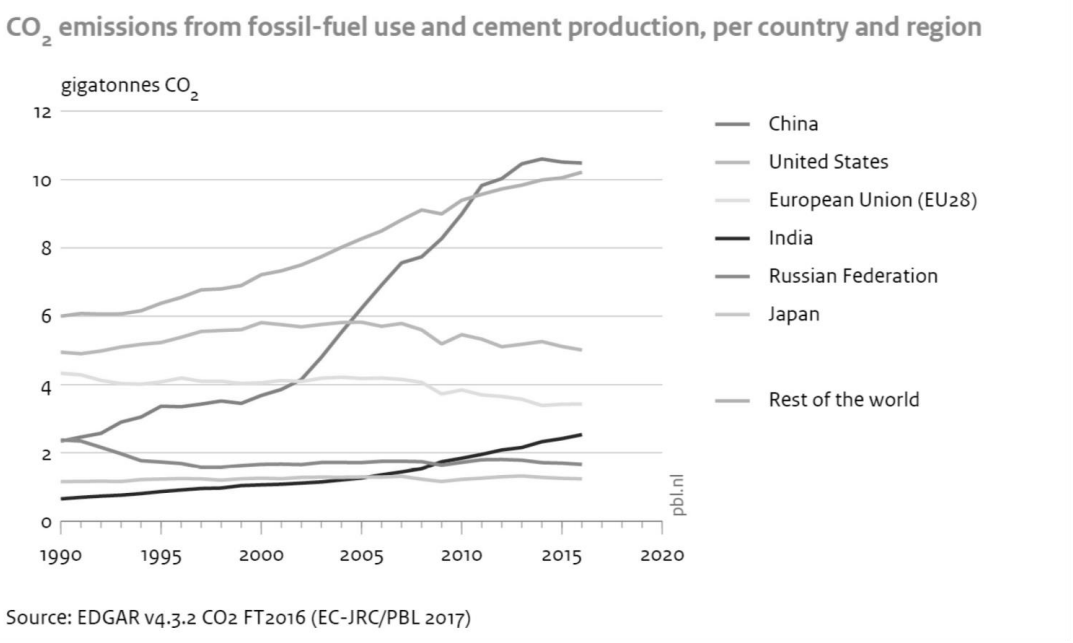


*Figure 1 $CO_2$ emission per country and region 1)[1]*

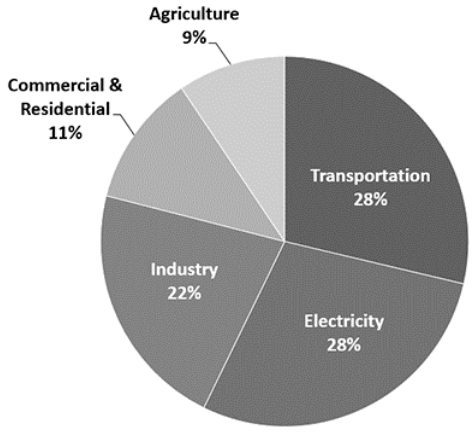


*Figure 2 Sources of GHG [2]*

Thus, when considering the reduction of GHG emissions, the above three sources are in priority. The electricity generation can be replaced by renewable energy, like biomass, wind, solar power etc. But for the transportation and industry, it is merely possible to find alternative solution in a short period when considering the large base number worldwide. Therefore, a possible solution is $CO_2$ reutilization, which can be either transferring $CO_2$ into potential resources or direct using of $CO_2$ in some way. In Table 1 & 2, the existing and emerging $CO_2$ utilizations are listed.

*Table 1 Existing $CO_2$ utilization [3]*

| **Existing uses** | **Current non–captive $CO_2$ demand (Mtpa)** | **Future potential non–captive $CO_2$ demand (Mtpa)** |
|---|---|---|
| Enhanced oil recovery (EOR) | 30< demand < 300 | 30< demand < 300 |
| Urea yield boosting | 5 < demand < 30 | 5 < demand < 30 |
| Other oil and gas industry applications | 1< demand <5 | 1< demand <5 |
| Beverage carbonation* | ~8 | ~14 |
| Wine making | <1 | <1 |
| Food processing, preservation and packaging* | ~8.5 | ~15 |
| Coffee decaffeination | unknown | 1<demand <5 |
| Pharmaceutical processes | <1 | <1 |
| Horticulture | <1 | 1< demand <5 |
| Pulp and paper processing | <1 | <1 |
| Water treatment | 1 < demand < 5 | 1 < demand < 5 |
| Inerting | <1 | <1 |
| Steel manufacture | <1 | <1 |
| Metal working | <1 | <1 |
| Supercritical $CO_2$ as a solvent | <1 | <1 |
| Electronics | <1 | <1 |
| Pneumatics | <1 | <1 |
| Welding | <1 | <1 |
| Refrigerant gas | <1 | <1 |
| Fire suppression technology | <1 | <1 |

*Table 2 Emerging $CO_2$ utilization[3]*

| **Emerging uses** | **Future potential non–captive $CO_2$ demand (Mtpa)** |
|---|---|
| Enhanced coal bed methane recovery (ECBM) | 30 <demand <300 |
| Enhanced geothermal systems − $CO_2$ as a heat exchange fluid | 5< demand <30 |
| Power generation − $CO_2$ as a power cycle working fluid | <1 |
| Polymer processing | 5< demand <30 |
| Chemical synthesis (excludes polymers and liquid fuels/ hydrocarbons) | 1< demand <5 |
| Algae cultivation | >300 |
| Mineralisation | |
| Calcium carbonate and magnesium carbonate | >300 |
| Baking soda (sodium bicarbonate) | <1 |
| $CO_2$ concrete curing | 30< demand <300 |
| Bauxite residue treatment (‘red mud’) | 5 < demand < 30 |
| Liquid Fuels | |
| Renewable methanol | >300 |
| Formic acid | >300 |
| Genetically engineered micro–organisms for direct fuel secretion | >300 |
| $CO_2$ injection to conventional methanol synthesis | 1< demand <5 |

### 1.1 Methanol economy

Among all these usages, methanol is one of promising applications. As one of major industrial chemicals, the worldwide methanol market is growing rapidly. Based on IHS Market analysis [4], the global methanol demand in 2021 will increase to 95.2 million tons as shown in Figure 3.

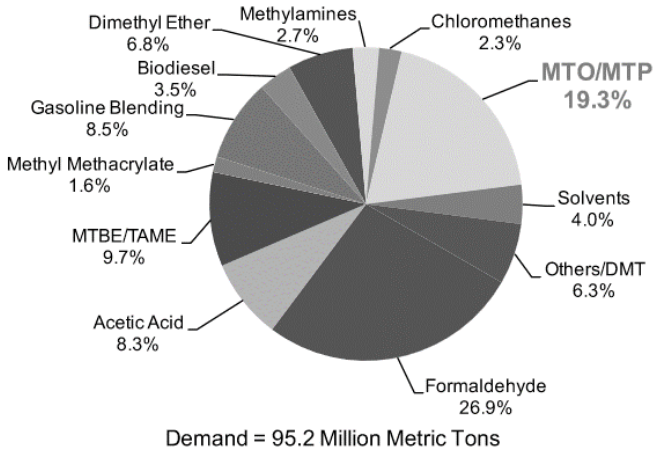


*Figure 3 Global methanol demand in 2021*

Methanol is widely used in making products such as plastics, plywood resins, paints, textiles and explosives. It also is a key intermediary and source for the production of dimethyl ether (DME) through dehydration and catalytic conversion, to gasoline in niche applications though the methanol–to–gasoline processes, and for the production of methyl tertiary butyl ether, which is a gasoline anti–knock additive primarily in use in Asia and Europe. Figure 3 shows the major applications of methanol which include many key intermediates for chemical industry. Even more, methanol can be directly used as fuel, or transformed to DME, a potential substitute of diesel.

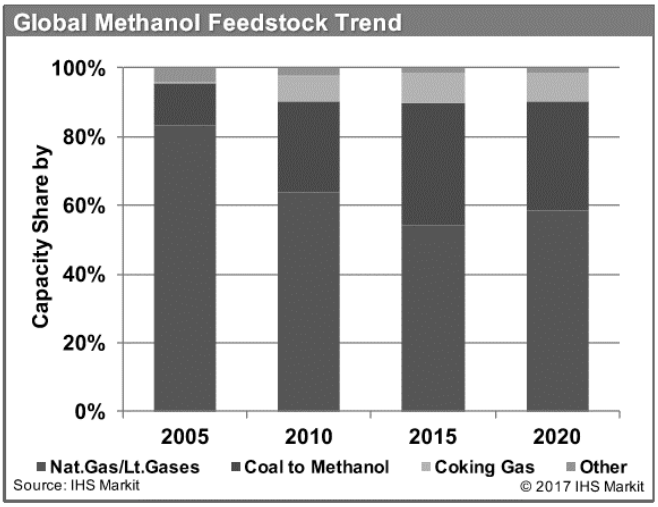


*Figure 4 Global methanol feedstock*

Figure 4 indicates the methanol feedstock, it includes four sources, they are natural gas,

coal, coking gas and others. Among them, coal and natural gas are two major feedstocks. Especially, China has dominated more than half of methanol markets in recent years, and in China, the major methanol feedstock is coal, and $CO_2$ emission in coal to methanol process is 3.85 t ($CO_2$)/t(methanol) [5]. Therefore, if most of $CO_2$ can be reused to produce methanol, it can significantly reduce GHG emissions and costs from the product chain.

## 1.2 Methanol applications

As an alternative to fossil fuel, methanol can be used to replace the conventional petrochemical process. Methanol can be transformed to produce olefins, gasoline, aromatic hydrocarbons, dimethyl carbonate (DMC), poly (methoxy dimethyl ether ($DMM_n$), and other products. Which has a better additional value and the process is more environmentally friendly. At present, the syngas from coal to methanol, formaldehyde and other technology are very mature. Markets for methanol are now moving to production of synthetic oil, fuel oil additives and alternative fuels, which can effectively make up for the oil supply gap.

### *1.2.1 MTO, MTG and MTA*

Thermodynamic studies[6] [7] indicate methanol to olefin (MTO), methanol to gasoline (MTG) and methanol to aromatics (MTA), it can be found that high temperature and space velocity, low pressure, use of appropriate catalyst, and control of extent of reaction can produce high olefin yields, while a relative low temperature, appropriate catalyst and proper aromatization can benefit gasoline and aromatics production.

#### *1.2.1.1 MTO*

ZSM–5 or SAPO–34 [8] molecular sieve catalysts are used to produce low carbon chain olefin from methanol. The former is characterized by 2D straight channel structure and strong surface acidity, which however reduces the selectivity to ethylene and propylene. Also, byproducts include aromatics and paraffin. For this reason, the selectivity can be

improved by preparing small grain ZSM–5 molecular sieve and modifying the catalyst. The latter has 3D straight channels with high activity and olefin selectivity, but it is vulnerable to carbon accumulation. In order to reduce this weakness, SAPO–34 molecular sieve should be modified.

UOP (U.S) and Hydro (Norway) adopts the combination of fluidized bed and regenerator, selecting SAPO–34 as the main component of MTO–100 catalyst. Ethylene and propylene selectivities are 55% and 27% respectively [9]. Nowadays, most MTO capacity is in China, which usually is combined with coal chemical industry, like coal gasifier and other process.

*1.2.1.2 MTG*

MTG process uses ZSM–5 molecular sieve as catalyst. The reaction is strongly exothermic process, and the adiabatic temperature rise can be up to 600 ℃. Therefore, industrialization of this process will face the problem of heat transfer from the reaction. Mobil (U.S) has developed fixed bed, fluidized bed and multi–tube reactor technologies. Parallel converting reactor, inter–external heat exchanger and fused salt in shell are used to control the reaction temperature, respectively [10]. At present, fixed bed is the mainly used technology in industry.

*1.2.1.3 MTA*

The HZM–5 molecular sieve modified by Ag, Zn and Ga is used as catalyst to improve the aromatization activity and selectivity. Mobil uses fixed bed process with total aromatics yield of 15.5%. The selectivity of benzene, toluene and xylene mixture is 14%, while the yield is very low (about 3%) [11].

*1.2.2 Methanol to DMC (dimethyl carbonate)*

*1.2.2.1 DMC process*

Processes for DMC production mainly includes: phosgene method, ester transformation, methanol carbonylation method, urea alcoholysis method, and carbon dioxide methanol synthesis method. Because of safety and environmental problems, the phosgene has been phased out. Ester transformation and methanol carbonylation method are the main technologies in the industrial production of DMC, but the former investment costs are higher and therefore only production in large–scale is economically feasible. Epoxy ethane (propane) is used as raw material, which may cause equipment and environmental issues. Thus, any new technology has potentially good economic and environmental benefits.

Ube Industries (JPN)[12] adopts low–pressure heterogeneous method (improved methanol carbonylation process) and takes activated carbon adsorbed $PdCl_2$ /CuCl as solid catalyst. At 0.2 to 0.5 MPa, DMC is synthesized directly. The yield is high, and the conversion of methanol is close to 90%.

Urea alkylation is a new method for industrial process of DMC [13]. Direct synthesis of DMC from carbon dioxide and methanol is an economical and environmentally friendly technology. However, problems such as low yield of DMC and catalyst deactivation have not been solved. At present, the process is still in the research and development stage.

**2. 2 DMC as mixed diesel additive**

The oxygen mass fraction in DMC is 53.3%, which is higher than in methyl tert–butyl ether (18.0%). Therefore, combustion brings less smoke and tar particles than pure gasoline and diesel oil. Its toxicity is similar to that of anhydrous ethanol. Adding DMC to diesel engine, the thermal efficiency is higher than for pure diesel. In the gasoline engine, with the use of DMC and gasoline fuel mix, total hydrocarbon, NOx and

benzene emissions can be significantly reduced.

### *1.2.3 Methanol to $DMM_n$*

$DMM_n$ is a homologue with the general form of $CH_3O(CH_2O)_nCH_3$. It can be used as a great diesel additive which can greatly reduce smoke particles, $NO_x$ and CO in vehicle exhaust

#### *1.2.3.1 $DMM_n$ process*

The key problem of $DMM_n$ synthesis is the selection and preparation of the catalyst. At present, the catalysts for $DMM_n$ synthesis mainly include acid catalyst, super strong acid catalyst, molecular sieve catalyst and ionic liquid catalyst. The preparation of $DMM_n$ in the early studies was mainly based on low polymerization degree polyformaldehyde (or oligoformaldehyde) and methanol, which was obtained under the catalysis of trace sulfuric acid or hydrochloric acid. DoPunt (U.S) was the first to study this subject, however they only obtained a yield of 10%. British BP, German BASF and other companies have also explored, but the yield is still low. The main disadvantages of this process are the low conversion and the strong corrosion caused by the catalyst.

Using solid super strong acid as catalyst to produce $DMM_n$ can solve some of the problems, such as difficulties in catalyst separation, low conversion and poor product selectivity [14]. Using molecular sieve as the catalyst, the yield can reach 47% [15].

Using room temperature ionic liquids as catalyst, methanol and trioxymethylene can be used as raw material to produce $DMM_n$. The catalyst has high catalytic activity and high conversion rate, and reaction is simple and easy to operate and control. One–way $DMM_n$ yield reaches 50%, where with n as 3~8, the selectivity is 70~80% [16].

#### *1.2.3.2 $DMM_n$ as diesel additive*

$DMM_{3\sim8}$ has a similar boiling point as diesel, but with higher relative molecular mass,

lower vapor pressure and higher viscosity. No further changes in diesel engine is needed when it is used as additive. Similarly, to DMC, there are no long C–C chains, therefore, combustion efficiency is high and less smoke particles, $NO_x$ and CO are generated.

# 2. Literature review

Assuming a total new concept needs very strong theoretical supports, in this work, reactive distillation is used in $CO_2$ hydrogenation process. Thus, the literature review consists of researches for methanol synthesis from carbon dioxide and reactive distillation. For $CO_2$ hydrogenation, the different catalysts, mechanism and reactors are studied, for reactive distillation, the design and control method, column internals are discussed. And information given in this chapter can be used in the process simulation.

$CO_2$ hydrogenation is nowadays a widely studied topic due to the greenhouse gas emission and fossil fuel crisis. However, most researches only stay in laboratory scale and very few pilot factories and industrial applications can be found in public. There are three major parts in the literature review, which are catalyst modification, process modification and mechanism.

Reactive distillation, which is actually not a very new concept, have been proven to be a very efficient solution in many chemical industrial processes. The combination of reaction and separation process reduces process complexity, and in some cases, increases the process efficiency. Although the manufacturing of the RD column brings some challenges, it is still a very promising technology.

## 2.1 $CO_2$ hydrogenation to methanol

According to different active components, the catalytic agents of $CO_2$ hydrogenation to methanol can be roughly divided into two categories, copper based catalyst and other types using precious metals as active component.

### *2.1.1 Catalysts*

#### *2.1.1.1 Copper based catalysts*

The early catalysts used in $CO_2$ hydrogenation have been developed on the basis of F–T synthesis catalyst. Although since the 1960s, produced by ICI company, $Cu/ZnO/Al_2O_3$ has become a commercial catalyst for methanol synthesis from syngas, there is still an issue about the active center, especially Cu state. When the copper catalyst is used for $CO_2$ hydrogenation, the problem becomes more complicated.

Some researchers believe that copper exists in the form of $C^0$ and $Cu^+$ (or $C^{\delta+}$) in the reaction of $CO_2$ hydrogenation, both of them can be seen as active center. Słoczyński et al. [17] used $Cu/ZnO/ZrO_2$ catalyst for $CO_2$ hydrogenation, after 10 days of reaction, the catalyst was tested, and the presence of $Cu_2O$ was found. Toyir et al.[18][19] prepared Cu/ZnO/SiO2 catalyst by using methoxy copper and ethyl acetone zinc as precursors, and the presence of $Cu^+$ was detected in the reaction. They found that the presence of $Cu^+$ increased the selectivity of methanol, and the ratio of $Cu+/Cu^0$ could be adjusted by changing the addition of gallium (Ga). Saito et al.[20] also proposed a similar view and believed that when the ratio of $Cu^+/C^0$ was 0.7, the performance of the accelerator was the best. Xu et al. [21][22] studied $CO_2$ hydrogenation on the CuO–ZnO catalyst, it is believed that active center exists in the oxygen hole on the CuO–ZnO structure, Cu valence on it is Cu + and $Cu^0$. Other test methods also proved existence of $Cu^+$. Such as Fierro [23] used $H_2 – CO_2 – H_2$ REDOX cycle confirmed Cu is partially oxidized by CO2 in the CuO/ZnO, which shows the existence of $Cu^+$, while the same situation does not occur in the pure CuO. In situ EXAFS studies showed that 76% of $Cu^0$ have been oxidized in the $Cu/ZrO_2$, and 27% is $Cu^+$, rest are $Cu^{2+}$[24]. Arena et al. [25] used CO as probe molecules, detected the formation of $Cu^{\delta+}$ by infrared spectrum in the Cu/ZnO/Zr catalyst, it is also confirmed that the $Cu^{\delta+}$ is in the metal oxide interface, and the interaction between Cu and ZnO, $ZrO_2$ is advantageous to the $Cu^{\delta+}$ stability. In addition, the close degree of functional theory calculations showed that $Cu^{\delta+}$ appeared on the interface of

Cu/metal oxide, methanol formation reaction is mainly happened in the $Cu^{\delta+}$, and inverse water gas shift reaction on the $Cu^0$ [26]. Wang et al. [27][28] used the UBI–QEP (Unity Bond Index–Quadratic Exponental Potential method) to calculate the $CO_2$ hydrogenation reaction on Cu (100). The results show that the ratio of $Cu^+/Cu^0$ is the key factor to the reaction.

However, many researchers believe that the copper–based catalyst exists only in the form of $Cu^0$ in the catalytic $CO_2$ hydrogenation of methanol reaction. Clausen et al. [29] used in situ XRD technology to study the changes of copper–based catalyst during methanol synthesis, only $Cu^0$ is detected. Xu et al. [30] used XPS – Auger technology to test Cu/ZnO catalyst, the results found catalyst exists in $Cu^{2+}$ form before reduction, after reaction only $Cu^0$ exists, but partial Zn is found as form of $Zn^{\delta+}$ after reduction and reaction. Yoshihara et al. [31][32] studied methanol synthesis reaction and $CO_2$ reverse water gas shift reaction hydrogenation in polycrystalline Cu and single crystal Cu (100) with low pressure and low conversion rate, and measured the reaction kinetics data. They found that polycrystalline Cu and single crystal Cu (100) has a similar TOF value (in terms of metal copper as active center) of methanol generation with value of Cu/ZnO catalyst, this suggests that the active center of all of them is the same, which is $Cu^0$. Rasmussen et al. [33] studied the $CO_2$ hydrogenation reaction on single crystal Cu (110) and obtained similar conclusions. In addition, Chinchen group [34] and Pan [35] work found that methanol yield and the metal copper surface area follow very strong linear relationship, which can also prove that $Cu^0$ is only active center.

Yoshihara et al.[32] think $Cu^0$ is extremely susceptible to be oxidized to $Cu^+$, the emergence of $Cu^+$ could be generated by accident when analyzing the, since it is merely possible to avoid any air contact. Some detected $Cu^+$ experiments are not strictly "in situ" experiments. However, there are many authors reported that although the methanol yield is associated with the surface area of copper, but not always

follows linear relationship, this could be an indirect proof that $Cu^0$ is not the only active center. [36][37][38]

Most researchers believe that it is unwise to study the active center while separating Cu from the rest of catalyst. In fact, copper components often interact with carriers and auxiliaries, which affect the state and activity of copper components. Many researchers believe that the addition of $ZrO_2$ can interact with the Cu, increasing the stability and activity of Cu [26][39][40][41], and similar interaction also exists between Cu and ZnO. [32][37] Zhang et al. [22] also believed that Cu and ZnO formed solid solution, $Cu_2O$ and ZnO together as the active center. Also, there are some articles on oxygen hole and Cu as active centers [29][42]. Arena et al. [25] believe that the copper/metal oxide interface plays an important role in $CO_2$ adsorption and hydrogenation. In the study of the hydrogenation properties of Cu–Ni bimetallic catalyst, the active center was considered to be Cu–Ni alloy. Even copper single active center, there are still some authors [28] believes that it should be metal copper clusters, rather than a single copper atom.

*2.1.1.2 Precious metal catalysts*

Precious metals can also be used as the active component of methanol catalyst for $CO_2$ hydrogenation. The catalysts are usually prepared by impregnation method.

Shao et al. [45] reported that $PtW/SiO_2$ and $PtCr/SiO_2$ catalysts had higher methanol selectivity, at 473 K, 3 MPa, with $CO_2$ and $H_2$ molar ratio of 1:3, the conversion rate of $CO_2$ was 2.6%, and the methanol selectivity was 92.2%. They also studied the $SiO_2$ supported RhM (M=Cr, Mo, W) [46], and the results of in–situ FT–IR showed that the intermediate contains the methyl acid salt, and the $CO_2$ and CO have different hydrogenation behaviors. Inoue et al. [47] reported the test results of $CO_2$ hydrogenation on the Rh catalyst supported by $ZrO_2$, $Nb_2$, and $TiO_2$. $Rh/ZrO_2$, $Rh/Nb_2O_5$ showed high catalytic activity, but the product was mainly methane, and the methanol on Rh/Ti obtained the most selectivity.

Solymosi et al. [48] investigated the effects of $CO_2$ and $H_2$ on the load Pd catalyst of $SiO_2$, MgO, $TiO_2$ and $Al_2O_3$. The results show that Pd plays a role in activating $H_2$, and the activated H reflows to the carrier to generate formate for the adsorption of carbon. They also found that the dispersion of Pd affected the product distribution of the reaction. When the dispersion degree of Pd is high, methane is mainly generated. When the dispersion degree of Pd is low, the reverse water gas shift reaction occurs, and methanol is produced. Therefore, they believe that $CO_2$ hydrogenation is mainly carried out by the CO that is generated by the reverse water gas shift reaction. Shen et al. [49] prepared the Pd/$CeO_2$ catalyst and studied the effect of reduction temperature on the structure and properties of the catalyst. With the increase of the reduction temperature, the Pd is sintered, along with reduction of part of $CeO_2$, which results the decrease of conversion of $CO_2$ and methanol selectivity.

Sloczynski et al. [17] prepared Au (or Ag) /ZnO/$ZrO_2$ and compared the performance of Cu/ZnO/$ZrO_2$. The active order of catalyst was Cu>Au>Ag, while methanol selectivity was Au>Ag>Cu. Baiker group [50] using the sol–gel method Ag/$ZrO_2$ catalysts, discusses the influence of preparation conditions on the physicochemical and catalytic properties, under optimized conditions, the Ag particles was only about 5~7 nm. However, compared with Cu/$ZrO_2$, though the methanol selectivity is similar, the conversion rate of $CO_2$ is much lower. These experimental results show that compared with Cu, the effect of Ag and Au on $CO_2$ and hydrogen is poor.

In addition, there are also reports of precious metal loaded on copper–based catalysts. In the Fierro group, Pd/Cu/ZnO/ $Al_2O_3$ catalysts were prepared by impregnation method [51]. The results showed that Pd promoted the reduction of CuO and increased the yield of methanol per unit area of Cu. They also explained the mechanism of hydrogen flow. However, as the result of the Pd impregnation in the rotary evaporation apparatus (the equivalent of hydrothermal process), will lead to the Cu/ZnO/$Al_2O_3$ hydrotalcite structure rearrangement, CuO particles get bigger. At the same time, the loaded Pd covers the partial surface Cu bit, and the surface area of Cu

is reduced. Therefore, the total methanol yield is lower than that of unloaded Pd. They also prepared the Pd/Cu/ZnO catalyst by means of co–precipitation and fractional precipitation [52]. The coprecipitation method has a large copper particle, which caused a smaller specific surface area, it is difficult to reduce. The residual $Na^+$ has a large influence, and the catalytic performance is poor, and the loaded Pd cannot compensate for the loss of Cu surface. In the catalyst prepared by cascade precipitation method, Pd and Cu have a synergetic effect. The method of cascade precipitation is to maintain the original copper dispersion degree, and the catalytic performance is improved due to the catalytic effect of Pd.

In addition to copper – based catalysts and precious metal supported catalysts, other elements are used as active components. For example, Calafatat et al. [53] found that $CoMoO_4$ has catalytic effect on the synthesis of methanol from $CO_2$ hydrogenation, and the addition of K can improve the selectivity of methanol.

In the above–mentioned catalysts, copper–based catalyst is the most studied and the comprehensive performance is the best. Therefore, the following discussion is mainly aimed at the copper base catalyst.

### *2.1.2 Carrier*

The carrier not only supports and disperses the active component, but also interacts with the active component, or influences the interaction between the active component and the auxiliary agent. Therefore, the suitable carrier plays an important role of the catalyst. In terms of copper base catalyzer for $CO_2$ hydrogenation, the carrier mainly includes ZnO, $Al_2O_3$, $ZrO_2$, $TiO_2$ and $SiO_2$. According to the number of oxide components used by the carrier, it can be divided into single component oxide carrier (including modified single component) and compound oxide carrier.

*2.1.2.1 Single component oxide carriers*

For single component oxide carrier, the acid and alkali, morphology and structure of the carrier will affect the performance of the catalyst. Tagawa et al. [54] believed that the acid carriers showed higher methanol selectivity and lower catalytic activity, and the neutral and alkaline carriers only produced CO, only amphoteric carriers showed high activity. Among them, $TiO_2$ is the best, which can inhibit the generation of CO. At the same time, they also used auxiliaries $K_2O$, $P_2O_5$ and $B_2O_3$ to regulate the acid and alkalinity of the carrier [55]. However, they only described the acid and alkalinity of the carrier but did not measure and characterize the surface acid and base position of the carrier. Guo et al. [56] also investigated the effects of $La_2O_3$ on the catalytic performance of $CuO–ZrO_2$ catalyst. The results showed that the addition of $La_2O_3$ increased the base number and base density of the surface of $CuO–ZrO_2$, and the selectivity of methanol was closely related to the alkaline position distribution of the catalyst surface. Liu et al. [41] prepared nanoscale mesoporous $ZrO_2$ and used it as a carrier of copper–based catalyst. They found that this kind of $ZrO_2$ have more oxygen flaws, which resulting the change of active component and carrier of electronic states, as a result, the reduction temperature of CuO decreases, thus improves the catalytic performance. Jung et al. [57] studied the influence of the phase state of $ZrO_2$ on the catalytic performance of copper–based catalysts. The results showed that $CO_2$ hydrogenation activity was higher on $m–ZrO_2$ than on $t–ZrO_2$. The reason is that the concentration of methanol intermediate on $m–ZrO_2$ is higher than that of $t–ZrO_2$.

*2.1.2.2 Composite oxide carrier*

Compared with single – component oxide carriers, composite oxide carriers usually exhibit better catalytic performance. Among them, ZnO is most studied. Xu et al. [58] added $ZrO_2$ in Cu/ZnO and found that the addition of $ZrO_2$ increased the dispersion of Cu, which helped to improve the activity of catalysts and methanol selectivity. Cong et al. [44] used EPR and XPS technology to analyze $Cu/ZnO/ZrO_2$ catalysts, the results showed that the addition of $ZrO_2$ changed the surface of the catalyst structure

and coordination, improved the dispersion of active components and the stability of the catalyst. Xu et al. [59] also investigated the influence of the addition of $ZrO_2$ on the Cu/ZnO catalyst performance, and the results showed that a proper addition of $ZrO_2$ increased the selectivity and yield of methanol. Experiment also found that $CO_2$ stripping temperature on the Cu/ZnO surface is above 500℃, after adding $ZrO_2$, stripping temperature dropped to 200 ~ 300 C, namely, $ZrO_2$ changed the $CO_2$ state on the Cu/ZnO catalyst surface, improved the ability of $CO_2$ hydrogenation to methanol. Li et al. [60] studied the function of $Al_2O_3$ on Cu/ZnO/$Al_2O_3$ catalyst. It was believed that $Al_2O_3$ does not only support the structure, but also disperses catalyst active component, moderate amounts of $Al_2O_3$ can improve methanol yield and selectivity of $CO_2$ hydrogenation, and excessive $Al_2O_3$ may decrease methanol yield. Nomura et al. [61] added ZnO or $ZrO_2$ in Cu/$TiO_2$ and Cu/$Al_2O_3$ catalysts, results showed that the performance of composite oxide carrier was improved, among them, CuO–ZnO/TiO2 is the best. Saito et al. [20] investigated the effects of $Al_2O_3$, $ZrO_2$, $Ga_2O_3$ and $Cr_2O_3$ on Cu/ZnO catalyst. It is found that the addition of $Al_2O_3$ and $ZrO_2$ increases the specific surface area of copper, while $Ga_2O_3$, and $Cr_2O_3$ can stabilize $Cu^+$ and improve the activity per unit copper. Arena et al. [36] and Ma et al. [62] reported that the commercial Cu/ZnO/$Al_2O_3$ catalyst used in syngas methanol was not as good as Cu/ZnO/$ZrO_2$ for $CO_2$ hydrogenation, and the reason was that $Al_2O_3$ had a strong affinity for water.

In addition to the compound oxide carrier containing ZnO, other compound oxides have also been reported. Zhang et al. [39] investigated the effects of $ZrO_2$ on the physical and catalytic properties of Cu/ γ–$Al_2O_3$. The addition of $ZrO_2$ raised the dispersion of copper, while the interaction between $ZrO_2$ and CuO can improve the catalytic performance. Qi et al. [63] used Cu–$MnO_x$/$Al_2O_3$ catalyst for $CO_2$ hydrogenation to methanol. The addition of $Al_2O_3$ significantly increased the conversion rate of $CO_2$ and the selectivity of methanol. When the molar fraction of $Al_2O_3$ was 5% ~ 10%, the catalytic effect was better. Zhong et al. [43] used the surface modification to prepare $SnO_2$ – $SiO_2$ (SnSiO) compound carrier, SnSiO is

$SnO_2$ monolayer linked on the surface of $SiO_2$ composite oxide, the pore structure and specific surface area remained the same as $SiO_2$ carrier. The introduction of $SiO_2$ on the surface of $SnO_2$ can effectively promote the reduction of CuO and NiO, which is conducive to the improvement of catalytic performance. Zhu et al. [64] prepared $Cu/ZnO/SiO_2 – ZrO_2$ catalyst for $CO_2$ hydrogenation, the catalyst has the characteristics of large surface area, uniform pore size distribution, which showed high activity and methanol selectivity.

To sum up, the role of the carrier can be summarized as the following aspects. One is to support the active component as skeleton; The second is to disperse the active components and increase the number of active sites. The third is to interact with the active component to stabilize some activity and improve its activity. In addition, there are reports of direct involvement of the carrier in the catalytic reaction, such as Fisher et al. [65] and Bianchi et al. [66], that the hydrogenation of carbon intermediates such as formate is carried out on the carrier $ZrO_2$.

### *2.1.3 Additives*

Additives are added in copper–based catalyst can make the dispersion of Cu and Cu electronic state, the interaction between Cu and the carrier and the properties of carrier itself have changed, which leads to the change of catalyst performance. Therefore, additives in copper–based catalysts are an important part of the research.

#### *2.1.3.1 Addition of rare earth elements*

The study of Chi et al. [67] showed that the conversion rate of $CO_2$ was significantly increased after the mixing of $La_2O_3$ and $CeO_2$ in $Cu/ZnO/SiO_2$, while methanol selectivity decreased slightly, the yield of methanol increased. $La_2O_3$ improved the reduction temperature of $CuO/ZnO/SiO_2$ catalyst, and $CeO_2$ reduced the reduction temperature. Adding $La_2O_3$, $CeO_2$ can affect interactions between $Cu/ZnO/SiO_2$. Liu et al. [68] studied the effects of $La_2O_3$ on the physicochemical properties of Cu/ZnO

catalyst and $CO_2$ hydrogenation. The $La_2O_3$ modified catalyst has a finer CuO crystal, and catalytic activity increases. Guo et al. [56] was also found appropriate amount of $La_2O_3$ can improve the dispersion of copper in the $CuO/ZrO_2$ catalyst, change of alkaline distribution on the surface, so as to improve the conversion rate of $CO_2$ and the selectivity of methanol. Wang et al. [42] added $CeO_2$ or $Y–CeO_2$ in Cu/ $\gamma–Al_2O_3$, catalyst activity and methanol selectivity increased significantly. Such increase is due to coordination between the Cu and $CeO_2$ which later formed to an active center, while dispersion of carrier $Al_2O_3$ and BET have nothing to do with it. The oxygen hole produced by the addition $CeO_2$ is beneficial to the activation of $CO_2$, Moreover, $CeO_2$ also affected the reduction peak temperature of CuO. Huang et al. [69] investigated the performance of $CO_2$ hydrogenated methanol reaction by modified $Cu/ZnO/Al_2O_3$ modified catalyst, and the results showed that the activity of $La_2O_3$ and $CeO_2$ decreased after doping.

*2.1.3.2 Addition of transition elements*

Zhang et al. [70] found that the doping of V increased the dispersion of copper in Cu/ $\gamma–Al_2O_3$ catalyst, thus enhancing the activity of the catalyst. The best addition of V is 6% (quality ratio). Wang et al. [71] has similar reports. The Cu/Zn/Al/Mn catalyst of four components was prepared by coprecipitation method [74], and it was found that adding a moderate amount of manganese fertilizer could significantly improve the activity and thermal stability of the catalyst. The structure and morphology of the catalyst were characterized by SEM and XRD method, and the results showed that the manganese fertilizer could prevent CuO grain growth and promote CuO dispersion. Lachowska et al. [73] and Sloczynski et al. [38] also reported that Mn has promoted the catalytic agent of Cu/ZnO/ZrO.

*2.1.3.3 Addition of IIIA elements*

Toyir et al. [19] prepared Ga doped Cu/ZnO and $Cu/SiO_2$ catalysts by impregnation method. The results showed that $Ga_2O_3$ had a positive effect, such effect was related

to the size of $Ga_2O_3$ particles, which means a smaller $Ga_2O_3$ particles bring more benefit to the generation of $Cu^+$. Inui et al. [74] prepared the Cu/ZnO catalyst doped with Pd and Ga. The hydrogen adsorbed on Pd has overflow phenomenon, and Ga has reverse overflow phenomenon. The reduction state of metal oxide in the catalyst can be adjusted by these two flows which brings a better catalyst performance. The yield of methanol increased significantly under the large space velocity. Liu et al. [40][41] found that the doping of $Ga_2O_3$ and $B_2O_3$ could lead to changes in CuO content on the catalyst surface, thus affecting its catalytic performance. Sloczynski et al. [75] investigated the influence of B, Ga, and In doping in Cu/ZnO/$ZrO_2$ catalyst. The results showed that the addition of additives changed of the dispersion of copper and the surface of the catalyst and changed the water (which is against methanol synthesis) adsorption ability, thus affecting the catalyst activity and stability. Among them, Ga has the best promotion effect, while In in addition, the catalytic activity is significantly reduced.

#### *2.1.3.4 Addition of alkali/alkaline earth metals*

There are also a number of reports on the copper – based catalysts used in alkali and alkaline earth metals. For example, the catalysts of CuO–ZnO–$SiO_2$ doped by Li, Na, K and Mg were studied. Słoczyński et al. [38][75] added Mg to Cu/ZnO/$ZrO_2$, increasing the specific surface area and dispersion degree of copper.

### *2.1.4 Catalyst pre–treatments*

The preparation of catalysts usually includes two processes: roasting and reduction.

The roasting temperature has great influence on the structure of the copper–based catalyst, which can furtherly affect $CO_2$ hydrogenation catalytic performance. With the increase of roasting temperature, the particle size increases, and the surface area of BET is decreased and the specific surface area of copper decreases, and the activity of the catalyst decreases as well [63][81][94]. However, the roasting temperature should

not be too low, otherwise the precursor cannot be completely decomposed into oxide, and the interaction between each component is not enough. Generally, roasting temperature at 350 ~ 400℃ the performance of the catalyst is the most preferred [80][94]. In addition, the heating rate of the roasting process also influences the performance of the catalyst. Fujita et al. [95] found that when green copper zinc is chosen as precursor for catalyst, the copper particle size was affected by the heating rate, and the low heating rate could obtain the ultra–fine CuO grain. But when malachite is chosen, particle size is irrelevant to the heating rate.

Reduction conditions also affect the performance of the catalyst. Chi et al. [94] found in 275 ~ 375℃, the reduction temperature of $Cu/ZnO/SiO_2$ has a little influence on the catalyst activity, but after 430℃, catalyst activity declines, it is believed that the presence of the $C^0$ grain. The results of Fujita et al. [95] showed that the Cu/ZnO catalyst obtained best performance after reducing 17 h under 170 ℃. Cao et al. [96] used $KBH_4$ solution for fresh carbonate precipitation in liquid phase, a highly activity and high selectivity of $Cu/ZnO/Al_2O_3$ catalyst is obtained, and dosage change of $KBH_4$ can modify $Cu^+/C^0$ ratio, so as to achieve the better catalyst activity and selectivity.

### *2.1.5 Reaction mechanism*

Although the reaction of CO hydrogenation to methanol has been studied more than half a century, the reaction mechanism remains controversial. There is an inherent relation between $CO_2$ hydrogenation and CO hydrogenation to methanol, and there are many unsolved problems. The research on methanol reaction mechanism of $CO_2$ hydrogenation is mainly focused on the following aspects.

#### *2.1.5.1 Carbon source*

Three reactions are involved in the process of $CO_2$ hydrogenation, see equation (1)–(3).

$$CO_2 + 3H_2 \rightleftharpoons CH_3OH + H_2O \quad (1)$$

$$CO_2 + H_2 \rightleftharpoons CO + H_2O \quad (2)$$

$$CO + 2H_2 \rightleftharpoons CH_3OH \quad (3)$$

Whether methanol is from $CO_2$ hydrogenation or from CO hydrogenation, i.e. what is the carbon source, remains a problem. Weigel et al. [97] believed that after adsorption of $CO_2$ on the surface of the catalyst, carbonates would be formed, and the latter would generate CO through the reverse water gas shift reaction. Then CO is hydrogenated to generate formaldehyde or methoxyl until methanol. Therefore, CO is the carbon source of methanol. Klier et al. [98] also believed that CO is the carbon source of methanol. However, many authors believe that methanol synthesis mainly comes from the direct hydrogenation of $CO_2$. For example, Chinchen et al. [99] used $^{14}C$ as a marker to track the synthesis of methanol, which proved that CO2 was the carbon source of methanol. Sun et al. [100] also showed that $CO_2$ is a carbon source. Mao et al. [101] studied the hydrogenation reaction of $CO_2$ in $Cu/ZnO/ZrO_2$ catalyst by TPSR technology, indicating that methanol synthesis was through $CO_2$ hydrogenation. At mean time, some researchers think both $CO_2$ and CO are the carbon sources of methanol synthesis, but $CO_2$ hydrogenation is at the leading position [38][65][102]. The reason can be attributed to the rate of $CO_2$ hydrogenation rate in the same condition is greater than that of CO. Cong et al. [103] found the particle size of the catalyst can also affect the reaction mechanism of methanol synthesis. When the catalyst particle size is very small, CO tends to generate $CO_2$ through the water gas shift reaction, and then the methanol is synthesized by $CO_2$ hydrogenation. When the particle size is large, CO is easy to directly be hydrogenated to methanol.

*2.1.5.2 Reactive center*

The main active component is copper in the copper–based catalyst. The question on copper state in the catalytic reaction has been not unified so far. Especially, more and more studies show that ZnO and $ZrO_2$ "carrier" is directly involved in the catalytic

reaction. They act on $CO_2$ adsorption and on activation of the active center [26][56][65][66]. The role of copper is adsorbing and desorbing $H_2$, therefore both the "carrier" and the copper are active centers.

*2.1.5.3 Hydrogen overflow*

Hydrogen overflow plays an important role in $CO_2$ hydrogenation to methanol on copper–based catalyst. Bianchi et al. [66] systematically studied the $ZrO_2$ loaded copper–based catalyst. It is believed that the free hydrogen desorbing from the copper reaches the surface of $ZrO_2$, then the carbon intermediates were hydrogenated. Jung et al. [104] discussed the effect of hydrogen overflow on $CuO/ZrO_2$ catalyst through isotope tracking experiments. The exchange rate of H atom on $CuO/ZrO_2$ was much higher than that on $ZrO_2$, indicating that the hydrogen overflow on copper has certain effect. Water on $ZrO_2$ can block the exchange of H atom while in $CuO/ZrO_2$, H atom exchange is promoted. This is because water prevents $H_2$ decomposition on the surface of $ZrO_2$, but it does not block the decomposition of $H_2$ on $CuO/ZrO_2$, which is beneficial to hydrogen overflow. It is also determined that the rate of hydrogen overflow is much greater than the rate of methanol generation. Therefore, hydrogen overflow is not the rate–determining step of methanol synthesis.

*2.1.5.4 Intermediates and rate controlling steps*

$CO_2$ hydrogenation is a complex reaction, composed of multiple simple reactions (primitive reactions), forming a variety of reaction intermediates. The researchers generally detected the presence of formate and methoxy intermediates in [30][102][106][107]. Recently, Hong et al. [107] studied the reaction mechanism of $CO_2$ hydrogenation to methanol on $CuO–ZrO_2$ catalyst by using the dynamic Monte Carlo simulation of the first principle. The results of theoretical calculation also indicate that methanol and CO are converted by the same intermediate formate. The results of IR spectra showed that the formate is mainly in bridge adsorption state [100][103]. Fujitani et al. [108] used scanning tunneling microscope to test the

formate adsorbed on Cu (111), the results show that under normal pressure, formate is adsorbed as a form of linear form, but under high vacuum no chain formate is observed. The hydrogenation of formate or methoxy is generally considered to be a rate–controlling step in $CO_2$ hydrogenation [30][100][103].

*2.1.5.5 Reaction path*

Researchers [26][65][100][106] have proposed a variety of catalytic reaction pathways for the synthesis of methanol reaction from $CO_2$ on copper–based catalyst. For example, Cu/ZnO, Cu/$ZrO_2$ and Cu/ZnO/$ZrO_2$ catalysts have been described. Fujita et al. [108] proposed the mechanism of the synthesis of methanol on Cu/ZnO catalyst, as shown in Figure 5

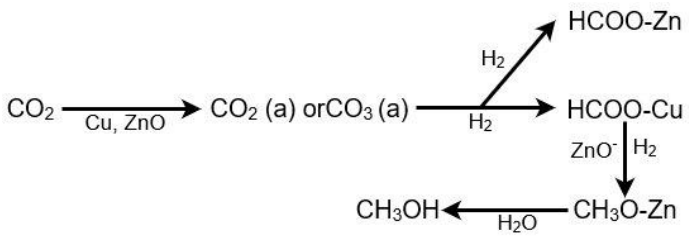


*Figure 5 $CO_2$ hydrogenation mechanism on Cu/ZnO catalyst*

$CO_2$ is first adsorbed on the Cu/ZnO catalyst and by hydrogenation transformed to copper and zinc formate intermediate, which are then converted into methoxy zinc and then hydrogenated to methanol. Fisher et al. [65] believed that in the hydrogenation on Cu/$ZrO_2$, $CO_2$ is adsorbed on $ZrO_2$ as hydroxyl as bicarbonate and $H_2$ is desorbed from the copper. The hydrogen carbonate is generated by hydroxy adsorbing $H_2$ on $ZrO_2$, and further hydrogenated to methanol. The reaction path is shown in Figure 6.

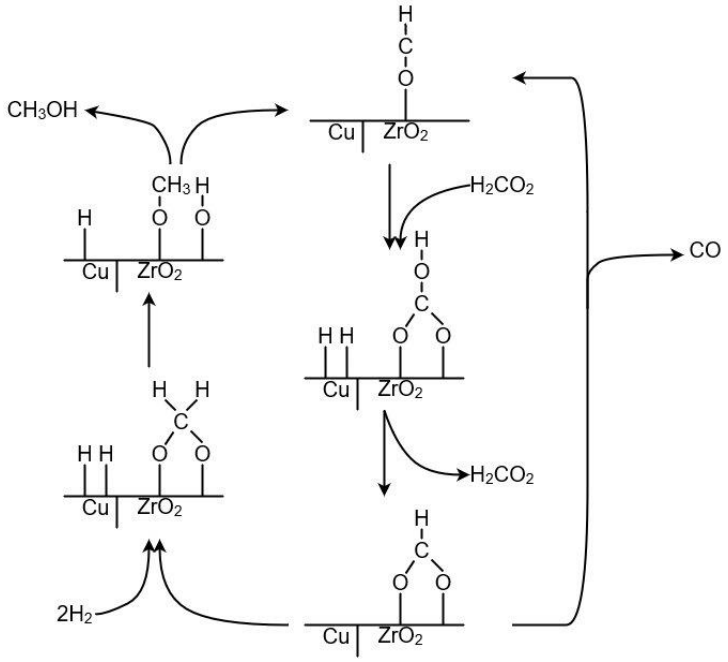


*Figure 6 $CO_2$ hydrogenation mechanism on $Cu/ZrO_2$ catalyst*

Arena et al. [25] studied the $CO_2$ hydrogenation mechanism on $Cu/ZnO/ZrO_2$ catalyst. They believed that both ZnO and $ZrO_2$ can adsorb $CO_2$ to generate formate, and the copper desorbs hydrogen through the efflux to reach the $Cu/ZnO$ and $Cu/ZrO_2$ interface with formic acid and is hydrogenated methanol, as shown in Figure 7.

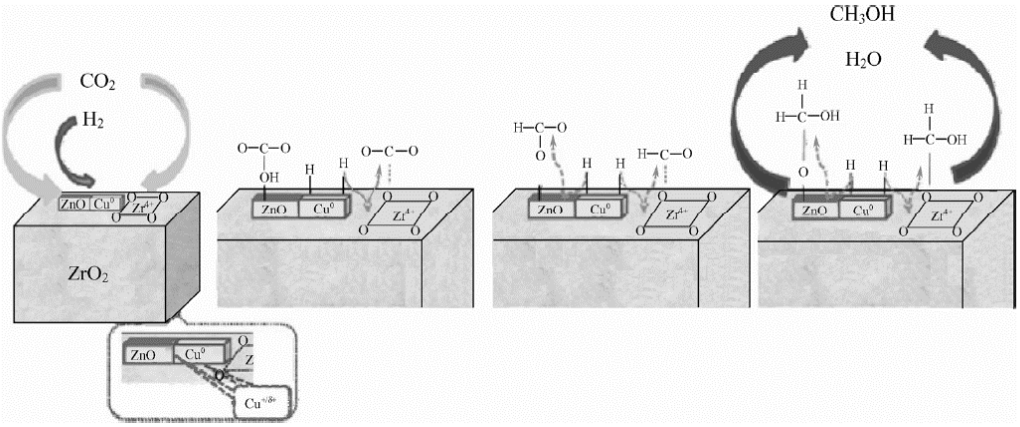


*Figure 7 $CO_2$ hydrogenation mechanism on $Cu/ZnO/ZrO_2$ catalyst*

### *2.1.6. Liquid phase $CO_2$ hydrogenation to methanol*

At present, industrial methanol synthesis uses CO and $H_2$ as the feed materials, and usually a gas phase reactor is implemented. Like in $CO_2$ hydrogenation, copper–based

catalyst is the mostly common catalyst in–use. Restricted by thermodynamic equilibrium in industrial production conditions of 300℃ and 5 MPa, the one–way conversion is lower than 15% [109]. Therefore, multi–loop reactors or complex circulation are used to improve the conversion, which means that a complicated process and a lot of equipment is required.

Both the CO and $CO_2$ hydrogenation reactions are exothermic, the reaction enthalpy at 25℃ is –90.64 kJ/mol and –49.47 kJ/mol, respectively. Therefore, increasing reaction temperature brings disadvantages to the methanol synthesis. Taking the raw material gas $CO/H_2$ as an example, as shown in Figure 8 [110], to achieve high methanol conversion, the energy consumption of the reaction increases since higher pressures are needed. Therefore, low temperature liquid phase methanol synthesis under low pressure can reduce energy consumption and increase carbon conversion.

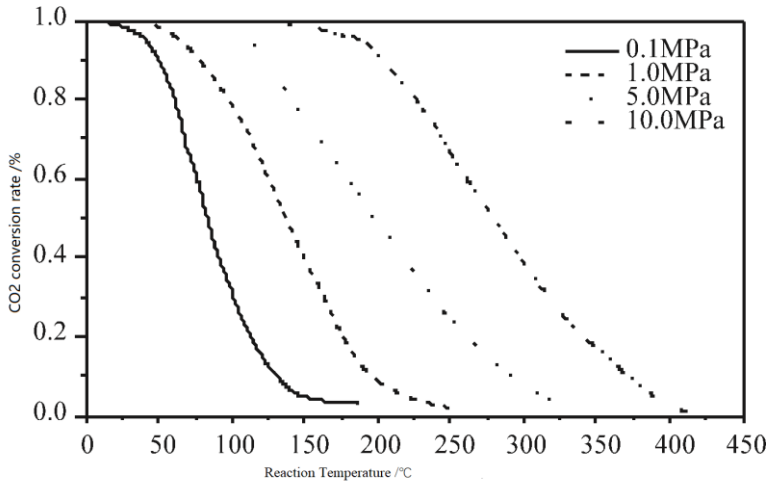


*Figure 8 Methanol conversion rate at various temperature*

*2.1.6.1. Mechanism of $CO_2$ hydrogenation to methanol in liquid phase*

Although there are no specific articles related to liquid phase $CO_2$ hydrogenation, syngas methanol synthesis can be used as a reference due to the similar materials and reactions. Zeng etc. [111] used $CO/CO_2/H_2$ as raw materials for low temperature methanol synthesis in liquid phase. Its reaction mechanism is mainly composed of three steps (Figure 9): (1) the raw materials $CO_2$ and CO react with $H_2$ to generate

formate; (2) the synthesis of esters between formate and alcohols from the catalyst or liquid; (3) esters are hydrogenated to produce methanol.

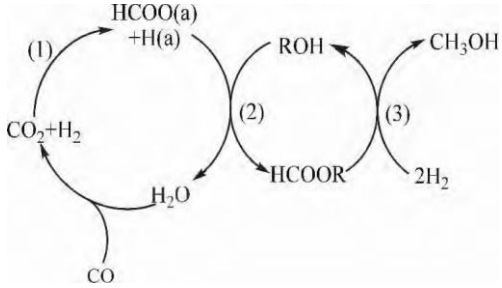


*Figure 9 Mechanism of $CO_2$ liquid hydrogenation [111].*

Yang et al. [112][113][114][115] observed the reaction process using in situ diffuse reflection infrared spectroscopy and found that the carbonylation reaction followed the Rideal–type mechanism. Zhang [116] studied methanol dynamics on the Cu/ZnO catalyst and found that alcohol carbonylation rate is greater than that of ester hydrogenation rate, hence the hydrogenation reaction rate is the controlling step. This is different from the $CO/H_2$ methanol synthesis.

*2.1.6.2. Catalysts at low temperature in liquid phase*

Most $CO/CO_2/H_2$ catalyst system consists of two kinds of catalysts, namely, alcohol catalyst system composed of copper–based catalyst and alcohol solvent, and paraffin catalyst system composed of copper–based catalyst and inert liquid paraffin wax. Also, new kinds of catalysts, which are not based on conventional F–T synthesis catalysts, have been studied recently, such as precious metals, cobalt and ionic liquids.

(1) Alcohol catalyst system

The alcohol catalyst system operates at 150~170 ℃ and 3 ~5 MPa. The Cu/ZnO catalyst in alcohol catalyst system has been studied comprehensively. Reubroycharoen et al. [117][118] found that when n(Cu): n(Zn)=1:1, the catalyst showed the highest activity, and the total carbon conversion was 47%. Bao et al. [119] found that addition of Zn can improve pore diameter distribution of Cu–O, and

prevent the accumulation of Cu during reduction, resulting in high dispersion of Cu and Cu–$ZnO_x$ grains.

Alkali metal salt can catalyze the carbonylation reaction to methanol and improve the conversion. Catalysts such as Cu–MnO alone brings low catalytic activity, but addition of $K_2CO_3$ as modifier can significantly improve the activity of the whole reaction system [120]. The total carbon conversion was 90.2 % and the selectivity to methanol about 99.1%, but the author has no further reports on the catalyst.

In $CO/CO_2/ H_2$ reaction system, the influence of solvent on reaction rate and selectivity is mainly related to its spatial structure and electronegativity. The carbonylation reaction of solvent alcohol molecules is a nucleophilic reaction [111][121], high hydroxyl electronegativity and low space position resistance are beneficial to the reaction. For example, 1– butanol has less steric resistance, but the oxygen on the hydroxyl group is less electronegative, which makes the activity lower than for 2–butanol. The oxygen atom of the iso–butanol hydroxyl group is highly electronegative, but the space resistance is larger and therefore the activity is not as good as for 2–butanol. 2– butanol hydroxyl oxygen atoms have good electronegativity and suitable space resistance and therefore exhibit high catalytic activity. From table 3, it can be found that 2–propanol, 2–butanol and 2–pentanol have the best catalytic performance.

*Table 3 The influence of different solvent on methanol synthesis [118]*

| Solvent | Total Carbon conversion /% | Selectivity /% | | |
|---|---|---|---|---|
| | | $CH_3OH$ | $HCOOCH_3$ | HCOOR |
| 1–propyl alcohol | 35.2 | 98.1 | 0.0 | 1.9 |
| 2–propyl alcohol | 44.4 | 99.8 | 0.2 | 0.0 |
| 1–butanol | 34.4 | 98.9 | 0.4 | 0.0 |
| 2–butanol | 47.0 | 99.6 | 0.4 | 0.0 |
| t–butanol | 29.9 | 99.7 | 0.3 | 0.0 |
| 1–amyl alcohol | 34.2 | 99.7 | 0.3 | 0.0 |
| 2–amyl alcohol | 44.0 | 99.7 | 0.3 | 0.0 |

(2) Paraffin catalyst system

Paraffin catalyst system operates at 200~240 ℃ and 4~5 MPa, s. In this process, a liquid paraffin is added as an inert medium. The paraffin has good thermal conductivity, which makes the reaction temperature uniform and temperature control simple and effective.

Zhang et al. [116] used $Cu/ZnO/Al_2O_3$ as the catalyst at 240 ℃ under 4 MPa. The carbon conversion was 44.5% with 99.4% methanol selectivity. Because the reaction temperature is relatively high, the copper–based catalyst is easily sintered and deactivated. Therefore, this catalyst system is not widely used in industrial process.

(3) Other catalysts

Precious metals have been used as industrial catalyst in various applications for many years. For example, platinum net is used in catalytic reforming and palladium can be used to purify exhaust gases from vehicles. Despite the price, precious metals always have relatively high activity, selectivity and endurance to catalyst poisons.

Filonenko et al.[122] prepared nanoparticulate gold catalysts for conversion of $CO_2$ to formates, and the performance $Au/Al_2O_3$ was studied. The XPS and STEM showed that $Au^0$ played an important role in the catalyst. The existence of Au can promote heterolytic dissociation of $H_2$, and the best activity was obtained with 1 wt.% $Au/Al_2O_3$ catalyst. Liu et al.[123] also tested Au catalyst in $CO_2$ to formates synthesis. From theoretical calculations and spectral analysis, the activation of $CO_2$ can be achieved through a weakly bonded carbamate zwitterion intermediate derived from a simple Lewis base adduct of $CO_2$. However, this can only occur with a hydrogen lacking Lewis base center in a polar solvent. Ganguly et al.[124] studied Au (111) function in Au photo–catalyst for $CO_2$ hydrogenation to methanol, the results showed that the reaction can have appreciable rates at room temperature. Zhan et al. [125] used Pt to prepare a nanoreactor, namely ZIF–67/Pt/m$SiO_2$ nanocubes, which have a

sandwich–structure. The results showed that such nanoreactor was around six times as active as other comparative catalysts with shorter diffusion times Vourros et al. [126] studied Au catalyst with different supporters in $CO_2$ hydrogenation to various products. The results showed that Au–ZnO has the highest selectivity to methanol (nearly 90%), while Au–$CeO_2$ gives 83%. If CO is considered as the product, the Au–$TiO_2$ has almost 100% selectivity, and for methane, Au–$Fe_2O_3$ is the best option (85%).

*2.1.7 Process conditions and reactor type*

The most important factors of pilot experiment and further industrial application are proper process conditions, they are temperature, pressure, space velocity and C/H ratio. But the challenges are those conditions are heavily depended on different catalyst, reactor types and products. So, it is unwise to discuss process conditions without reactor type.

Although at current stages, most studies remain in laboratory scale, they can be used as good reference for further study.

*2.1.7.1 Fixed bed reactor*

Fixed bed reactor is the most common reactor for catalytic reaction for industrial use, it is often used in gas phase reaction. Fixed bed reactor has a simple structure, catalyst is packed in the bed, which means catalyst loss is less compared with other reactors. But, it is hard to maintain the temperature constantly and one–way conversion is low (compared with other reactor types). Thus, when implemented into practice, it always requires loop structure and multiple reactors are needed to satisfy the total conversion rate.

Willauer et al [127] studied $CO_2$ hydrogenation under Fe catalyst to produce different carbohydrate in a stainless–steel tube. They also compared the fixed bed and continuously stirred tank/thermal reactor (CSTR) under different space velocity while

other conditions unchanged. The result showed that under low space velocity, the fixed bed has a higher $CO_2$ conversion rate than in that of CSTR. When space velocity was 0.000093 L/s–g, the $CO_2$ conversion is 60%, then conversion rate decreased while space velocity increased. Gesmanee et al [128] used Cu–Zn catalyst to produce methanol from $CO_2$ in fixed bed, and different catalyst combinations were examined. The result indicated copper–zinc catalyst brought the highest methanol yield, but $CO_2$ conversion rate is relatively low. Guo et al [129] used combustion synthesis to prepare CuO–ZnO–$ZrO_2$ for $CO_2$ hydrogenation to methanol, the different catalysts have been tested. The results showed that the highest methanol yield is 8.5%, but the precise space velocity was not given. Bahruji et al [130] studied Pb/ZnO catalyst to produce methanol from $CO_2$, and different Pd loading dosages were tested. The result showed methanol selectivity is 60%.

The various studies indicate that although different catalysts are used, the temperature remains the same, and pressure somehow is different due to different catalysts. One major obstacle in fixed bed is its poor conversion rate as it proves in the Tab, most catalysts used in fixed bed have conversion no more than 20%.

*2.1.7.2 heterogeneous tank reactor (slurry bed)*

Tank reactor or tank mixer is widely used in laboratory or pilot factory, and it is always used in heterogeneous reaction, especially liquid phase reaction. when catalysts are used, they can be either packed in the small pocket and placed in the tank or suspended in the liquid phase, the latter is also called slurry bed reactor.

When studying liquid phase $CO_2$ hydrogenation, tank reactor is always used. Yan et al [131] studied Fe–Cu catalyst for CO2 hydrogenation in slurry reactor, and analyzed different catalysts composition, the results showed that Fe–Cu–Al–K catalysts has the best performance with 17.9% of $CO_2$ conversion rate, and they also found that for Fe–Cu catalyst, the product is various, which means a poor selectivity. Zhang et al [132] used Cu/ZnO/$Al_2O_3$/$ZrO_2$ catalyst to produce methanol from $CO_2$, total $CO_2$ conversion

was 25.9% and methanol selectivity was 61.5%, the rest were CO. Shaharun et al [133] used the same catalyst as Zhang did, and they studied effect of different Cu/Zn ratio, the results indicated that higher Cu/Zn ratio brings higher $CO_2$ conversion rate but poor in methanol selectivity and vice versa. When Cu/Zn ratio was 5, the conversion rate was 15.81% and methanol selectivity was 40%, while Cu/Zn ratio was 0.5, the conversion was 6.3% but methanol selectivity was 93%.

The studies on slurry bed always give a higher $CO_2$ conversion rate and milder reaction conditions compared with fixed bed reactor, the reason can be included as larger catalyst contacting surface and uniform reactant distribution. The major challenge of tank reactor (slurry reactor) is separation of end products, therefore, a separation unit like distillation column or extraction tank is always needed.

*2.1.7.3 Fluidized bed*

Fluidized bed is very suitable for industrial use because its large capacity and intensive fluid dynamics. When used in catalytic reaction, fluidized bed has uniform temperature distribution and large contacting area. But its structure is complex, and capital cost is relatively high, which somehow limits its application in laboratory.

Kim et al [134] studied characteristics of $CO_2$ hydrogenation in multi–section fluidized bed with Fe–Cu–K–Al catalyst, and different operating conditions are optimized. The results indicated that best $CO_2$ conversion is 46% when column temperature is 300℃, and pressure is 1 MPa. And product ranges from CO to C5, the selectivity is relatively poor. For now, there are no specific researches related to $CO_2$ hydrogenation to methanol in fluidized bed.

*2.1.7.4 Membrane reactors*

Membrane reactor is first used in waste water treatment, it combines both reaction and separation in the same equipment, when used in $CO_2$ hydrogenation, it can remove product instantly which is good for reaction.

Gallucci [135] used zeolite membrane reactor for $CO_2$ hydrogenation to methanol and compared membrane reactor with conventional reactor, the $Cu/ZnO/Al_2O_3$ catalyst was packed inside reactor. The results showed that one–way conversion of $CO_2$ was 11.6%, and methanol selectivity was 75%. Chen et al [136] designed silicone rubber/ceramic composite membrane reactor, and $Cu/ZnO/Al_2O_3$ catalyst was used. the study optimized membrane reactor and operating conditions, and mathematical model was built, and optimal conversion was 6.4%.

*2.1.7.5 Chapter conclusion*

Currently, most researches on $CO_2$ hydrogenation focus on catalysts and its mechanism, there are very few specific articles related to reactors and process conditions, it is still worthwhile when considering pilot factory or even industrial applications in the future.

Generously speaking, fixed bed reactor has the lowest conversion rate compared with other types, and the strictest reaction conditions. For other reactors, the temperature and pressure are the same, the reaction temperature is around 170–250 ℃, and operating pressure is around 10–30 bar. The conversion rate differs due to different catalysts and end products. Besides membrane reactor, when improving conversion rate, the methanol selectivity decreases in most reactors. Each reactor conditions and conversion rate are listed in Table 4.

*Table 4 Reactor conditions for CO2 hydrogenation*

| Author | Catalyst | Target product | Temperature (℃) | Pressure (bar) | Space velocity | Conversion (%) | Ref |
|---|---|---|---|---|---|---|---|
| **Fixed bed reactor** | | | | | | | |
| Willauer | Fe | C2–C5 | 300 | 18.2 | 0.000093 L/s–g | 60 | [127] |
| Gesmanee | Cu–Zn | MeOH | 270 | 40 | 500 $h^{-1}$ | 0.192 | [128] |
| Guo | CuO–ZnO–$ZrO_2$ | MeOH | 150 | 30 | – | 12 | [129] |
| Bahruji | Pb/ZnO | MeOH | 250 | 20 | 30 mL/min | 10.7 | [130] |
| **Heterogeneous tank reactor (slurry bed)** | | | | | | | |
| Yan | Fe–Cu | C1–C5 | 250 | 5 | – | 17.9 | [131] |
| Zhang | Cu/ZnO/$Al_2O_3$/$ZrO_2$ | MeOH | 220 | 30 | 2000 mL/ g/h | 25.9 | [132] |
| Shaharun | Cu/ZnO/$Al_2O_3$/$ZrO_2$ | MeOH | 170 | 30 | 20 mL/min | various | [133] |
| **Fluidized bed reactor** | | | | | | | |
| Kim | Fe–Cu–K–Al | C1–C5 | 250–350 | 0.5–1.5 | 0.07–0.2 | 46 | [134] |
| **Membrane reactor** | | | | | | | |
| Gallucci | Cu/ZnO/$Al_2O_3$ | MeOH | 206 | 20 | $6*10^3$ $h^{-1}$ | 11.6 | [135] |
| Chen | Cu/ZnO/$Al_2O_3$/$ZrO_2$ | MeOH | 220–230 | 16 | – | 6.4 | [136] |
| Shaharun | Cu/ZnO/$Al_2O_3$/$ZrO_2$ | MeOH | 170 | 30 | 20 mL/min | various | [137] |

## 2.2 Reactive distillation

Reaction distillation (RD) technology, one of the successful concepts of process intensification in chemical industry, combines both chemical reaction and distillation in the same equipment. The interaction between the reaction and distillation processes improves both sides, distillation is used to improve reactions and break the limitation

of chemical equilibrium, improve reaction conversion and product selectivity, improve energy utilization efficiency, save the process energy consumption, and decrease the size of equipment. Reactions are used to improve distillation separation on the other hand with comprehensive utilization of reaction heat, to facilitate complete separation of azeotropic mixtures or obtain product with high purity requirement. As known, almost all chemical industrial systems contain the two important unit operations, reaction and separation. Almost 70% of separation processes use distillation technology. As the reaction distillation technology has many advantages, it has a wide application prospect in chemical industry and has attracted wide attention in the academic and industrial circles in recent years.

Despite the RD advantages and wide application field the technology also has certain limitations and difficulties, such as high coupling between reaction and separation with strong nonlinearity. This makes process simulation and design difficult. The relative volatility of the system must meet certain requirements. Babcock et al.[138] classified the reaction system into three classes according to the relative volatilities of reactants and products, in the class I, volatilities of all reactants are between that of products, in this class, reactive distillation is applicable. In class II, volatilities of all products are greater than (or less than) that of the reactants, and heterogeneous catalytic rectification is suitable. When volatilities of all product are between that of reactants, which belongs to class III and Ⅳ, the reactive distillation technology is not suitable. For gas liquid reactive system, it is possible that reactants and products are coagulation components, which means their relative volatilities are the same, but coagulation components have very small solubilities in the liquid phase, as long as the relative volatilities of all condensable reactants and products meet the requirements of the rule of Babcock, the reactive distillation can be used. The reactive distillation column may be larger if the reaction part needs a certain amount of liquid holdup to obtain enough residence time. The optimized operation of the reaction and separation conditions is difficult. In the system, there may be reactive azeotropes and nonreactive azeotropes, which may not have existed before. The coupling of reaction and

rectification makes the system more complex, which brings inconvenience to the process design and control. At present, the above problems limit the application of reactive distillation technology in chemical industry. To this end, this chapter about the RD technology in recent years was reviewed from basic research to practical applications of some representative work. This part also puts forward and systematically summarizes the RD process development methods (Figure 10), including feasibility analysis, preliminary concept design, process simulation and optimization, and key equipment design.

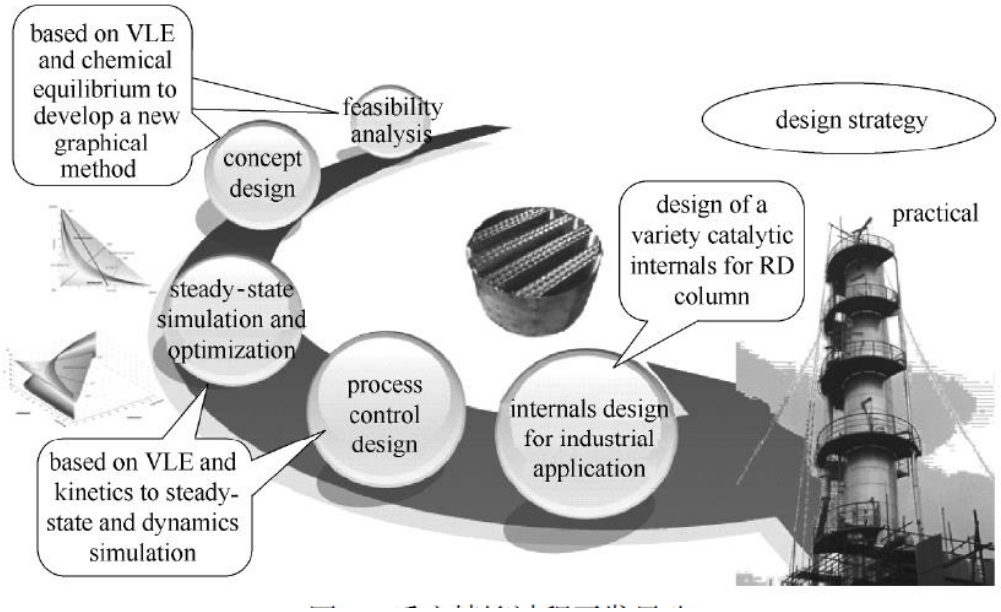


*Figure 10 The process of reactive distillation feasibility study[139]*

### *2.2.1 Feasibility analysis*

Although the potential application of reactive distillation technique is very extensive, not all chemical reactions and separation processes are suitable for coupling by reaction distillation. Therefore, the RD process development must first carry a feasibility analysis before any further studies. Its purpose is to study whether the component of product can meet the production requirements. If so, then the method is feasible. The feasibility analysis methods include residual curve/bifurcation analysis, static analysis, pinch design method, feasible regions, driving force and cascade reactions method [137][140][141], Different feasibility methods and their properties are listed in Table 5.

*Table 5 Feasibility study methods*

| Method | Input | Assumption | Output |
|---|---|---|---|
| RCM | Phase equilibrium; chemical reaction equilibrium; chemical reaction kinetics; feed composition; product composition | Phase equilibrium; negligible heat effect; equilibrium or kinetically controlled regime | Feasibility of RD process; process superstructure; feed stage; number and location of (non–) reactive azeotrope |
| SA | Phase equilibrium; chemical reaction equilibrium; reaction stoichiometry; feed composition; reaction operating condition | Phase equilibrium; negligible heat effect; equilibrium–controlled regime; steady–state operation; component no more than 3; constant molar flow; infinite vapor and liquid flows; one reversible reaction | Feasibility of RD process; feasible region; process superstructure; multi–steady state; number and location of (non–) reactive stage |
| Pinch–point | Phase equilibrium; chemical reaction equilibrium; chemical reaction kinetics; feed composition; product composition | Equilibrium or kinetically controlled regime; film theory; constant mess transfer coefficient | Feasibility of RD process; process superstructure; operation condition; feed stage; number of (non–) reactive stage; location of (non–) reactive azeotrope |
| AR | Phase equilibrium; chemical reaction equilibrium; chemical reaction kinetics; feed composition; product composition | Phase equilibrium; kinetically controlled regime | Feasibility of RD process; process superstructure; multi–steady state |

Table 6: (continued)

| | | | |
|---|---|---|---|
| Driving force | Phase equilibrium; chemical reaction equilibrium; chemical reaction kinetics; feed composition; product composition | Phase equilibrium; equivalent binary element; single feed; equilibrium–controlled regime | Feasibility of RD process; process superstructure; feed state; stage number; minimum reflux ratio |
| Reactive cascade | Phase equilibrium; chemical reaction equilibrium; chemical reaction kinetics; feed composition; product composition | Phase equilibrium; negligible heat effect; equilibrium or kinetically controlled regime; steady–state operation; constant liquid holdup | Feasibility of RD process; process superstructure |

*2.2.1.1 Residual curve/bifurcation analysis (RCM)*

For simple distillation process, the liquid phase composition changes over time in a triangle phase diagram are called the residual curve. The residual curve corresponds to different distillation time of all components. The arrows point to the direction of time, but also to the direction of temperature increase. The graph (RCM) can be understood as representing the real material balance remaining and can be used to analyze the existing system of non–ideal mixtures and azeotrope. It can also be used to predict total reflux conditions of the liquid phase trajectory. If the same residual curve can connect the top and bottom products, and the products exist in all nodes, the reaction distillation process is feasible. The residual curve technique is a powerful tool for process development and preliminary design of traditional multi–component separation processes.

Venimadhavan et al. [142] studied the effects of reaction kinetics on RCM and revealed the limitations of the equilibrium analysis. Then they expanded the RCM method to any stoichiometric reactions, obtained all available starting points by bifurcation analysis and from solution of the boiling point temperature of the mixture. According to the

solution, the boiling point temperature of the mixture is D which relates to the Damköhler numbers, dimensionless numbers are used in chemical engineering to relate the chemical reaction timescale (reaction rate) to the transport phenomena rate occurring in a system. The branches were calculated using the pseu–doarc–length continuation method [143]. Since then, Ung et al. extended this method to multi–balance reactions. The method uses transformed coordinates to express phase equilibrium and chemical equilibrium. These can be further used to judge the existence of azeotropes and nonreaction azeotropes and to limit the reflux ratio of the distillation [144]. On this basis, they further studied the influence of the feed composition and presence of inert component. Also, they discussed the feasible process scheme [145]. Chiplunkar et al. [146] explored the feasibility of dynamic control systems for reaction distillation through experiments and bifurcation analysis. Mixed coordinates (i.e., composition of the mole fraction and conversion components) were used in the RCM. Figure 11 shows the remaining curves of the MTBE synthesis system [144], where n–butane is an inert component, and using conversion composition as variables can reduce the dimension of RCM.

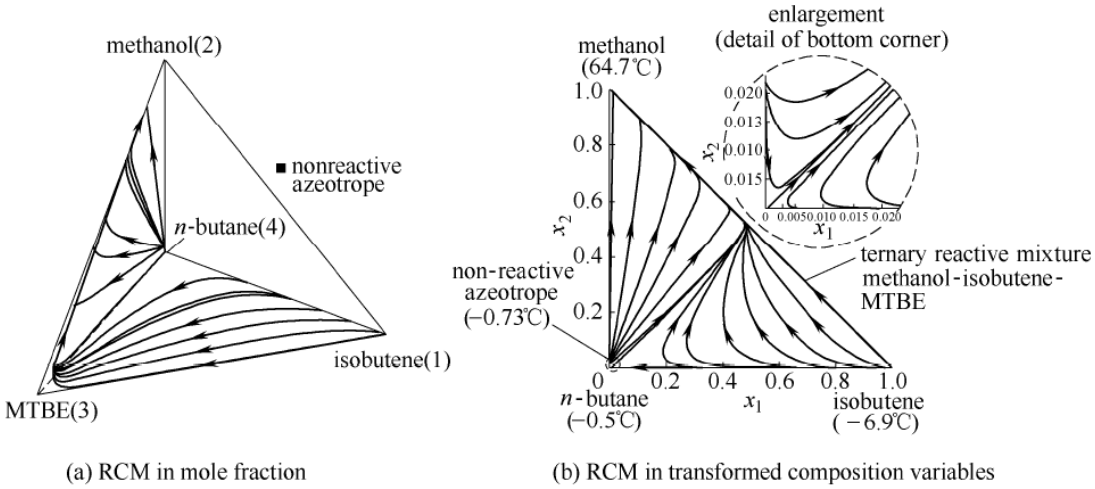


*Figure 11 Residue curve map of MTBE synthesis system*

*2.2.1.2 Static analysis*

In static analysis [147][148][149][150], the RD process is decomposed into two independent units, i.e. the reaction and distillation units, assuming that after a certain

amount of reaction, the feed containing a composition of $X^*$ is set as the initial mixture going into the distillation unit (Figure 12 (a)). Figure 12(b) is a typical phase diagram of the static analysis, consisting of several important curves, including the distillation line, the chemical equilibrium manifold (CEM), the line of mass balance (LMB), and the line of chemical interaction (LCI). The rectifying line is used to determine the extreme boiling points. The CEM is the dividing line between the positive and the negative reactions. The LCI connects the initial feed composition and the assuming initial composition, and each point on the line corresponds to a different degree of reaction. Then the limiting path is determined, which restricts the trajectory of the steady–state (LLS). The limited steady–state is the steady–state with maximum conversion and the feasible condition. Feasible condition is met on the rail line that satisfies mass balances when part of the rail line is in the positive reaction zone.

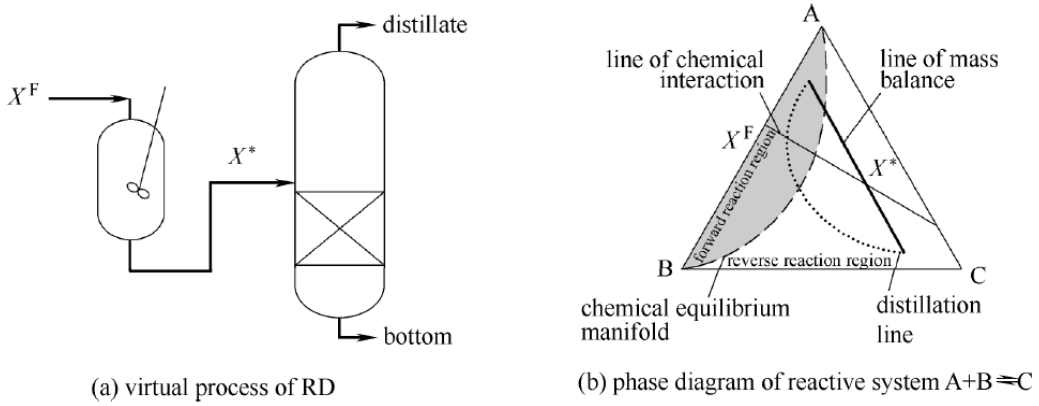


(a) virtual process of RD

(b) phase diagram of reactive system A+B⇌C

*Figure 12 Statics analysis method*

The static analysis method is based on the following assumptions: (1) separation efficiency is infinite, and the traditional distillation curve can be used for analysis. (2) gas–liquid flow is infinitely large; therefore, changes of plate composition caused by the reaction can be ignored; (3) only one reversible equilibrium reaction is considered; (4) theoretical plates are assumed in steady–state operation. The static analysis method requires known feed composition, phase equilibrium and reaction equilibrium model parameters, stoichiometric numbers and operating conditions, such as conversion, feasible region, length of the reaction zone and its location, and other information. According to the obtained results, the feed composition is divided into several sub–

regions, each sub–region has different products, and each sub–region has the same product composition. Of course, the inert components in the feed will also affect the feed sub–region [150].

*2.2.1.3 Pinch design method*

The design methods based on the pinch point include the fixed point, the boundary value design and the feed angle methods [140]. Under total reflux, composition of some regions remains constant. Those regions usually appear as pure component and azeotropic composition and their location changes with the change of reflux ratio, ratio of external reboiler and Damköhler number. The points represent chemical and physical balance, known as the "fixed point" [151]. The fixed point can be a stable node, unstable node or saddle point. The judgement can be made by the eigenvalue of the point's Jacobian matrix. Figure 13 [151] shows the design process by the fixed point method for a reaction $2B \rightleftharpoons A+C$. First of all, the fixed point is set as a function of the external reboiling ratio and tracking all the points that meet material and energy balances, the arc length of continuation method is used in the space of composition–reaction–reboiling ratio [branch 1, 2, 3 in Figure 13 (a)]. Once the reboiling ratio is determined, the position of the fixed points in the rectification and stripping sections are determined. The reboiler is used to calculate the distillation section after which the the location of feed plate is determined [FTR in Figure 13 (b)]. The feeding plate is the plate which can meet the requirements of the top product and the overall material balance. The feed plate location is parameterized from 0 to 1 to ensure that the distillation section and the rectifying section intersect. Otherwise the solution is not feasible. Huss et al. [152][153] carried out the bifurcation analysis of fixed point with CAD and studied the feasibility of methyl acetate reaction distillation system.

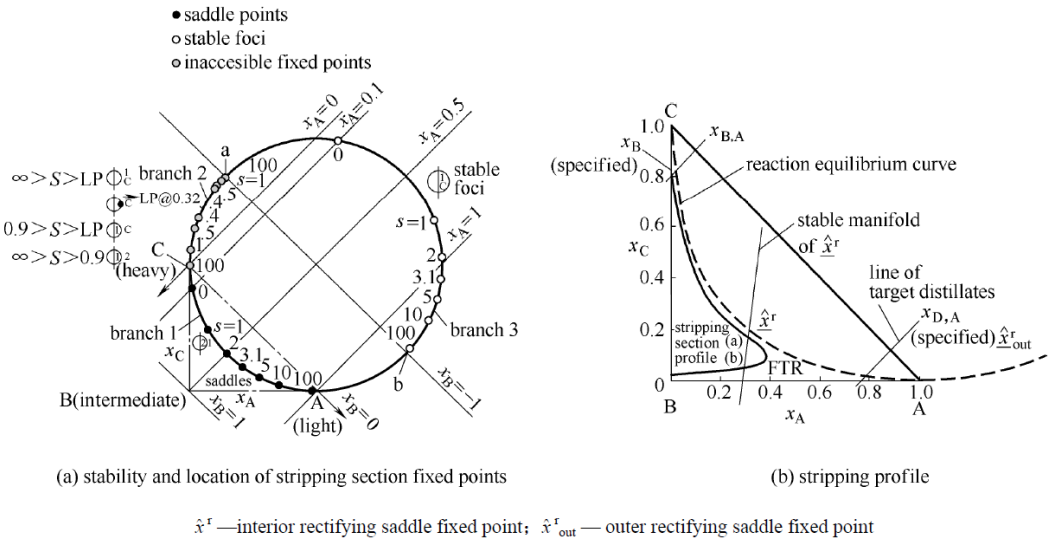


(a) stability and location of stripping section fixed points (b) stripping profile

$\hat{x}^r$ —interior rectifying saddle fixed point; $\hat{x}^r_{out}$ — outer rectifying saddle fixed point

*Figure 13 Fixed point method for reactive system 2B⇌A+C*

### *2.2.1.4 Attainable region method*

The attainable region method (AR) was initially applied to study reactor network synthesis and was then successfully expanded to reaction, mixing and separation. This method defines a reaction–separation composition vector based on thermodynamic activity. The composition vector has the same properties as the reaction vector and it can be built through the existing reaction–mixing process. The AR region is determined by the reaction composition vector that points to the inside of the AR boundary, is either tangent or zero. The region outside AR does not have a reaction vector going through the AR. Gadewar [154][155] used AR and bifurcation analysis to analyze the feasibility of reactive distillation. A two–phase countercurrent cascade model was established to replace the reactive distillation column of rectifying and stripping section. The results showed that gas–liquid CSTR cascade can significantly expand the accessible region of the single–phase reactor (Figure 14 [155]). Separation of components can broaden the accessible region of reaction and obtain higher yield and product purity.

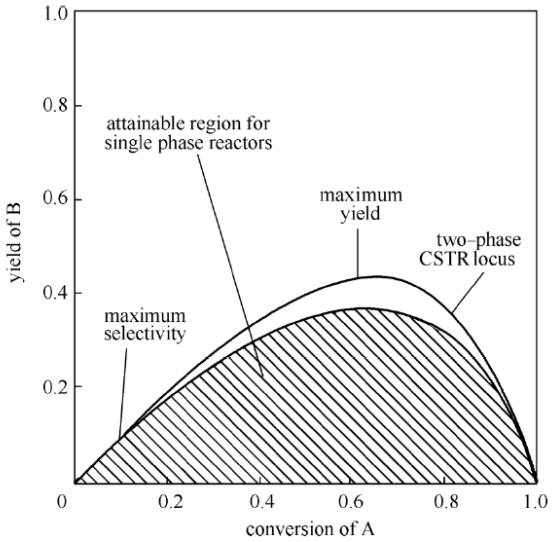


*Figure 14 Attainable region of reactive system A→B→C*

### *2.1.5 Driving force method*

Jantharasuk et al. [156] developed a new method of design and analysis of reactive distillation systems based on the combination of elemental method and driving force, namely the driving force method, as shown in Figure 15. Based on the element method, an element is used to represent the components in the reactive distillation system. A pair of key elements is selected to establish an equivalent binary key element system. Then a reaction driving force diagram [Figure 15 (a)] is constructed. Through calculations using reactions and bubble point algorithm, the equilibrium curve of the reaction is calculated. The driving force at the top and bottom of the column can then be obtained [Figure 15 (b)] to determine optimal design structure. This method can be also applied to multi–reaction systems.

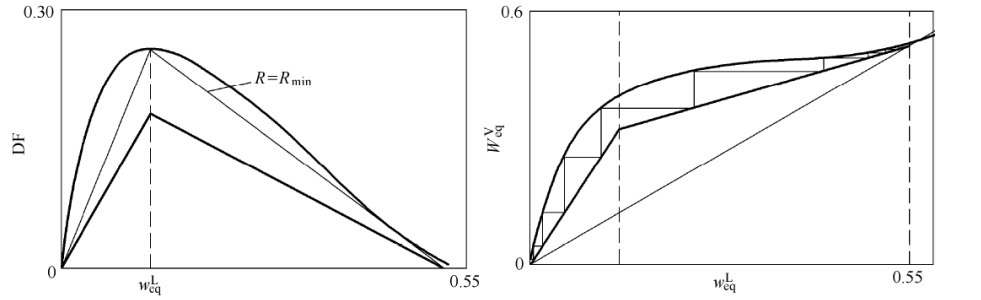


(a) equivalent binary element driving force diagram (b) equivalent binary element reactive-equilibrium diagram

DF—equivalent binary driving force; $w^L_{eq}$—equilibrium element fraction in vapor phase; $w^V_{eq}$—equilibrium element fraction in vapor phase

*Figure 15 Driving force method for MeOAc synthesis system*

### *2.2.1.6 Reaction cascade method*

Chadda applied the concept of cascade reaction to judge the possible reactive distillation system, the two phase CSTR and flash cascade are used to analyze fixed point [Figure 16 (a)] to predict a possible separation at given feed conditions by flash calculation and lever rule. [157]. They then extended the reaction cascade to the upstream cascade [Figure 16 (b)] and applied to the double feed condition [158]. Gadewar[154] used two phase CSTR cross–flow cascade model [Figure 16 (c)], the heavy component of reacting liquid from enter the first grade, and the light component of gas phase enter the system step–by–step, this method can greatly simplify the complexity of prediction for composition at middle section of double feed column.

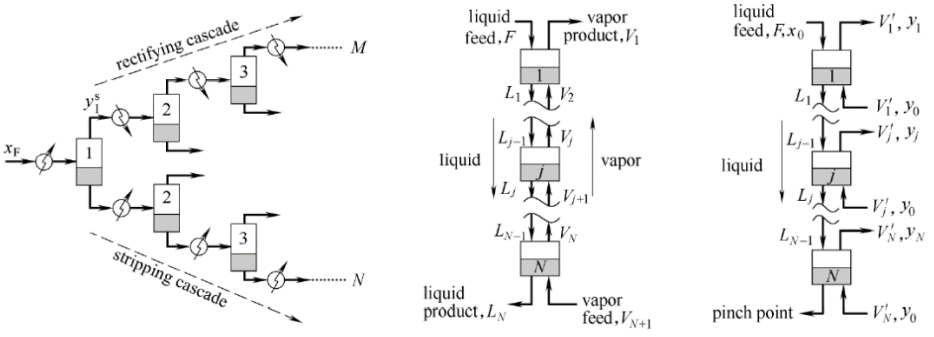


(a) concurrent cascade (b) countercurren cascade (c) crosscurrent cascade

*Figure 16 Reactive cascade*

### 2.2.2 Conceptual design

Due to the interaction of multi–component mass transfer, heat transfer, flow and chemical reaction, the design of reactive distillation is very difficult. It needs to determine the design parameters include: separation and reaction sequence and feeding location, operating conditions, including pressure, distillate/feed ratio, etc.), suitable catalysts, column internals (including catalytic dose and liquid holdup), and others. A preliminary conceptual design can provide reasonable initial value and basic design information for the subsequent process simulations. At present, the conceptual design of reactive distillation is divided into three categories: graphical method, evolution/heuristic method and method based on optimization. Before 2000, there were a lot of studies on the graphical method. After that, scholars improved all kinds of graphical methods, and began to study the evolution/heuristics and optimization methods.

#### *2.2.2.1 Graphical method*

The graphical method plays an important role in rapid feasibility analysis of reactive distillation process and in screening of different process structures. The method is based on the characteristics of the reaction and distillation process, combined with constraint equations and experimental data to generate the nomograph. According to the graphical information provided, reactive distillation is designed [140], which can simplify the complicated calculation work, provide initial value for mathematical modeling, and analyze complex problems, which are inconvenient for mathematical expressions [159]. Graphical method can reduce the dimensions of the chart through the transformation of variables, or replacing molecular group by substitute elements, application of the above two methods can make effectively simplified diagram, more intuitive. The application of graphical method is usually limited by the group and reaction number, thermodynamics and reaction equilibrium are assumed. Besides, Graphical method does not include column internals, which means it is not suitable for economic analysis.

*2.2.2.2 Evolution/heuristic method*

Evolutionary/heuristics is evolved from traditional distillation, it is based on empirical rules, overcame the limitation of graphic method, considering the influence of column internals, which can combine the economic analysis, and be applied to many components and multiple reaction systems. However, because there is no specific empirical rule to ensure the optimal integration of chemical reaction and distillation, this method cannot get the optimal design of the column. Evolution/heuristics is a late–stage design algorithm that has been successfully applied to the response rectification of equilibrium constraints. Shah, etc. [160] designed the system framework based on a series of experience rules for feasibility analysis of reactive distillation process and a preliminary process of conceptual design and made technical evaluation of possible application process.

*2.2.2.3 Methods based on optimization*

This method overcomes the shortcomings of the graphic method and the evolution/heuristic method and can find the global optimal or local optimal [161]. However, this method requires a lot of computation, which relies on calculating program and precise solver to solve complex mathematical problems. At present, the main optimization design methods include mixed integer nonlinear programming (MINLP), orthogonal collocation on finite element (OCFE) and mixed integer dynamic optimization (MIDO), etc. There are two methods for optimization problems: deterministic algorithm and stochastic algorithm [163]. The deterministic algorithm includes DICOPT++, generalized Bender decomposition algorithm, external approximation/ relaxation/enhancement penalty algorithm, external approximation algorithm by logics, etc. Random algorithms include simulated annealing, evolutionary algorithm, particle swarm optimization and differential evolution, etc. [164]

**Mixed integer nonlinear programming (MINLP)** RD problem usually consists of two basic aspects, namely annual operating cost and annual equipment investment. Keller, etc. [163] used the MINLP evolutionary algorithm adopted for the multiple main reactions and the reactive distillation system, took DMC with methyl ester transfer system as an example to carry on the design, chose selectivity of EMC and DEC to establish objective function and penalty function and calculated multi–objective optimization. Niesbach etc. [165] applied the MINLP evolutionary algorithm to design industrial scale of n–butyl acrylate production process, on the basis of considering RD column amplification effect, an optimal design was done aiming at production per ton product (CPT) as the objective function. Rugerio etc. [166] used the MINLP improved differential evolution algorithm to study multicomponent and multi–reactions of catalytic RD column design, and considered the influence of column internals, this method can be divided into three steps, first to split RD to chemical reactor and nonreaction distillation column, analyzed theoretical plate number and volume of catalyst; Then the equilibrium level model is established to calculate the column diameter and operating conditions. Finally, a strict non–equilibrium level model is established to design the column parameters.

**Orthogonal collocation on finite element (OCFE)** because of long calculation time and complexity of MINLP, it is very difficult to design a column with many plates or design multi–distillation units at the same time. Moreover, if the initial value is out of the feasible region, it can lead to convergence difficulties. Therefore, Seferlis et al. [167] proposed the design and optimization of the OCFE technology of RD column, which transformed the discrete column number variable into a continuous variable, and the composition and temperature as a function of position.

**mixed–integer dynamic optimization (MIDO)** is a kind of design and control method at the same time, which can include the discrete variables (number of process structure, control circuit, etc.) and continuous variables (design/operation parameters and the parameters of the controller to adjust, etc.) into an optimization framework

[168]. Fernholz [169] studied dynamic optimization problems of acetic acid methyl ester semi–batch RD column, adopted the intermittent operation time and yield as function, solved optimization problem into a nonlinear programming (NLP) through the gOPT tool in gPROMS.

*2.2.2.4 Other design methods*

In 1990~1992, BP chemical, Hoechst, BASF and other companies carried out "reactive distillation" three–year plan, set up BRITE EURAM team to carry out a series of reactive distillation feasibility analysis and researches of concept design [170][171][172].

(1) The SYNTHESISER prediction tool was developed to determine whether the reactive distillation process was feasible, the separation effect and column design information can be preliminarily given. The tool can be used for multiple reaction systems, and input includes stoichiometric number of each reaction, reaction type, and vapor–liquid equilibrium data. Moreover, the user can define the minimum concentration of product streams. The following steps are included: establishment of elimination standards; To find binary and ternary azeotropes, a simple distillation method was used to study the reactive distillation. The rectifying zone and reaction zone of the column were determined by the reactive distillation line and the nonreactive distillation line. Determine feed stage, the plate number in reaction section and rectification section.

(2) the DESIGNER process simulator was developed to design and study the complex behavior in the reactive distillation column. DESIGNER uses a rate–based approach that includes several interrelated major modules, including databases, solvers, initializers, and model libraries. Model library includes: fluid mechanics model applicable to different column internals and flow state; three types of reaction models, namely the effective kinetic model, homogeneous catalytic reaction model (including liquid membrane reaction), and non–homogeneous catalytic reaction model based on

the concept of catalyst effective factor; Different column model, including the mixed liquid and gas phase model, liquid phase CSTR and gas phase PFR model, mixing pool model, eddy diffusion model based on the linear eddy diffusion equation of desorption agent and numerical solution based on eddy diffusion equation is strictly eddy diffusion model. The solution is a combination of relaxation method and Newton method.

(3) the integrated tool of PREDICTOR synthesis and design was developed, and the results of SYNTHESISER could be improved as the input of DESIGNER.

Overall, both graphic method and evolutionary/heuristics and the method based on optimization in the reactive distillation concept design are increasingly obvious, but do not form a comprehensive related design method, system, effective theory system, need to be studied in–depth.

### *2.2.3 Process design and optimization*

After a preliminary concept design, a reasonable mathematical model is usually established and simulated to complete the detailed design and optimization of the reactive distillation process, the process of technological design, engineering amplification, the practical production operation, etc all have important guiding significance. The reactive distillation process model includes steady–state model and dynamic model. The steady–state model assumes that the parameters of the process do not change with time, which is the basis of the design and optimization of the reactive distillation system. The dynamic model cancels the assumption that the liquid volume and energy of the tray are constant, and the dynamic change of material and energy is studied by using its differential equation of time [173].

#### *2.2.3.1 Steady state model and process design*

The steady–state mathematical model of reactive distillation includes the equilibrium model, non–equilibrium model, non–equilibrium pool model, differential model and

artificial neural network model [174]. The mathematical model is established to describe the thermodynamics, kinetics, mass transfer, fluid mechanics and chemical reaction in the reactive distillation process. According to the reaction rate, it can be divided into three categories, namely, extremely low rate very slow (no reaction), medium rate (reaction speed control), fast reaction rate (chemical equilibrium), and whether kinetics and reaction is considered are based on reaction rate.

**Equilibrium model** equilibrium model assumes that the whole column can reach equilibrium, each stage is assumed as CSTR, the stream can reach gas–liquid phase equilibrium when leaving the stage, reaction can occur either in liquid phase or gas phase. The equilibrium model is divided into two types [175], namely, the equilibrium model of chemical equilibrium (EQ–EQ) and the equilibrium level model (EQ–Kin) considering the reaction kinetics. In general, the description of the system is quite different from the real situation, but because of its relatively simple application and solution, it can be used in the initial stage of the design of reactive distillation process [176][177].

In the study of the solution of equilibrium model, Xu et al. [178] proposed the block tridiagonal matrix technique, which was used to solve the reactive distillation mathematical model with a series of reactions. Kuang et al. [179] applied the block tridiagonal matrix technology to the catalytic distillation process of methyl acetate hydrolysis. Wu et al. [180] proposed the two–diagonal matrix method, and the simulation results showed that its convergence and stability were better than the tridiagonal matrix method. Qi et al. [181], introduced the concept of transformation variable, and the modified newton–raphson method was used to calculate the reactive distillation process of various equilibrium reactions. and Yuan et al. [182] used relaxation method to get the initial value, with Newton Raphson method as the main calculation, the METB and ETBE reactive distillation system were used to solve the equilibrium model, the result showed that the calculation can be applied to nonlinear model. Lei et al. [183] established the equilibrium model for two different catalytic

distillation equipment for the synthesis of isopropyl benzene, and solved it with the new relaxation method, and the convergence rate was faster.

**Non–equilibrium model** non–equilibrium model assumes that equilibrium only reaches at phase interface, adopts double membrane theory to describe the behavior of the gas–liquid interface, considering the actual multicomponent mass transfer, heat transfer and chemical reaction rate. The non–equilibrium model includes the non–equilibrium model with Maxwell's equation and the non–equilibrium model with effective diffusion coefficient, which is less complex than the former.

Some literature discusses the models of different complexity [175][184][185][186][187], including the equilibrium/nonequilibrium model, effective diffusion coefficient / Maxwell–Stefan equations, no thermal effect/ thermal effect, the different reaction kinetics (homogeneous: liquid membrane and liquid phase reaction; Non–homogeneous: internal diffusion resistance and external diffusion resistance), constant molar flow hypothesis/non–constant molar flow, and whether to consider hydrodynamic effects (non–ideal flow). Of course, the more complex the model is set, the more difficult it is to apply and solve the problem, and to simplify the model without affecting the precision, making it easier to apply to industrial design. Some scholars have verified the non–equilibrium model of the reactive distillation system established by the pilot experiment [188][189][190][191][192] and determined the appropriate model. Also, some scholars studied the performance of reaction rectifying column packing through the experiment and simulation [193][194][195][196][197], considering the fluid mechanics performance and non–ideal flow, and applied to get the relational non–equilibrium model, in order to obtain more accurate simulation results.

**Nonequilibrium pool model** Normal nonequilibrium model usually cannot describe the gas liquid distribution in the packed column. Nonequilibrium pool model overcomes the defect of the model, which divide each stage into a series of tiny pools to describe the heat transfer, mass transfer and chemical reaction, such as using

Maxwell–Stefan equations to describe the interphase mass transfer, considering local concentration and the local temperature effect on the local reaction rate, and the influence of the flow pattern and uneven distribution is studied by reasonable way of connection, the influence of backmixing also can be implemented by setting the appropriate number of tiny pools [198].

**Differential model** Zhang, et al. [199] proposed a differential model mainly used in heterogeneous reactive distillation, setting any micro unit in column to establish the mass balance, and differential solution is calculated under given boundary conditions, if the differential equations of the boundary value is unknown, it can be still obtained solution by combining the shooting method and Newton Raphson method under the mass balance of whole column constraint. [200] The development of the above differential models is applied to both reversible equilibrium reaction and non–homogeneous catalytic distillation process with non–equilibrium reaction.

**Artificial neural network (ANN)** artificial neural network (ANN) sets simple nonlinear neuron as the processing unit, and the connection of each other constitutes a large–scale distributed parallel nonlinear dynamic system. The model does not need to consider the specific process of reactive distillation, which also does not rely on accurate mathematical model. All variables in chemical process are used as input to analyze the potential patterns and generate a high–dimensional nonlinear mapping from input to output. Zhao et al. [201] proposed a batch processing – non–monotonic linear search of ANN improved BP algorithm and applied to the simulation of catalytic distillation column of acetic acid methyl ester. Hu et al. [202] used ANN to predict the starting process of catalytic distillation tower. The results showed that ANN had high precision and significance for further optimization calculation.

*2.2.3.2 Dynamic model and process control*

Dynamic model is the key factor for the response to disturbance, design and optimization of start–up, appropriate control strategy, the analysis process of steady state and design intermittent and half batch process, etc.

Control method and structure the current process control have already used the more advanced model prediction control (MPC) than traditional proportional integral differential (PID) control, from the open loop control to the closed loop control, from linear to nonlinear control [203]. Different control structures can be obtained by selecting different control variables and operating variables.

(1) proportional – integral control method.

Proportional integral control (PID) is the most widely used industrial control technology, the circuit design is simple, flexible operation, also can obtain good control effect for nonlinear process, this method needs to select the appropriate control variables and operating variables. Sneesby et al. [204], proposed traditional linear PI controller for ETBE system, the bottom product is controlled by heat load at bottom reboiler and conversion rate is controlled by reflux ratio, comparing with only controlling bottom products, the sensitivity and resistance to disturbance are better. Al–Arfaj [205] developed six kinds of linear PI control structure for ideal two product reactive distillation system, and the open loop stability were studied, the control structure is: (1) controlling variables are the column top, distillated purity(CS1), operating variables are reflux ratio and reboiler heat load; (2) controlling variables are the impurities (CS2) at column top and bottom, and the operating variables are the same as CS1. (3) Single product concentration control (CS3), selecting one product purity to control; (4) The control variable is the concentration of reactants at both ends of the reaction section (CS4), and the operation variables are the feed flow of two reactants. (5) The control variable is the temperature of the sensitive plate of the distillation section (CS5), and the operating variable is the heat load of reboiler. (6)

The control variable is the purity of the column top product (CS6), and the operating variable is the feeding flow of the reactants with the upper end feed. Except them, a new kind of control structure was also studied (CS7), namely, two point of temperature control, control variables are two sensitive plate temperature, operating variables are two reactants feed flow rate respectively.

The dynamic complexity of reactive distillation process makes traditional PI control fail to provide satisfactory control performance, and modern control technology requires more advanced control methods and process models. Fernbolz et al. [206] designed a kind of linear MIMO PI controller, the control variables are two sensitive plate temperature, heat load of the reboiler and reflux ratio are operating variables, and controller is tested in the nonlinear process model for open loop and closed loop respectively, the results showed that it can improve the control performance. Gruner et al. [207] presented a nonlinear state feedback controller, combining the gradual accurate input output linearization and robust observer, compared with the linear MIMO PI controller, this controller has stronger resistance to disturbance, better performance in set–point tracking and unknown input lag. Vora et al. [208] developed a nonlinear input/output linear state feedback controller, the control variables were product purity and conversion rate, operating variables were reflux ratio and reboiler heat load, the ethyl acetate reactive distillation system was used for open loop and closed loop test respectively, the results showed that its performance is superior to the traditional PI controller. Chen et al. [209] applied a three temperature points multiloop PID control and applied in closed loop control of n–butyl acetate reactive distillation column and studied the structure of three kinds of temperature control, and the optimal control structure were reactive distillation column reboiler heat load, the ratio of n–butyl alcohol and total feed, stripping column reboiler heat load control three sensitive plate temperature respectively.

(2) Model predictive control method.

Model predictive control (MPC) is an optimal control algorithm based on prediction model, rolling optimization and feedback correction. Khaledi et al. [210] proposed a 2*2 unrestricted linear MPC control strategy, i.e. the product purity and conversion rate. Two control variables were reaction temperature and sensitive plate temperature; Operating variables were reflux flow rate and reboiler heat load. Both open–loop and closed–loop control for ETBE reactive distillation system were studied respectively. Results showed that comparing with the simple single point of control structure, the 2*2 PI control structure was better to solve the problem of interaction process and it was very effective and stable for set–point tracking and disturbance resistance. Seban et al. [211][216] put forward a kind of linear MPC based on GOBF – ARMA model, the control variables were top and bottom product concentration, operating variables were reboilering heat load and reflux flow rate and used open loop control for ideal reactive distillation system, the results showed that the scheme is a good way to track the set point and obtained conventional control, improved the ability of MPC prediction. Kawathekar et al. [212] presented a nonlinear model predictive control scheme (NLMPC), can be applied to the highly nonlinear reactive distillation system, the scheme used close loop control in methyl acetate reactive distillation system through regulating plate temperature to predict impurity concentration in the top and bottom products, operating variables were reboilering heat load and reflux ratio. Compared with traditional PI controller, the results showed that the performance of NLMPC was 2 ~ 3 times better than of PI control performance. Huang et al. [213] proposed a 2*2 nonlinear multivariate model predictive control, which controlled variables to be the top product concentration and sensitive plate temperature, operating variables. The results showed that the control scheme has high precision and good performance.

Simultaneous design and control method process design and control can affect each other, control of process design, thus, the study of interaction between process design and process control design and process operability has important significance to improve the dynamic performance of the process. Yuan et al. [168][214] introduced

the existing design and control methods, mainly including control index optimization method, mixed–integer dynamic optimization method (MIDO), the robust optimization method, the embedded control optimization method, the optimization of black–box method, etc.

Georgiadis, et al. [215] studied interaction between the process design, process control and operability in reactive distillation system systematically, based on the rigorous experimental verification of dynamic model, vector parameterization was used to solve the dynamic optimization problems. Two optimization strategies were proposed, one is sequence optimization design and control; The second is simultaneous design and control, both of them adopt multi–loop PI controller. Results showed that the operability can be used as a powerful function, at the same time, optimal strategy can obtain ideal process design, and it can obtain a cheaper and easier controllable process design without any increase in economic cost. Miranda, et al. [216] also conducted a similar study, used optimal control instead of the traditional PI controller in process control design, including two target functions containing design and control performance, and took two kinds of different solutions: optimization design method and optimization control. The former is included in the design constraint and can be solved by SQP technology. The latter, based on the minimum principle of Pontryagin, obtained the Euler–Lagrangian equation from the implicit optimization problem and solves it with the discretization technology.

### *2.2.4 Key equipment*

Homogeneous reactive distillation uses homogeneous catalyst or operates without a catalyst. Therefore, there is no distinction between the reaction, rectifying or stripping sections. The whole The column internals type and loading is kept the same in the whole column. Only if the reactant is corrosive, then internals with different materials are considered.

In heterogeneous reactive distillation, there are either solid catalyst or column internals with catalytic function, mainly in the reaction section. Catalytic distillation column internals can both accelerate the reaction and be used as separation unit. Thus, this chapter mainly summarizes the key equipment, such as catalytic packings, catalytic plates and other equipment.

### *2.2.4.1 Catalytic packings*

Taylor et al. [198] summarized the current catalytic packings, including (1) A "tea bag" structure, where catalyst particles are wrapped in metal wire mesh packings and then placed in RD column, including porous spherical structure, cylinder and other shapes (such as spherical, dice, circle, etc.) of the wire mesh; (2) a structure of horizontal arrangement, such as metal wire mesh with catalyst, metal screen tube with catalyst, etc.; (3) a binding catalyst structure where small particles of catalysts is put into a pocket of glass cloth and stitched together, then a metal mesh with a certain hole space is overlapped together into a catalyst package; (4) a composite corrugated board, where catalyst is sandwiched between corrugated webs, such as Katapak–S and KATAMAX; (5) catalytic internals, such as catalytic Raschig rings, zeolite catalyst coatings of structured packing, catalyst tubes, and so on, as shown in Figure 17.

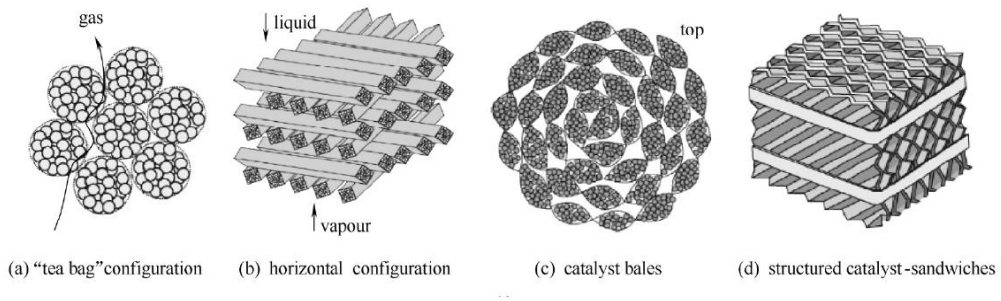


*Figure 17 Catalytic packing*

Yu et al. [217] designed a new type of catalytic distillation unit, which uses aβ–molecular sieve membrane (the carrier is ceramic Raschig ring). The catalytic performance in MTBE synthesis was better than that of resin D005. Du et al. [218] have developed a new type of solid acid catalyst for reactive distillation, where $Al_2O_3$

was used as the carrier. The catalyst has lower pressure drop and mass transfer efficiency is close to the θ ring packings. Sun et al. [219] developed a structured basket catalyst packing for gas–liquid–solid catalytic reaction. Stainless steel wire mesh basket and parallel stainless–steel wire mesh was put into basket framework, which was easy to handle and change, leakage resistance, and could improve the gas–liquid–solid three phase catalyst bed contact state, which is advantageous to the reaction.

*2.2.4.2 Catalytic trays*

There are several kinds of structures for catalytic distillation plate columns.

(1) The reactor can be installed outside the column (side catalytic reactor), so that the tray can be coupled with the reactor, and the gas–liquid channel on the tray is not affected, but the operation is more complicated.

(2) Direct loading of catalyst into the conventional downpour tube. This may affect liquid channeling so that liquid in the downflow tube cannot flow smoothly. The catalyst can be encapsulated in porous medium and placed in a common plate column downpour.

(3) Installing the catalytic packing layer and the non–reaction tray alternatively. Gas passes through the non–catalytic channel in the middle of the packing section and the liquid enters the reaction zone of the filling section after distribution on the separation tray.

(4) The catalysts can be loaded in sealed downcomers. But number of such structures is huge, which makes the maintenance inconvenient. In addition, due to small volume in the downcomer, the liquid in it moves slowly which affects the chemical reaction rate [220].

(5) Catalyst is arranged on plate along the flow direction vertically to ensure that the liquid and catalyst contact is good. A baffle plate in front should be completely submerged in liquid.

*2.2.4.3 Other advanced equipment*

In addition to catalytic packings and trays, scholars have also developed some advanced reactive distillation equipment successively. Wu et al. [221] and Zheng et al. [222] applied a side reactor in synthesis and hydrolysis of methyl acetate reactive distillation process with simulation and experiments, respectively. The results showed that such a structure can improve the conversion of reactants. Li et al. [223] and Lu et al. [224] studied the effect of a pre–reactor in the process of distillation etherification of light gasoline and searched for the optimal conditions of the process. Huang et al. [225][226][227][228] studied a two–stage reactive distillation column in two step continuous reaction and its control performance. The results showed that the structure can improve the efficiency of the reaction and separation and effectively resist disturbances in feed flow rate and composition. Furthermore, a three–stage reactive distillation column was applied in three step continuous reaction. Bao et al. [229] studied the simulation of an isolated reactive distillation column. The research showed that the structure can avoid backmixing and improve product purity and conversion of the reactants. Moreover, the energy consumption was relatively low. Li et al. [230] designed an external circulation reaction column, which can reintroduce the unreacted reactants into the reaction zone. Zhao et al. [231] introduced a chemical heat pump system into tert–butyl alcohol dehydration reactive distillation and demonstrated its feasibility through simulations. Lee et al. [232] designed two kinds of thermally integrated reactive distillation equipment, namely, a HIDiC reactive distillation column and a multi–effect reactive distillation column and studied the optimal structure of the two designs with strict simulations. Wu et al. [233] designed a direct sequence thermo–coupling reactive distillation system, combining two reboilers into one, reducing utility costs.

European project INTINT is committed to developing new reactive rectification column internals. In the project, CFD technology and rate–based process simulations are combined together [234]. The column geometrical shape is obtained by CFD simulations, which can improve fluid mechanics. The new method used in process simulations can provide basis for process optimization.

### 2.2.5 Coupled reactive distillation process

In recent years, the researchers have coupled the reactive distillation with other techniques, and there have been many new processes of reactive distillation, such as enzymatic reactive distillation, microwave reactive distillation, membrane reactive distillation, etc.

#### *2.2.5.1 Enzymatic reaction rectification*

Wierschem et al. studied the enzymatic reactive distillation (ERD) for the production and separation of chiral molecules and established corresponding models [235]. The enzyme is highly enantioselective and can only be used by the enantiomers in chiral molecules. The catalytic conditions are mild, and the reaction rate was high, and cost was cheap. Then they studied the ultrasonic enzymatic reactive rectification (US–ERD) [236], which activated the enzyme with ultrasound. Compared with ERD, US–ERD can increase the reaction rate, reduce the height of the reaction section and the total column height, but the installation cost of ultrasonic equipment was higher. The technical and economic analysis indicated that the cost of the two plans as similar. Only a higher reaction rate was brought by US–ERD, can later significantly have more advantages.

#### *2.2.5.2 Microwave reactive distillation*

Microwave can rapidly provide energy for the reaction system, make the temperature of the distillation process rapid rise to the value to match the reaction temperature,

and temperature can accelerate the reaction rate, studies have confirmed that the microwave reinforcement for some reactive distillation systems [237].

Altman et al. [238][239] studied the effects of microwave irradiation on physical separation and heterogeneous liquid phase reaction respectively. In the process of molecular separation, when the gas–liquid contact surface is exposed to the microwave, the traditional vapor liquid equilibrium is broken, which brings advantages to separation. If only the liquid was exposed to microwave irradiation, the separation was not affected. Compared the equilibrium curve of esterification reaction under microwave irradiation and traditional conditions, the results showed that the microwave did not increase the conversion rate of esterification reaction. Gao et al. [240][241] developed microwave reactive distillation process with or without the presence of microwave assisted vapor liquid equilibrium and studied microwave experiment of DOP esterification reactive distillation process, combined with the steady equilibrium stage model of microwave reactive distillation process, completed the comparison between microwave reactive distillation and conventional distillation process, the results showed that isooctyl alcohol stripping microwave reactive rectification process has more advantages. And Werth et al. [242] studied effect of the microwave reactive distillation with DMC ester exchange reaction as example, the experimental results showed that for binary mixture, the irradiation of microwave field has no effect on the separation on both system and micro scale.

*2.2.5.3 Membrane separation reactive distillation*

The reactive distillation process may result forming non–ideal aqueous–organic phase mixture, which leads to the formation of azeotrope, and the membrane separation technology can overcome this phenomenon because it is not limited by vapor liquid equilibrium. Lutze et al. [243] comprehensively summarized the current situation and development of the combination of membrane and (reaction) distillation. Yang [244][245], coupled reactive distillation and pervaporation membrane separation technology, used in the synthesis of ETBE process, the relevant mathematical model

was established, and the model calibration and operation parameters optimization, the results showed that the reactive distillation and compared with the traditional technique of reactive distillation, membrane separation coupling can improve the conversion rate and yield, under the same conversion, membrane reactive distillation can obviously increase the capacity. Buchaly et al. [246] used the membrane reactive distillation for the heterogeneous catalytic synthesis of n–propyl propionate and established the corresponding non–equilibrium model for simulation and optimization. Mitkowski et al. [247] applied the membrane separation to the batch reactive distillation process and carried out the computer–aided design.

### 2.2.6. Application field

The application field of reactive distillation is very extensive, and its function is mainly reflected in two aspects, namely, separation–intensified reaction and reaction–intensified separation. The related applications are listed in Table 7 and Table 8 respectively. The separation–intensified reactions are mainly reversible reaction and chain reaction, especially the reaction rate is limited by equilibrium, which are suitable for the reaction of etherification and ether decomposition, esterification and ester decomposition, esterification, alkylation, carbonylation, hydrogenation, hydrolysis, chlorination, condensation and isomerization. Niesbach et al. [248] studied biomass reactive distillation. Neumann et al. [249] applied the esterification reaction of fatty acids which carbon chain number is beyond 18 (such as oleic acid or linoleic acid). Took the process of methyl acetate of Eastman chemical company as example, the alternative reactive distillation scheme can reduce the main equipment from 28 to 3 and increase the conversion rate [250].

The reaction–intensified separation mainly used in the separation with similar boiling point or azeotrope. Which can be applied to the separation between isomers, such as the separation of C4 olefins and heterogeneous olefins [251][252], the separation of p–xylene and m–xylene [253][254], separation of p–xylene and o–xylene [181]; The separation and purification of alcohols, such as the preparation of anhydrous ethanol

[255], the purification of coal based ethylene glycol, and the separation and purification of 2, 3–butanediol prepared by the fermentation method [256]; the separation of chiral molecules [235][257].

The application of catalytic rectification technology in chemical industry is becoming more and more extensive. At present, the technology has been used for etherification, esterification, ester hydrolysis, alkylation, etc. Table 9 summarizes the reaction distillation apparatus which has been successfully used and put into production in some industries.

*Table 7 The application of separation intensified reaction*

| Reaction type | Application | Ref. |
|---|---|---|
| Etherification | MTBE synthesis | [185] |
| | ETBE synthesis | [245] |
| | TAME synthesis | [258] |
| | TAEE synthesis | [191] |
| Esterification | MeOAc synthesis | [153] |
| | EtOAc synthesis | [171] |
| | n–butyl acrylate | [259] |
| Transesterification | DMC synthesis | [260] |
| | Butyl butyrate | [236] |
| Alkylation | Ethyl Benzene production | [261] |
| | Cumene Production | [183] |
| | Dodecyl benzene production | [192] |
| Carbonylation | Methanol to DMC synthesis | [262] |
| | 3–amino–2–oxazolidone synthesis | [263] |
| | Diethoxy methane synthesis | [264] |
| Hydrogenation | C3 selectively hydrogenation | [265] |
| | Diene in FCC gasoline hydrogenation | [266] |
| | FCC gasoline hydrodesulphurization | [267] |
| | MIBK production | [268] |
| Hydrolysis | EO to EG production | [151] |
| | IB to TBA production | [269] |
| Chlorination | Chlorination of benzene | [270] |
| Aldolization | Several aldol condensation systems | [271] |
| | Diacetone alcohol production | [272] |
| | Methylal production | [273] |
| Isomerization | Transformation between C4 olefin isomers | [274] |
| Others | Biomass based RD process | [248] |
| | Esterification of fatty acid | [249] |

*Table 8 The application of reaction intensified separation*

| Separating system | Application | Ref. |
|---|---|---|
| Hydrocarbon isomers | Separating C4 olefin isomers by dimerization | [250] |
| | Separating C4 olefin isomers by isomerization | [251] |
| | Separating PX and MX by transorgano sodium | [252][253] |
| | Separating PX and XO by trans alkylation | [181] |
| Alcohols | Separating ethanol–water azeotrope by hydrolysis | [190] |
| | Separating EG and 1,2–BG by aldolization | [191][192] |
| | Purifying 2.3–BG from broth by aldolization | [256] |
| Chiral molecules | Separating chiral molecules by transesterification | [235] |
| | Separating chiral molecules by hydrolysis | [257] |

*Table 9 Implemented reactive distillation process*

| Case | Company | Scale | Implemented time |
|---|---|---|---|
| MTBE synthesis | CR&L company | 20–100 kt/a | 1979 |
| | Charter International Oil Company | 222.6m3/d | 1981 |
| | Qilu Petrochemical corporation | 191m3/d | 1988 |
| | Jinjiang Oil Plant | 2000t/a | 2015 |
| MeOAc synthesis | Eastman Chemical | 180kt/a | 1980 |
| Dimethoxymethane synthesis | Asashi–kasei | 35kt/a | 1984 |
| Ethylbezene synthesis | CDTECH Company | 850kt/a | 1990 |
| PO to PG production | Yuxi Tianshan Chemical Company | 6000kt/a | 1999 |

## 3. Process simulation

When considering the application of RD technology in $CO_2$ hydrogenation, the conventional method is building the lab–scale RD column to justify the assumption, which costs lot of time and has certain potential risk. Thus, computer assisted design (CAD) can solve such situation, all the assumption can be justified on the computer in a relative short time with less cost.

There several software that can satisfy the simulation requirement, and users can even build their own models based on different mathematical models by using different programing language. Among them, Aspen Plus is a better choice, its strong database includes properties data for most common chemicals used in process, and it offers different models to design and test different equipment even lack of input.

Since application of RD technology in $CO_2$ hydrogenation is a novel idea, there are no articles or researches related to this field. It can only be done based on the use of existing experiment data. Aspen Plus is used in the current work to simulate the whole process.

## 3.1. Simple distillation and kinetic reactive distillation model

In this chapter, firstly, a simple distillation simulation is built to obtain initial data for reactive distillation. Then, two $CO_2$ hydrogenation simulation models are built based on a kinetic model obtained from earlier experiments [275]. The first conclusions can be obtained comparing the simulation results from the two simulations.

### *3.1.1 Thermodynamic equations*

The accuracy and validity of the used thermodynamic model directly affects the results of the simulations calculated based on material and energy balances. Therefore, suitable thermodynamic model can accurately calculate physical properties such as density, free energy, heat of formation, heat of vaporization, freezing point temperature, dipole moment, eccentric factor and critical pressure, relative density boiling point, boiling point, critical temperature, critical molar volume, critical volume, standard liquid volume, critical compressibility factor and other parameters of thermodynamic properties. There are two main type of thermodynamic models that can be selected: the equation of state models and the activity coefficient models.

Researches in separation and synthesis of methanol [276][277][278] have shown that the results are correlated well with experimental data by the PSRK model. The results obtained were consistent and satisfactory. Alcohol and water form a very strong polar

mixture system. The PSRK thermodynamic model is an extension of the SRK model. It is suitable for mixtures of polar components. Even though it is difficult to obtain binary vapor–liquid equilibrium data experimentally, the PSK model can be used for estimation according to the chemical structure of each component and the corresponding functional groups, not only in practice, but also the estimation error is small for most systems. Table 10 shows the physical properties of all components in PSRK model.

In this chapter, considering reactive distillation and reactants, products and intermediate, $H_2$, $CO_2$, water, MeOH, 1–butanol and butyl formate will form a mixed liquid system, so the PSRK is chosen as the thermodynamic model.

*Table 10 Physical properties of components calculated using the PSRK model in Aspen Plus 9.*

| Parameter | Units | Components | | | | | |
|---|---|---|---|---|---|---|---|
| | | $H_2$ | $CO_2$ | $H_2O$ | MeOH | 1–butanol | Butyl formate |
| Density | | 340.00 | 340.00 | 10.00 | 46.20 | 42.40 | 27.65 |
| Standard free energy | kJ/mol | 0 | –394.12 | –228.42 | –162.22 | –150.60 | –284.22 |
| Standard enthalpy of formation | kJ/mol | 0 | –393.26 | –241.66 | –200.81 | –274.92 | –426.82 |
| Enthalpy of vaporization | kJ/mol | 0.90 | 16.36 | 40.67 | 35.24 | 42.97 | 34.53 |
| freezing point | ℃ | –259.20 | –56.57 | 0.00 | –97.68 | –89.30 | –91.90 |
| Dipole moment | debye | 0.00 | 0.00 | 1.85 | 1.70 | 1.67 | 2.03 |
| Molecular weight | | 2.02 | 44.01 | 18.02 | 32.04 | 74.12 | 102.13 |
| Acentric factor | | –0.22 | 0.22 | 0.34 | 0.57 | 0.59 | 0.39 |
| Critical pressure | bars | 13.13 | 73.83 | 220.64 | 80.84 | 44.14 | 35.10 |
| Relative density | | 0.30 | 0.30 | 1.00 | 0.80 | 0.81 | 0.89 |
| Boiling point | ℃ | –252.76 | –78.45 | 100.00 | 64.70 | 118.75 | 106.10 |

Table 9: (continued)

| | | | | | | | |
|---|---|---|---|---|---|---|---|
| Critical temperature | ℃ | −239.96 | 31.06 | 373.95 | 239.35 | 289.95 | 285.85 |
| Liquid molar volume at TB | cc/mol | 28.57 | 35.02 | 18.83 | 42.75 | 103.36 | 127.97 |
| Critical volume | cc/mol | 64.15 | 94.00 | 55.95 | 117.00 | 273.00 | 336.00 |
| Standard liquid volume | cc/mol | 53.56 | 53.56 | 18.05 | 40.33 | 91.30 | 115.16 |
| Critical compressibility factor | | 0.31 | 0.27 | 0.23 | 0.22 | 0.26 | 0.25 |

*3.1.2 Azeotrope analysis*

It is necessary to analyze the existence of possible azeotropes before any distillation simulations to guarantee that distillation is a suitable separation method.

The major liquid phase components are 1–butanol, $H_2O$ and methanol. Considering the possible butyl formate intermediate, it should be also put into consideration. The results from azeotrope analysis carried out with Aspen Plus are given in Table 11.

*Table 11 Azeotrope analysis*

| **AZEOTROPE at 30 bars** | | **MOLE BASIS** | **MASS BASIS** | **Temperature** |
|---|---|---|---|---|
| 1 | BUTANOL | 17 % | 45 % | 218,15 |
| | WATER | 83 % | 55 % | |
| 2 | BUTANOL | 14 % | 33 % | 218,54 |
| | WATER | 79 % | 47 % | |
| | BUTFORMA | 7 % | 21 % | |
| 3 | WATER | 64 % | 27 % | 215,51 |
| | BUTFORMA | 36 % | 73 % | |

Azeotrope occurs in the situation when large amount of water exists or generates, since both methanol and butanol need to be separated completed, it means azeotrope can

occurs when separating water from the butanol. So, in the further design, how to break azeotropic system need to be considered.

*3.1.3 Basic distillation model*

In order to get enough initial data to simulate the reactive distillation process, basic distillation simulation can provide information about the distillation parameters, like reflux ratio, distillate rate, reboiler heat load and etc.

Firstly, the DSTWU model can provide basic simulation settings. Since $CO_2$ and $H_2$ exist in gas phase, and butyl formate only exists in a small amount, only $H_2O$, MeOH and 1–butanol is considered in the simulation.

Today, the only industrial $CO_2$ hydrogenation to methanol plant is located in Iceland, its capacity is 5000 t per year. Thus, the same capacity is chosen as reference, which is 20 kmol/h, according to the Eqn (1), $H_2O$ is the same as MeOH. Butanol is used as promoter, according to the experiment result, butanol amount is 5 times than the gas phase, which means 200 kmol/h. the feed temperature is 180 ℃, and pressure is 30 bar. The column pressure is set as 30 bar, same as the experiment conditions. Since $H_2O$ can inhibit catalyst, it should be removed from butanol, which means distillate contains $H_2O$ and MeOH, only butanol is left in the bottom. The distillation setting is listed in Table 12.

*Table 12 Distillation setup information*

| Feed information | |
|---|---|
| $H_2O$ | 20 kmol/h |
| MeOH | 20 kmol/h |
| 1–butanol | 200 kmol/h |
| Feed temperature | 180 ℃ |
| Feed pressure | 30 bars |
| Column information | |
| Column pressure | 30 bars |
| Column pressure drop | 0.5 bars |
| Key light component | $H_2O$ |
| Recovery rate | 0.99* |

*: means 99% of water will go into distillate.

The simulation results are listed below in Table 13.

*Table 13 DSTWU simulation result*

| | | |
|---|---|---|
| Minimum reflux ratio: | 3.58 | |
| Actual reflux ratio: | 5.00 | |
| Minimum number of stages: | 13.06 | |
| Number of actual stages: | 22.52 | |
| Feed stage: | 9.59 | |
| Number of actual stages above feed: | 8.59 | |
| Reboiler heating required: | 1229622.49 | cal/sec |
| Condenser cooling required: | 734121.90 | cal/sec |
| Distillate temperature: | 209.64 | ℃ |
| Bottom temperature: | 240.30 | ℃ |
| Distillate to feed fraction: | 0.18 | |

The DSTWU result provides necessary data for RadFrac simulation. the initial simulation result provides further data for precise simulation, and precise simulation follows 4 steps, they are:

1) Stage numbers, feed stage, reflux ratio, and distillate to feed fraction is calculated by the DSTWU model,
2) In RadFrac model, using Design Specs to constrain the $H_2O$ fraction in distillate, calculate the reflux ratio,
3) Based on the above data, using sensitivity analysis to find optimized feed stage based on reboiler heat duty,
4) Then using sensitivity analysis to find the best number of stages.

Table 14 to 16 show the simulation result of optimal distillation column, and initial simulation result in Table 14 is used to as comparison. After several modification, the result shows that most methanol and water can be successfully separated, while due to the azeotrope between water and butanol, there are certain amount of butanol cannot be separated and stay in distillate. From Table 16, it can be seen that although number of stages are not many, but reflux ratio remains high, which means potential high cost in operation, and it can be improved by increasing the stage number.

*Table 14 Initial stream result*

| | Feed | Distillate | Bottom |
|---|---|---|---|
| Mole Flow kmol/h | | | |
| METHANOL | 20.00 | 19.71 | 0.29 |
| BUTANOL | 400.00 | 39.75 | 360.25 |
| Total Flow kmol/h | 440.00 | 79.20 | 360.80 |
| Total Flow kg/h | 30650.27 | 3933.47 | 26716.80 |
| Total Flow l/min | 978.34 | 150.46 | 1218.22 |
| Temperature ℃ | 180.00 | 209.64 | 240.24 |
| Pressure bars | 30.00 | 29.50 | 30.00 |
| Vapor Frac | 0.00 | 0.00 | 0.00 |
| Liquid Frac | 1.00 | 1.00 | 1.00 |

*Table 15 Optimal stream result from the RadFrac model.*

| | Feed | Distillate | Bottom |
|---|---|---|---|
| $H_2O$ | 20.00 | 19.96 | 0.04 |
| METHANOL | 20.00 | 19.96 | 0.04 |
| BUTANOL | 400.00 | 39.27 | 360.73 |
| Total Flow kmol/h | 440.00 | 79.20 | 360.80 |
| Total Flow kg/h | 30650.27 | 3910.41 | 26739.86 |
| Total Flow l/min | 978.34 | 149.38 | 1220.42 |
| Temperature ℃ | 180.00 | 209.44 | 240.38 |
| Pressure bars | 30.00 | 29.50 | 30.00 |
| Vapor Frac | 0.00 | 0.00 | 0.00 |
| Liquid Frac | 1.00 | 1.00 | 1.00 |

*Table 16 Optimal distillation column data*

| | | |
|---|---|---|
| Actual reflux ratio: | 9.00 | |
| Number of actual stages: | 23.00 | |
| Feed stage: | 7 | |
| Reboiler heating required: | 7288.10 | kw |
| Condenser cooling required: | –5212.25 | kw |
| Distillate temperature: | 209.44 | ℃ |
| Bottom temperature: | 240.38 | ℃ |
| Distillate to feed fraction: | 0.18 | |

*Table 17 Split fraction*

| Component | Distillate | Bottom |
|---|---|---|
| H2O | 0.998 | 0.002 |
| MeOH | 0.998 | 0.002 |
| 1–butanol | 0.098 | 0.902 |

*3.1.4 Reactive distillation simulation*

Aspen Plus provides three alternative reaction models for reactive distillation. They are the conversion, equilibrium and kinetic models. For most studies of reactive distillation simulation, the equilibrium model is used, for example in esterification. However, the $CO_2$ hydrogenation reaction in this case is not reverse reaction, thus, the equilibrium model is not feasible. Also, since there are no reliable data related to conversion rate, the conversion model is not a choice. Therefore, only the kinetic model can be used.

The previous experiments [275] provides enough data to obtain the kinetic parameter.

It is assumed that the reaction rate, in units mol/kg cat h, can be expressed with the following formula where the rate is dependent on the overall pressure of the reacting gases and on the retarding effect of water in the solution:

$$r_1 = k_1 \left(\frac{p_G}{p_{G,mean}}\right)^{n_1} \left(1 + k_{12} c_{H_2O}\right)^{n_3}$$

where $p_G$ is the pressure of the reacting gas ($CO_2$ + $H_2$), $p_{G,mean}$ is the mean pressure (50 bars) $k_1$ is the rate constant which is calculated from the Arrhenius equation:

$$k_1 = k_{1,mean} \left(-\frac{E_1}{R}\left(\frac{1}{T} - \frac{1}{T_{mean}}\right)\right)$$

where $k_{1,mean}$ is the rate constant at mean temperature (estimated parameter), $T_{mean}$ is the mean temperature (200 °C = 473.15 K)

For equation (2), the formation of CO.

$$r_2 = k_2 \left(\frac{p_G}{p_{G,mean}}\right)^{n_2}$$

And for the reverse reaction:

$$r_{-2} = k_2 K_{eq} c_{H_2O}^{n_4}$$

The final production rates of MeOH and water can now be calculated (in units mol/m$^3$ h) from equations:

$$R_{MeOH} = r_1 \frac{m_c}{V}$$

where $m_c$ is the mass of catalyst and V is the volume of liquid in the reactor.

$$R_{H_2O} = (r_1 + r_2 - r_{-2}) \frac{m_c}{V}$$

The model parameter values have been estimated by previous experiment [275]. The parameters are given in Table 18.

*Table 18 Kinetic parameters for alcohol promoted methanol synthesis*

| Parameter | Value | Unit |
|---|---|---|
| $k_{1,mean}$ | 3.0 | mol/kg h |
| $k_{2,mean}$ | 11.5 | mol/kg h |
| $k_{12}$ | 17.0 | – |
| $K_{eq}$ | 0.9 | – |
| $E_1$ | 24.6 | kJ/mol |
| $E_2$ | 89.7 | kJ/mol |
| $n_1$ | 1.0 | – |
| $n_2$ | 1.0 | – |
| $n_3$ | –1.0 | – |
| $n_4$ | 1.0 | – |

Besides the kinetic parameters, liquid holdup is also needed in the simulations. As catalytic reactive distillation, it is often recommended to choose structured packing for reaction section considering installation and maintenance. Therefore, it is assumed that liquid holdup is 4% [276]. The reaction section can be seen as external reactor, after reaction, all product and remaining reactants are going into the feed stage, which is 7$^{th}$ stage. The number of reaction stage is set as 30 stages as assumption. Distillation parameter will follow the result from simple distillation. The reactive distillation

column setting is in Table 19.

*Table 19 Column settings in reactive distillation simulations*

| | |
|---|---|
| Reflux ratio | 8 |
| Distillate to feed ratio | 0.18 |
| Number of stages* | 53 |
| Reaction stages | 16–45 |
| Gas feed stage | 45 |
| Butanol feed stage | 16 |
| Condenser type | Partial vapor |

*: Including condenser and reboiler

The non–condensable gases cannot be fully separated from the distillate; therefore, the condenser type is partial vapor. Dissolved $H_2$ and $CO_2$ can be separated by adding an extra flash tank in further simulations. The results of the reactive distillation simulations are given in Table 20, 20 and .

*Table 20 Reactive distillation simulation results.*

| | **Gas feed** | **Butanol** | **Bottom product** | **Distillate** |
|---|---|---|---|---|
| Mole Flow kmol/h | | | | |
| H2 | 60 | 0 | 6.13E–09 | 0.27 |
| H2O | 0 | 0 | 0.32 | 19.59 |
| CO2 | 20 | 0 | 4.10E–06 | 0.09 |
| METHANOL | 0 | 0 | 0.35 | 19.56 |
| BUTANOL | 0 | 400 | 353.11 | 46.89 |
| Total Flow kmol/h | 80 | 400 | 353.78 | 86.40 |
| Total Flow kg/h | 1001.15 | 29649.12 | 26190.50 | 4459.77 |
| Total Flow l/min | 1666.57 | 935.37 | 1193.91 | 1399.48 |
| Temperature C | 180 | 180 | 240.20 | 215.74 |
| Pressure bar | 30 | 30 | 30 | 29.50 |
| Vapor Frac | 1 | 0 | 0 | 1 |
| Liquid Frac | 0 | 1 | 1 | 0 |

*Table 21 Column utility cost*

| | | |
|---|---|---|
| **Condenser** | | |
| Temperature | 215.74 | ℃ |
| Heat duty | –4216.08 | kw |
| **Reboiler** | | |
| Temperature | 240.20 | ℃ |
| Heat duty | 6197.73 | kw |

### *3.1.5 Conclusions from reactive distillation simulations*

From the simulation, the conversion rate of $CO_2$ is 98.65%, and most of the generated water stays in the distillate, which benefits the catalyst. However, a large amount of butanol is not separated from the distillate.

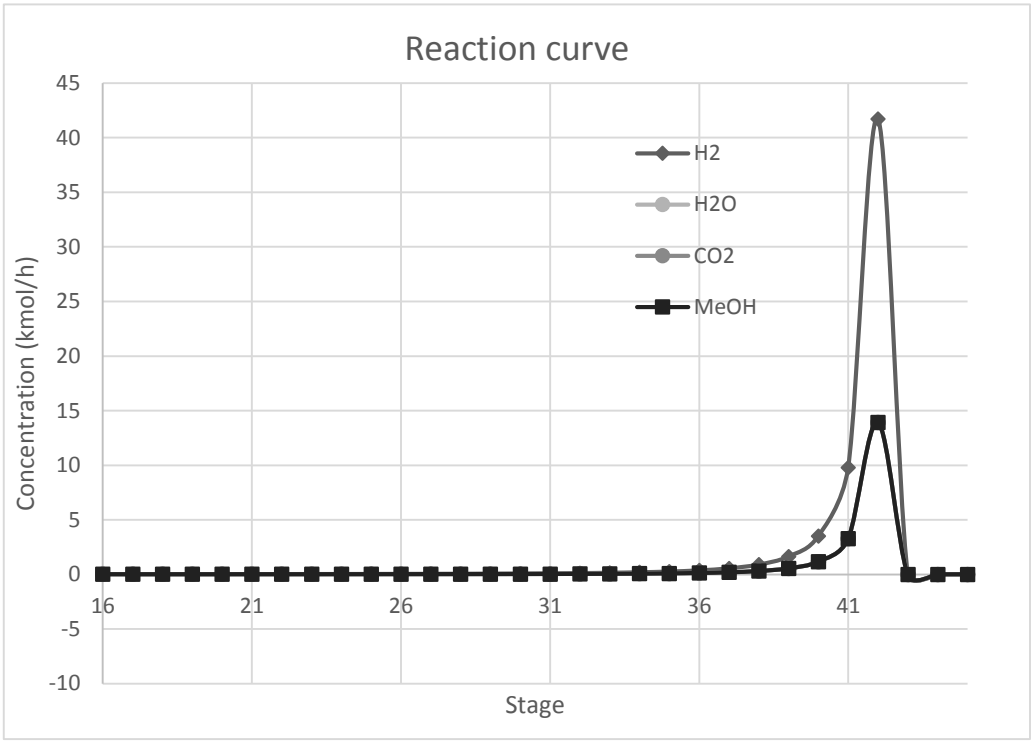


*Figure 18 Mole flow rate of reactants and products in reaction section in RD column*

From the reaction curve, the reaction stages are from 16 to 45, there is no further reaction after 42$^{nd}$ stage, considering the reacted $CO_2$, 99% is converted between 37$^{th}$ to 42$^{nd}$ stage.

### *3.1.6 Butyl formate model*

From earlier experiments (reference), it is assumed that butanol acts as a promoter. $CO_2$, $H_2$ and butanol first will react to form butyl formate and $H_2O$, where butyl formate is an intermediate. Then it reacts with $H_2$ and reduces to butanol and MeOH. The reactions are:

$$H_2 + CO_2 + C_4H_9OH = HCOOC_4H_9 + H_2O \quad (4)$$
$$HCOOC_4H_9 + 2H_2 = C_4H_9OH + CH_3OH \quad (5)$$

There is no clear experimental evidence of existing of butyl formate, but it is still worthwhile to test this assumption by Aspen.

To set such a simulation, the key point is the reaction. Unlike the previous simulation, there are no kinetic parameters available in this case. Therefore, only the conversion and equilibrium models can be used. Since the reactions are not reversible, the equilibrium model is also not suitable. Then the question becomes how to determine the level of conversion in each reaction. Butyl formate exists as an intermediate and theoretically there is nothing left in the end product, so conversion of Eq. (5) is 1.0. For Eq. (4) the conversion rate is assumed as 0.9. The other settings are the same as in the previous simulation. The results are listed in *Table 22*.

Table 22 Stream result of Butyl formate model

| | Butanol | Gas feed | Distillate | Bottom product |
|---|---|---|---|---|
| Mole Flow kmol/h | | | | |
| H2 | 0 | 60 | 0.97 | 0 |
| CO2 | 0 | 20 | 2.87E–21 | 9.42E–08 |
| H2O | 0 | 0 | 19.99 | 0.01 |
| METHANOL | 0 | 0 | 19.50 | 0.01 |
| BUTANOL | 400 | 0 | 36.33 | 363.18 |
| BUTYFORM | 0 | 0 | 0.00 | 0.49 |
| Total Flow kmol/h | 400 | 80 | 76.80 | 363.69 |
| Total Flow kg/h | 29649.12 | 1001.15 | 3680.03 | 26970.23 |
| Total Flow l/min | 703.86 | 1666.57 | 1335.64 | 1188.60 |
| Temperature ℃ | 40 | 180 | 226.42 | 263.18 |
| Pressure bars | 30 | 30 | 29.50 | 30 |
| Vapor Frac | 0 | 1 | 1 | 0 |
| Liquid Frac | 1 | 0 | 0 | 1 |

The result shows that the formate model has a very similar methanol yield than the kinetic model comparing 19.50 kmol/h with 19.74 kmol/h, but utility costs are higher. Also, the concentration profiles are more complicated. Most reactions occur between 41$^{st}$ and 45$^{th}$ stages, and there is still butyl formate left after the reaction part.

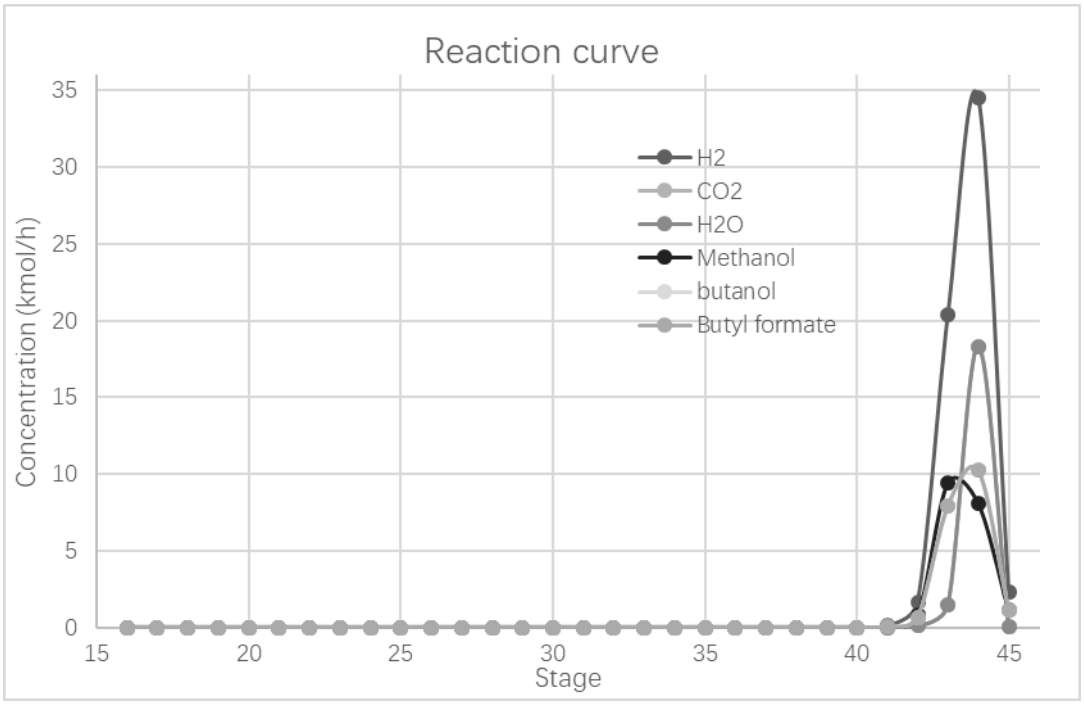


*Figure 19 Reaction curve from butyl formate model*

*Table 23 Column utility consumption*

| | | |
|---|---|---|
| **Condenser** | | |
| Temperature | 226.27 | C |
| Heat duty | –1772 | kw |
| **Reboiler** | | |
| Temperature | 263.18 | C |
| Heat duty | 8180 | kw |

### 3.2 Process optimization

In the previous chapter, both the kinetic model and the butyl formate model were simulated and the results are reasonable with a satisfying yield. In this chapter, several process optimizations will be done to improve yield and operation stability and to decrease utility costs. There are six parameters, which can be optimized. They are:

1) Butanol amount
2) Gas feed ratio
3) Feed temperature
4) Feed pressure and column pressure

5) Number of reaction stages
6) Location of reactive stages
7) 7. Reflux ratio

Since the butyl formate model is based on assumptions, which lacks experiment support, only the kinetic model will be optimized.

*3.2.1 Butanol amount*

Butanol provides the liquid reaction phase and it also acts as a promoter. Hence, the amount of butanol is a key factor. Insufficient liquid may cause poor extent of reaction and instability in reactive distillation column, but excessive amount brings high utility costs and larger equipment size.

In Aspen plus, sensitivity analysis is used to obtain the optimized butanol amount since this parameter is relatively independent from other parameters. The butanol amount ranges from 40 to 1200 kmol/h, and methanol amount in distillate is set as the evaluation indicator.

*Table 24 Sensitivity analysis in butanol amount*

| Status | Butanol | Methanol |
|---|---|---|
| | KMOL/HR | KMOL/H |
| Errors | 40 | 15.09 |
| OK | 200 | 19.83 |
| OK | 360 | 19.75 |
| OK | 520 | 19.70 |
| OK | 680 | 19.63 |
| OK | 840 | 19.56 |
| OK | 1000 | 19.47 |
| OK | 1160 | 19.37 |
| OK | 1200 | 19.34 |

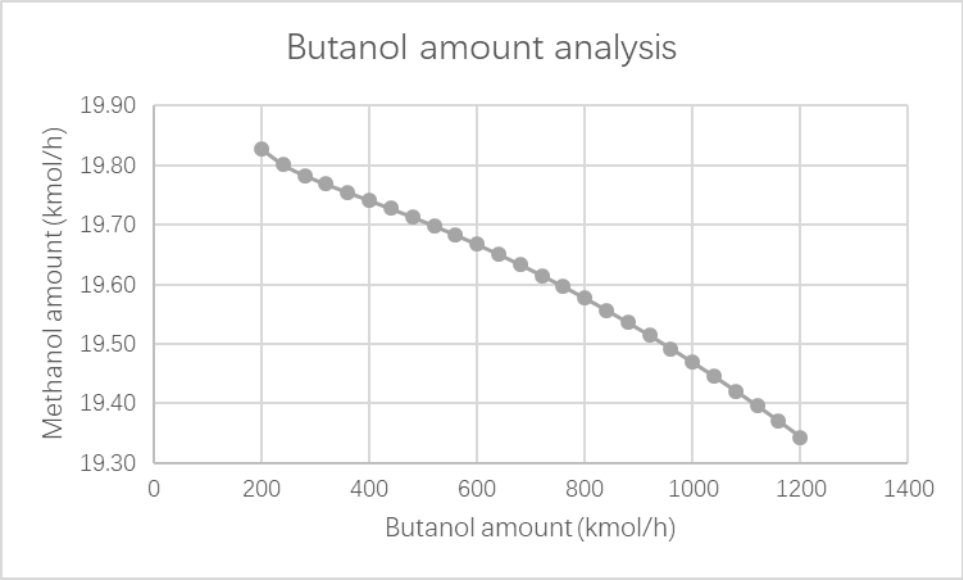


*Figure 20 Methanol product flow rate changes with different butanol amount*

The analysis indicates that butanol amount lower than 200 kmol/h is insufficient to support the distillation process. On the other hand, methanol production decreases when butanol amount increases.

A more detailed analysis was done to obtain the optimal butanol amount. When the butanol amount ranges from 160 to 200 kmol/h, the result show that 196 kmol/h gives the highest methanol yield. However, when considering industrial application, it is reasonable to set some margin to maintain operating stability. Usually the margin is ±20%. In the current case, 196 kmol/h is set as the lower limit, and the normal butanol amount is 250 kmol/h.

*Table 25 Detailed analysis in butanol amount*

| Status | Butanol | Methanol |
|---|---|---|
| | KMOL/H | KMOL/H |
| Errors | 192 | 19.83 |
| Errors | 193 | 14.58 |
| Errors | 194 | 18.03 |
| Errors | 195 | 18.03 |
| OK | 196 | 19.83 |
| OK | 197 | 19.83 |
| OK | 198 | 19.83 |
| OK | 199 | 19.83 |
| OK | 200 | 19.83 |

### *3.2.2 Gas feed ratio*

The previous simulation showed that some amount of $H_2$ is left unreacted. Since the $H_2$ price is much higher than the $CO_2$ price, it is better to increase the $CO_2$ amount to increase the conversion rate of $H_2$. Methanol yield is also simulated.

*Table 26 $CO_2$ feed amount*

| CO2 amount | Methanol | Remaining H2 |
|---|---|---|
| KMOL/H | KMOL/H | KMOL/H |
| 20 | 19.80 | 0.142049 |
| 21 | 19.85 | 2.68E–07 |
| 22 | 19.85 | 3.50E–11 |
| 23 | 19.86 | 5.97E–14 |
| 24 | 19.86 | 4.49E–16 |
| 25 | 19.86 | 8.87E–18 |
| 26 | 19.87 | 3.47E–19 |
| 27 | 19.87 | 2.24E–20 |
| 28 | 19.88 | 2.06E–21 |
| 29 | 19.88 | 2.91E–22 |
| 30 | 19.89 | 1.07E–21 |

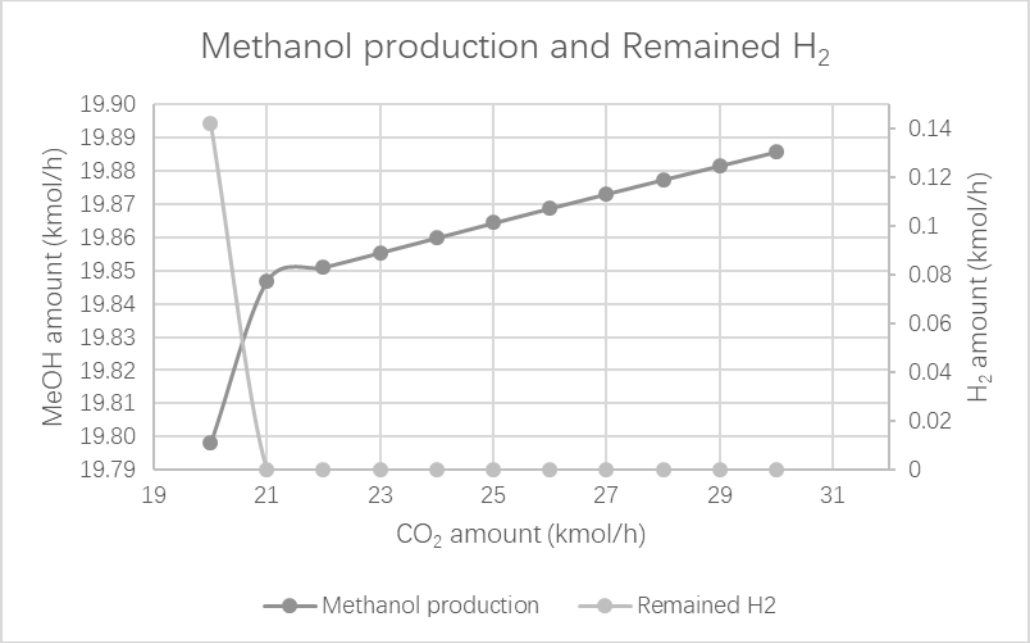


*Figure 21 Methanol production and remained $H_2$*

The $CO_2$ amount ranges from 20 to 30 kmol/h. It is obvious that increasing the $CO_2$

amount brings higher methanol production and less remaining $H_2$. In addition, any value beyond 30 kmol/h brings simulation failure. Therefore, the optimized $CO_2$ amount is 30 kmol/h.

### 3.2.3 Feed temperature

When optimizing the feed temperature, both gas and butanol feed need to be considered. Since the butanol amount is much more than $CO_2$ and $H_2$, it is obvious that the former has a stronger influence in heat duty of condenser and reboiler. The optimizing temperature ranges from 40 to 200 ℃ according to the previous simulation. Three variables are evaluated, they are methanol production rate, and condenser and reboiler heat duty.

First, butanol feed temperature was optimized. From Figure 6, the optimal methanol production is obtained when the feed temperature is around 80 to 90 ℃. With the feed temperature increasing, the condenser duty decreases while the reboiler duty remains stable.

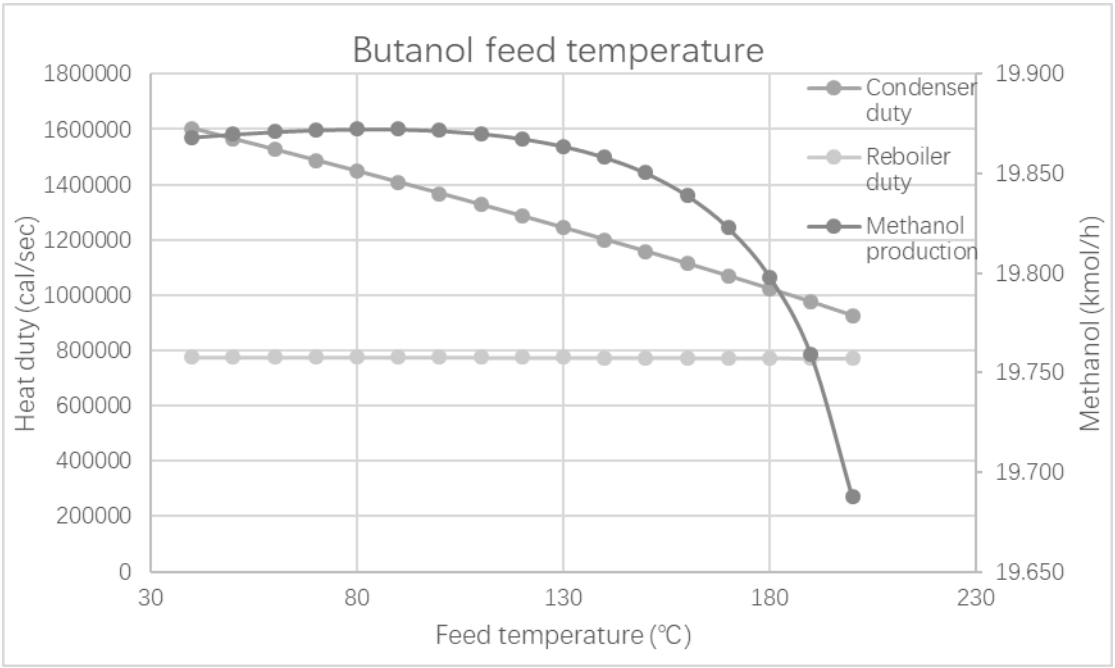


*Figure 22 Butanol feed temperature analysis*

Second, the gas feed temperature is also optimized. The methanol production decreases

while increasing the gas feed temperature, and the reboiler and condenser duties do not change much. However, when considering a real process, the relatively low temperature will cause poor reaction rate and high cooling costs in the compressing unit.

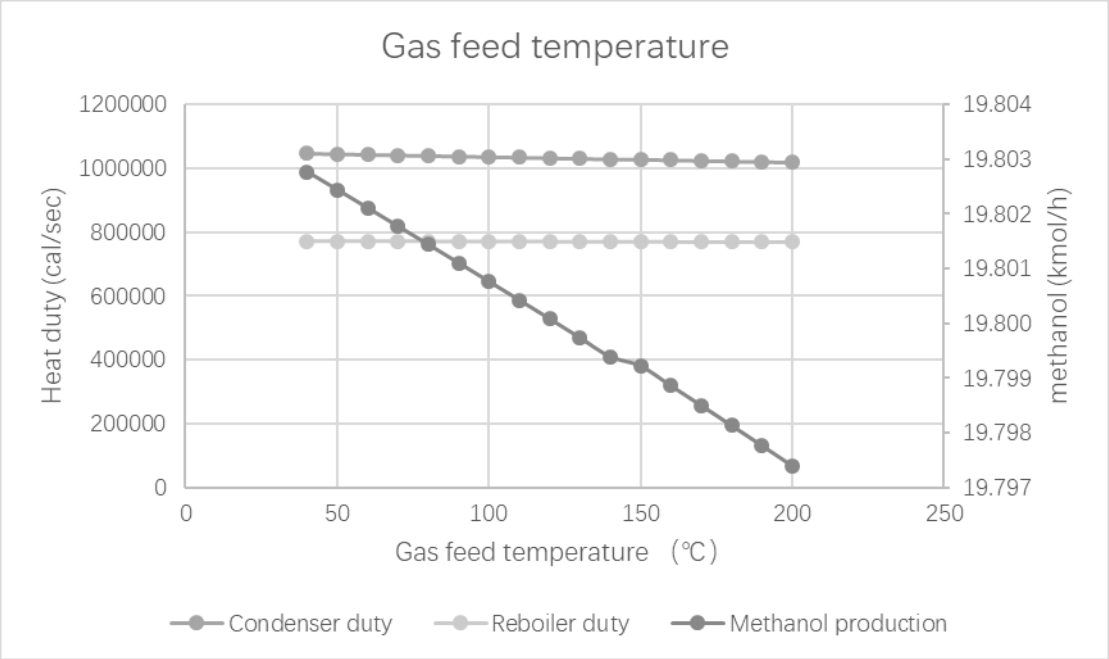


*Figure 23 Effect of gas feed temperature on methanol production and heat duties.*

### *3.2.4 Operating pressure*

From the reaction, the increasing pressure benefits the methanol production rate, but it also increases power consumption and the separating difficulties of soluble gas components in the later distillation column. Therefore, it is necessary to obtain optimal pressure. The tested feed pressure ranges from 10 to 50 bars. Column pressure drop is set as 0.5 bars. In Aspen plus, first Aspen Plus provides calculator model to maintain both feeds pressure equal and condenser pressure is 0.5 bars less than feed pressure. Then sensitivity analysis model can give the right answer. The table below shows the result that methanol yield reaches the top when feed pressure is 25 bars.

*Table 27 Pressure analysis*

| | Status | Feed pressure (bars) | Condenser pressure (bars) | Methanol production (kmol/h) |
|---|---|---|---|---|
| 1 | OK | 10 | 9.5 | 18.9277 |
| 2 | OK | 15 | 14.5 | 19.62325 |
| 3 | OK | 20 | 19.5 | 19.80589 |
| 4 | OK | 25 | 24.5 | 19.84809 |
| 5 | OK | 30 | 29.5 | 19.80418 |
| 6 | OK | 35 | 34.5 | 19.61782 |
| 7 | OK | 40 | 39.5 | 18.98801 |
| 8 | Errors | 45 | 44.5 | 17.46805 |
| 9 | Errors | 50 | 49.5 | 12.93059 |

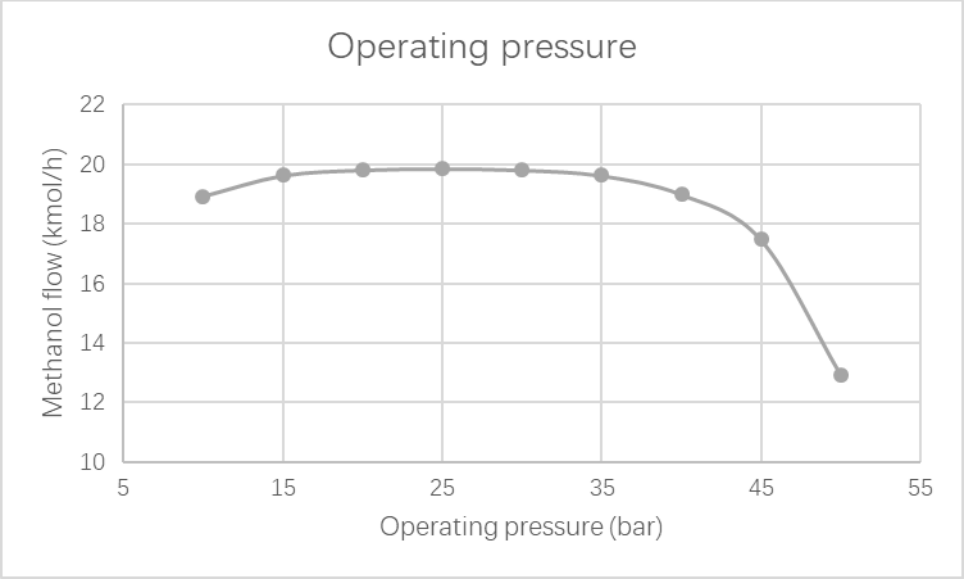


*Figure 24 Methanol production rate related to operating pressure*

### *3.2.5 Reaction stages*

In the last chapter, the simulation result shows that 99% of $CO_2$ is converted between $37^{th}$ and $42^{nd}$ stages. Hence, it is reasonable to reduce the number of reaction stages, although there will a reduction in reaction yield. Such losses can be compensated by adding a recycling line. Decreasing the number of reaction stages means lower catalyst load and equipment costs, which can make the process more economic.

*Table 28 Optimal number of reaction stages*

| | Previous column | Optimal column |
|---|---|---|
| Stage number | 53 | 40 |
| Reaction stage | 16–45 | 16–32 |
| Reflux ratio | 8 | 8 |
| Distillate to feed ratio | 0.18 | 0.18 |
| Methanol production (kmol/h) | 19.56 | 19.48 |

Comparing with previous simulation, the methanol yield only decreases 0.4%, but stage number decreases 24%.

### *3.2.6 Location of reaction stages*

In the previous simulation, the reaction section is simply determined by distillation simulation result which replace feed stage into multiple reaction stages. Through the last optimization, the reaction stages are reduced to 17 stages, and total stages are 40 including reboiler and condenser. Therefore, the number of reaction stages was kept constant changing only the feed stage location, because the two feeds stream determine the behavior of the reaction stages.

The butanol feed stage was ranged from $18^{th}$ to $39^{th}$ stage, and the gas feed stage from $2^{nd}$ to $23^{rd}$ stage. In Aspen Plus, the calculator model keeps the other parameters constant, and sensitivity analysis can measure the changes in methanol production, the amount of butanol remaining in the distillate, and the reboiler and condenser duties.

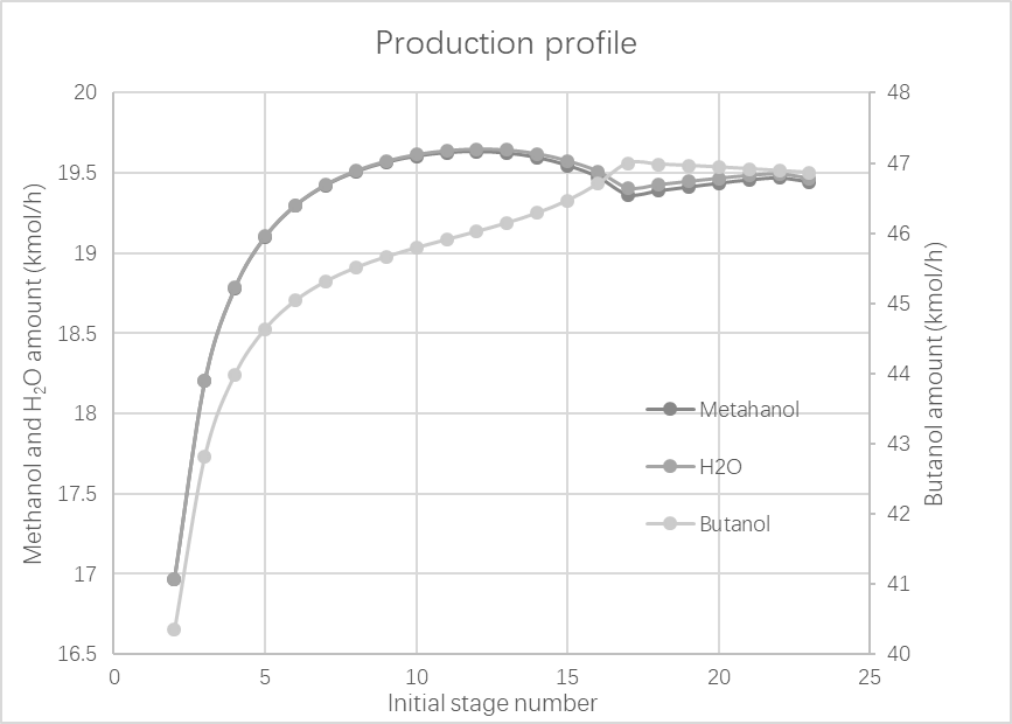


*Figure 25 Reaction stages location*

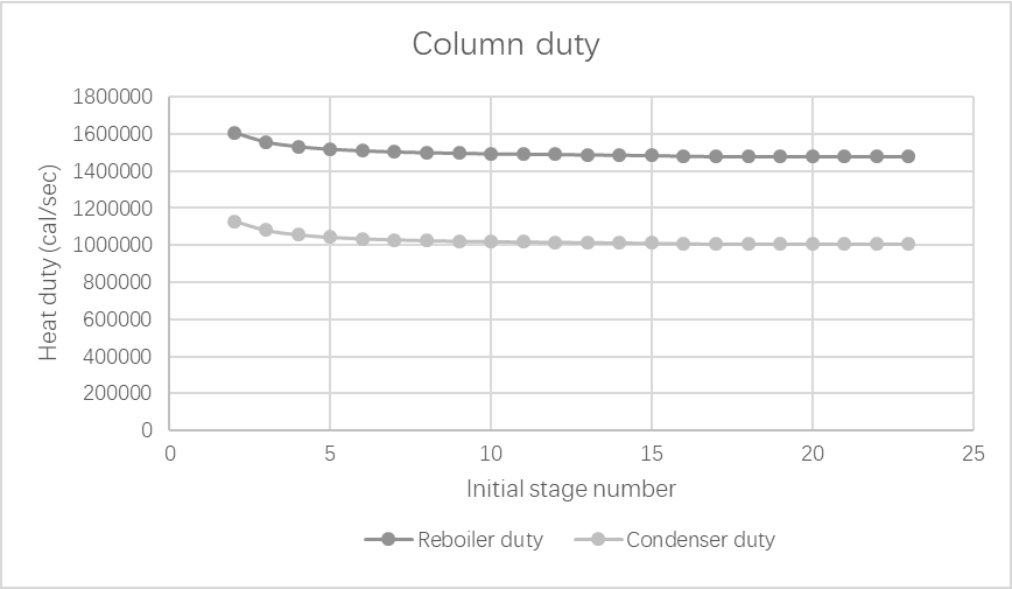


*Figure 26 Column duty*

From the simulation results, it can be seen that when the reaction stages are from 12$^{th}$ to 28$^{th}$, the methanol yield is the highest and the remained butanol in the distillate is relatively low. The column duty profiles show that the condenser and reboiler heat duties do not change much, which means the feed location do not have strong effect on

the column duties.

### *3.2.7 Reflux ratio (RR)*

The change of reflux ratio can determine the methanol production and remained butanol in distillate. An initial value for reflux ratio was calculated by distillation model and it may be not suitable anymore. Sensitivity analysis is used to measure the different reflux ratio and how it can affect methanol yield and remained butanol.

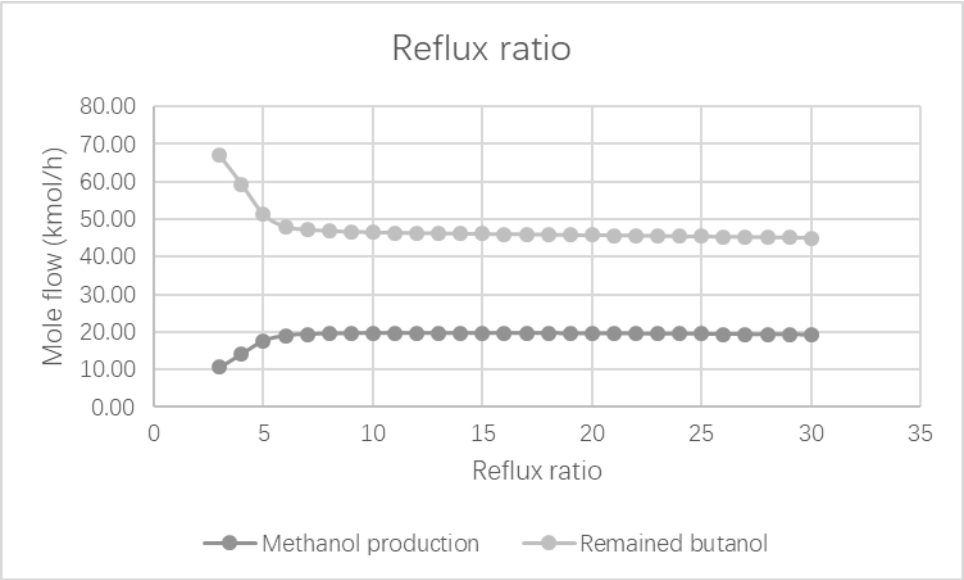


*Figure 27 Reflux ratio*

From the simulation, reflux ratio cannot affect the process much after a value of 8. Methanol yield keeps constant, although there is slight decrease in remained butanol, but increasing reflux ratio can significantly increase condenser load and operating cost, which is not economic.

### *3.2.8 Liquid holdups*

The $CO_2$ hydrogenation occurs in liquid phase; therefore, it is reasonable that liquid holdup in reaction section could have certain effect on the conversion rate along with the column pressure drop. and the liquid holdup amount can determine different packing type. In the Aspen Plus, liquid holdup is determined by reaction part in column

specification. Sensitivity analysis is applied to obtain the best liquid holdup.

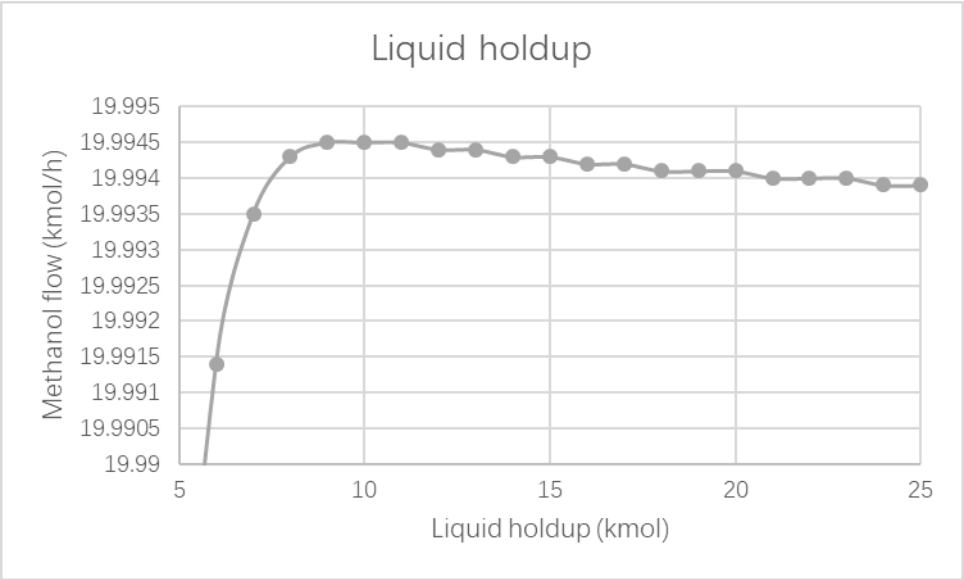


*Figure 28 Liquid holdup*

When liquid holdup is smaller than 7 kmol, the product methanol flow rate is less than 19.99 kmol/h, and best methanol flow rate is obtained when liquid holdup is 9 and 10 kmol, considering the potential column pressure drop, it is wise to choose a smaller holdup value. Thus, 9 kmol is selected as optimal liquid holdup.

### *3.2.9 Conclusions*

In this chapter, seven parameters have been optimized to improve the methanol yield and operating stability. The optimal result lists below:

*Table 29 Optimal RD column setting*

| Parameter | Value |
|---|---|
| Reflux ratio | 8 |
| Number of reaction stages | 17 |
| Reaction stages location | 12–28 |
| Feed temperature | Butanol 80 ℃<br>Gas feed 120 ℃ |
| Operating pressure | 25 bars |
| $H_2$/ $CO_2$ ratio | 2 |
| Butanol flow rate | 250 kmol/h |
| Liquid holdup | 9kmol |

*Table 30 Optimal simulation result –stream part*

| | Gas feed | Butanol feed | Bottom product | Distillate |
|---|---|---|---|---|
| Mole Flow kmol/hr | | | | |
| $H_2$ | 60 | 0 | 3.74E–16 | 2.31E–07 |
| $H_2O$ | 0 | 0 | 0.0053 | 19.99 |
| $CO_2$ | 30 | 0 | 1.80E–10 | 10.00 |
| METHANOL | 0 | 0 | 0.00600837 | 19.99 |
| BUTANOL | 0 | 250 | 238.79 | 11.21 |
| Total Flow kmol/hr | 90 | 250 | 238.80 | 61.20 |
| Total Flow kg/hr | 1441.25 | 18530.70 | 17699.98 | 2271.97 |
| Total Flow l/min | 1938.67 | 471.41 | 725.77 | 1334.48 |
| Temperature ℃ | 120 | 80 | 227.92 | 185.53 |
| Pressure bar | 25 | 25 | 24.5 | 24.5 |
| Vapor Frac | 1 | 0 | 0 | 1 |
| Liquid Frac | 0 | 1 | 1 | 0 |

*Table 31 Optimal simulation result –column part*

| | | |
|---|---|---|
| Condenser | | |
| Temperature | 185.53 | ℃ |
| Heat duty | –4065 | kw |
| Reboiler | | |
| Temperature | 227.92 | ℃ |
| Heat duty | 6663 | kw |

Comparing with previous simulation, the condenser temperature drops 30 ℃, but the heat duty does not change much, reboiler temperature decreases 13 ℃, and heat duty only increases 7%. But most $H_2$ is consumed, and bottom butanol is remains very high purity, which is easy to reuse in the further time. The only problem left is there are still some butanol remaining in the distillate, but it can be easily separated in the further distillation column.

### 3.3 Process design and simulation

In the previous chapter, the reactive distillation column has been optimized, but it is not enough when considering the real process. Therefore, in this chapter, the whole process is designed and simulated, and further optimization work can be done based on the

process simulation results.

In the chapter, crude methanol product is obtained from the distillate, but there are large amount of water, unreacted gas and butanol remaining, so when designing the whole process, it is key point to obtain high purity methanol, recover and reuse all necessary materials.

Since the process of $CO_2$ hydrogenation is very similar to methanol synthesis technology, and the latter is very mature technology, which can be used as a reference. For $CO_2$ hydrogenation, only the reactor type and product composition are different. The figure below indicates the major flows and equipment.

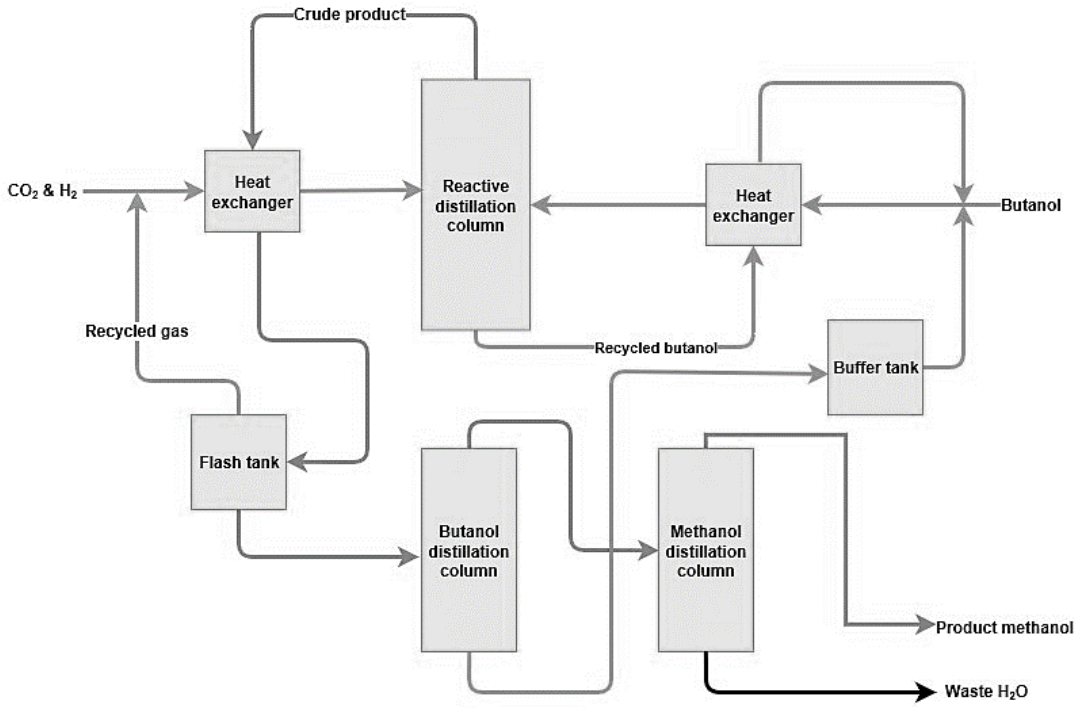


*Figure 29 $CO_2$ hydrogenation process block diagram*

First $CO_2$ and $H_2$ are compressed to the operating pressure, then mixed together. Butanol is also pumped to the operating pressure. All materials are heated by the product from the reactive distillation column and then enter the reactive distillation column. The distillate products are methanol, water, unreacted gas and butanol. The distillate is cooled by feed gas and in the flash tank, product feed is decompressed and

remaining $CO_2$ and $H_2$ are separated and directed back to the feed. The liquid from the flash tank then goes to butanol distillation column to separate butanol from the bottoms. The distillate then goes to methanol distillation column where pure methanol is produced. There are two parts of butanol, which can be recycled. One is from the bottom of the reactive distillation column. This part is first cooled by butanol feed and then reused. Another part is from the bottom of the butanol distillation column. This part is pumped to buffer tank and then pressurized and led to the butanol feed.

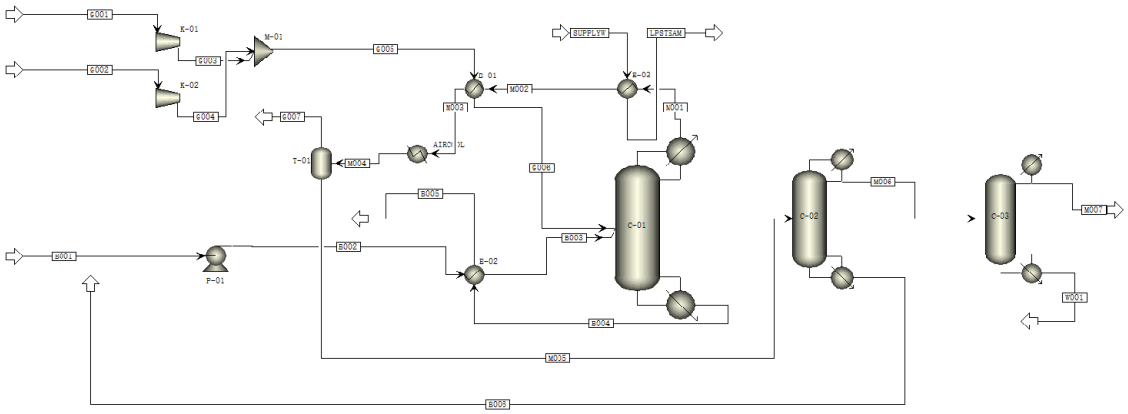


*Figure 30 Aspen flowsheet of methanol hydrogenation process*

In order to minimize the simulation work, the recycled lines will not be considered during the initial process simulation. The three material streams and all the major equipment in the simulation are listed below in Table 33.

*Table 32 Materials information*

| **Materials** | **Information** |
|---|---|
| $CO_2$ | Pressure: 1 bar<br>Temperature: 40 ℃<br>Flow rate: 30 kmol/h |
| $H_2$ | Pressure: 1 bar<br>Temperature: 40 ℃<br>Flow rate: 60 kmol/h |
| N–butanol | Pressure: 1 bar<br>Temperature: 40℃<br>Flow rate: 250 kmol/h |

*Table 33 Equipment checklist*

| **Equipment number** | **Description** |
|---|---|
| K–01 | $H_2$ compressor |
| K–02 | $CO_2$ compressor |
| P–01 | Butanol feed pump |
| M–01 | Gas mixer |
| E–01 | Gas feed heat exchanger |
| E–02 | Butanol feed heat exchanger |
| E–03 | Low pressure steam generator |
| E–04 | Distillate air–cooler |
| C–01 | Reactive distillation column |
| C–02 | Butanol removal distillation column |
| C–03 | Methanol refinery distillation column |

Since the aim of the initial simulation is to obtain initial data for the complete simulation, shortcut models are used to minimize the calculating load in some parts. Compressor model uses multi–stage compressors to control the outlet pressure. Heat exchanger uses shortcut model to obtain general data. For column simulations, only the reactive distillation column uses RadFrac model, the rest two columns use DSTWU model. Reactive distillation column setting follows the last chapter, and the rest of equipment settings is listed below in Table 34.

*Table 34 Initial specification*

| Equipment | Specification |
|---|---|
| K–01 | Outlet pressure: 25 bars |
| | Outlet temperature: 40 ℃ |
| K–02 | Outlet pressure: 25 bars |
| | Outlet temperature: 40 ℃ |
| P–01 | Outlet pressure: 25 bars |
| | Outlet temperature: 40 ℃ |
| E–01 | Gas feed outlet temperature: 120 ℃ |
| E–02 | Butanol feed outlet temperature: 80 ℃ |
| E–03 | Outlet steam vapor fraction: 1 |
| E–04 | Product outlet temperature: 40 ℃ |
| F–01 | Operating temperature: 40 ℃ |
| | Operating pressure: 7 bars |

Table 33: (continued)

| | |
|---|---|
| C–02 | Key light component: $H_2O$ |
| | Key heavy component: butanol |
| | Recovery rate: 0.001 |
| | Stage number: 30 |
| | Condenser pressure: 6.5 bar |
| | Reboiler: 7 bars |
| C–03 | Key light component: MeOH |
| | Recovery rate: 0.999 |
| | Key heavy component: $H_2O$ |
| | Recovery rate: 0.001 |
| | Stage number: 30 |
| | Condenser pressure: 6 bars |
| | Reboiler: 6.5 bars |

From the stream results, the final methanol production is 19.79 kmol/h, and methanol production after the reactive distillation column is 19.99 kmol/h, the separating efficiency is 99 %. Butanol can be recovered from two parts, and the total amount is 249.97 kmol/h, which can be seen as a 100 % recovery rate. And more remarkable, the $CO_2$ concentration in the product methanol (M007) remains at relative high level, which also causes a higher condenser duty in both distillation columns. Such situation can be explained by the $CO_2$ solubility in methanol. The solubility can be calculated by a simple 2–phase flash model. The solubility at different temperatures is shown in Figure 33.

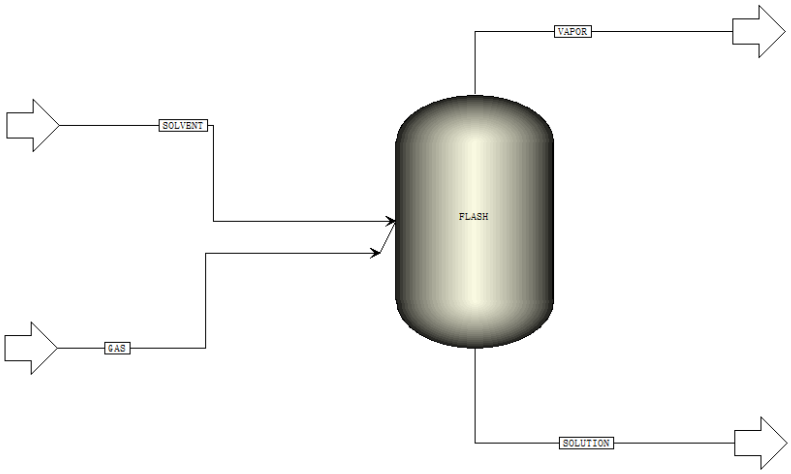


*Figure 31 Flash model to calculate $CO_2$ solubility in methanol*

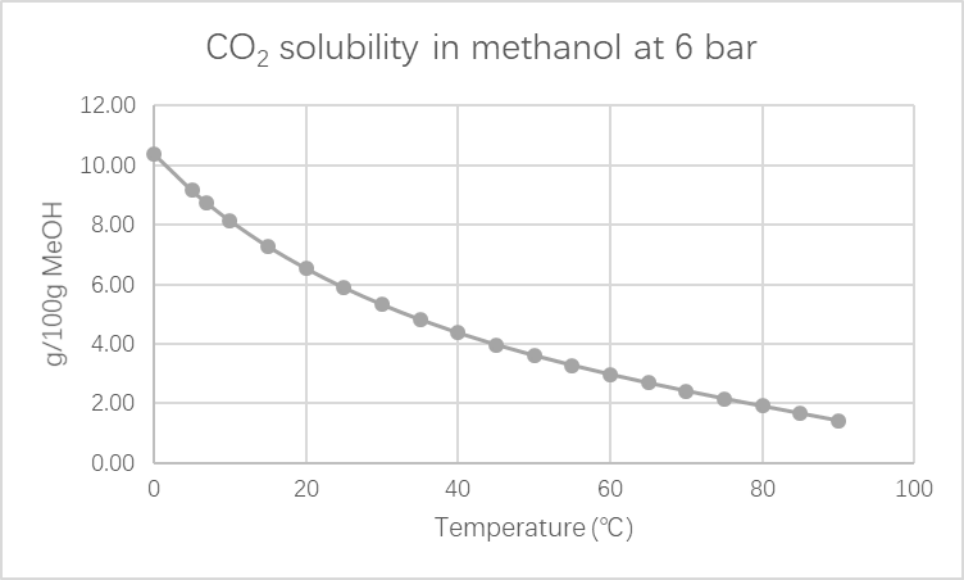


*Figure 32 $CO_2$ solubility in MeOH*

The dissolved $CO_2$ in methanol can bring significant impact on the further processes, for example, if the $CO_2$ concentration in methanol is beyond 50 ppm, it may cause higher decomposition in MTO process (methanol to olefins) [280]. Thus, the removal of $CO_2$ by means of stripping process is required when referring to the rectisol process, which is not economic when considering the whole process.

Besides, the operating temperatures in two condensers of two distillation columns are not reasonable. Therefore, it is necessary to optimize the process to obtain a more reliable process.

### *3.3.1 Feed optimization*

The excessive $CO_2$ in feed means another separating equipment to remove $CO_2$ from methanol and adding another stripping column will bring extra capital and utility costs. Since most unreacted gas can be recycled from the flash tank, it is better to increase $CO_2$ conversion by increasing $H_2/CO_2$ ratio.

In the last chapter, optimal $H_2/CO_2$ ratio was obtained to improve methanol yield, but it also brings a side effect when considering the whole process. Since $H_2$ has a low solubility in methanol, it can be easily separated by flash tank. Increasing the $H_2$ feed

while maintaining methanol yield becomes a reliable solution.

In Aspen Plus, sensitivity analysis is used to measure the optimal $H_2$ feed, while methanol concentration after the reactive distillation column, and the remaining $CO_2$ and $H_2$ in liquid product after the flash tank are set as evaluation criterion, while other settings remains the same, and $CO_2$ feed is 20 kmol/h. The simulation results are shown in Figure 33.

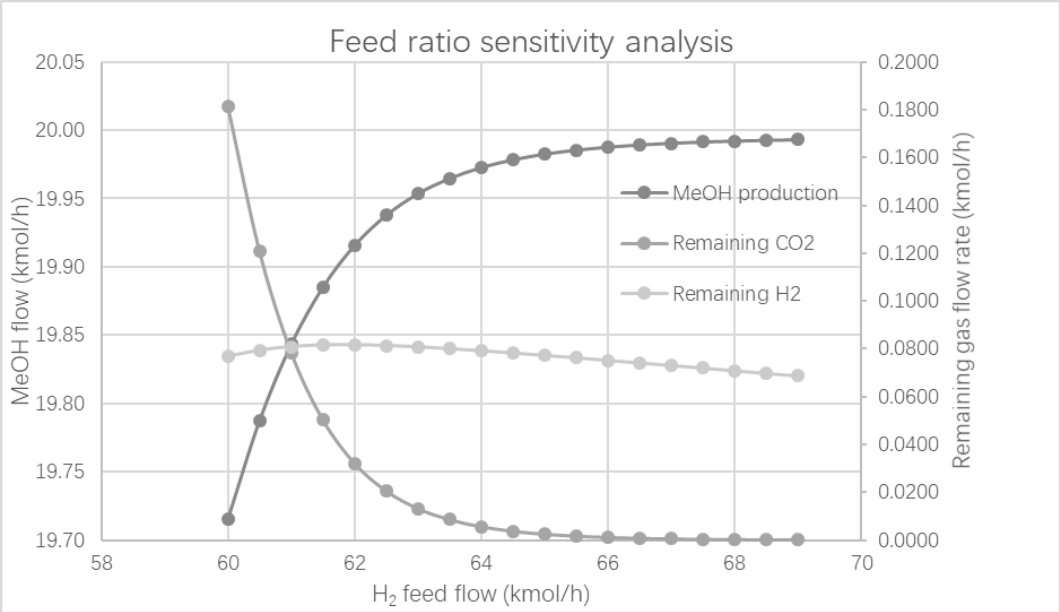


*Figure 33 Feed ratio sensitivity analysis*

The result indicates that when $H_2$ feed is 69 kmol/h, methanol flow rate reaches 19.99 kmol/h, while both remaining $CO_2$ and $H_2$ stay the lowest. Comparing to the initial simulation, the remaining $CO_2$ in methanol decreases a lot, and the excessive $H_2$ can be recycled.

The change of feed ratio may bring effect on liquid holdup, since excessive $H_2$ is hard to dissolve in the butanol. Therefore, to maintain the methanol yield, the liquid holdup in the reaction section needs to be increased. Based on the sensitivity analysis, the optimal liquid holdup should be 19 kmol.

### *3.3.2 Flash tank optimization*

Flash tank is the crucial equipment for separating and recycling excessive gas, and it connects the two parts of the whole process, the high–pressure and low–pressure zones, since the operating pressure of the flash tank is determined by the distillation process, which is like the conventional methanol separation process. Thus, optimizing the temperature in the flash tank is easier, and more notably, it determines the operating temperature of air the cooler. (E–04). Because a dramatic temperature drop in flash tank means large flash tank volume, which is not feasible for the real part of cooling duty needs to be carried by air–cooler

So, the operating temperature ranges from the distillate outlet temperature to 40℃, which is usually obtained by cooling water. In Aspen Plus, sensitivity analysis is used to determine the best temperature, and calculator model is used to guarantee that no temperature crossing happens between the flash tank and the air–cooler.

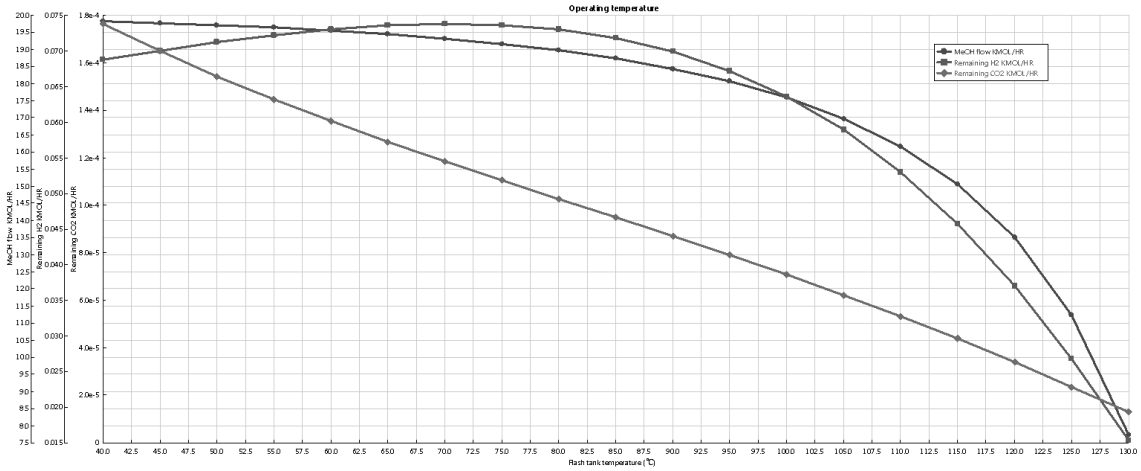


*Figure 34 Operating temperature*

From Figure 34, it is obvious that the lower temperature brings less methanol losses in the flash tank, but also a poorer separating efficiency. Thus, the flash tank is better to be kept in a low temperature.

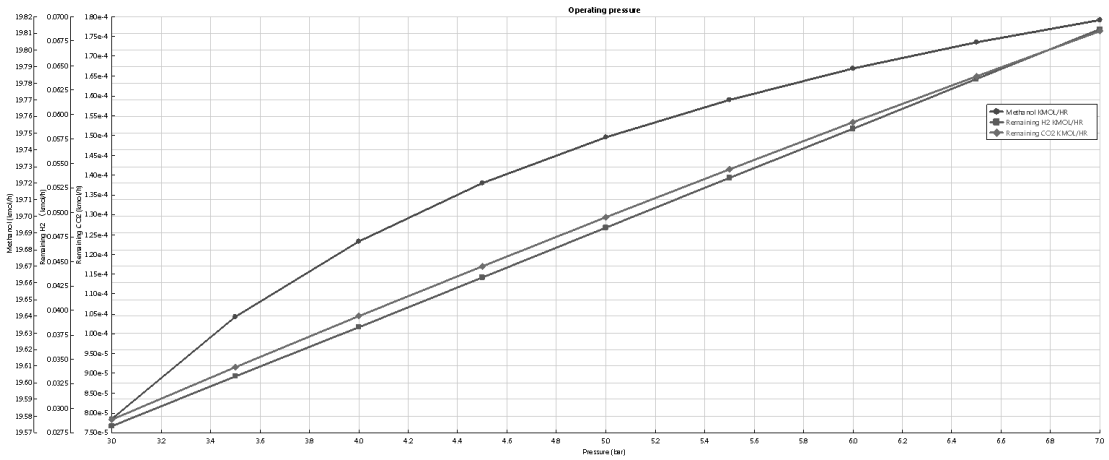


*Figure 35 Operating pressure*

Operating pressure in the flash tank follows the same trend as the operating pressure. Higher operating pressure can provide less methanol losses with poorer gas separating efficiency. Since the operating pressure in the reactive distillation column is relatively high, a dramatic pressure drop in the flash tank means higher equipment cost, so the operating pressure of the flash tank is kept at 7 bars.

### *3.3.3 Methanol purification unit*

The methanol refinery unit includes two columns to separate methanol from water and remaining butanol. The unreacted gas can be purged in one column. From Chapter 3.2, settings of ternary distillation are known, the only difference is the amount of butanol. In azeotrope analysis, large amount of water may form azeotrope with butanol. Therefore, it is impossible to obtain butanol from the mixture by simple distillation column based on trinary distillation diagram. In the initial process simulation, the DSTWU model cannot respond to the azeotrope. Therefore, when going into detailed simulations, the separating sequence has to change.

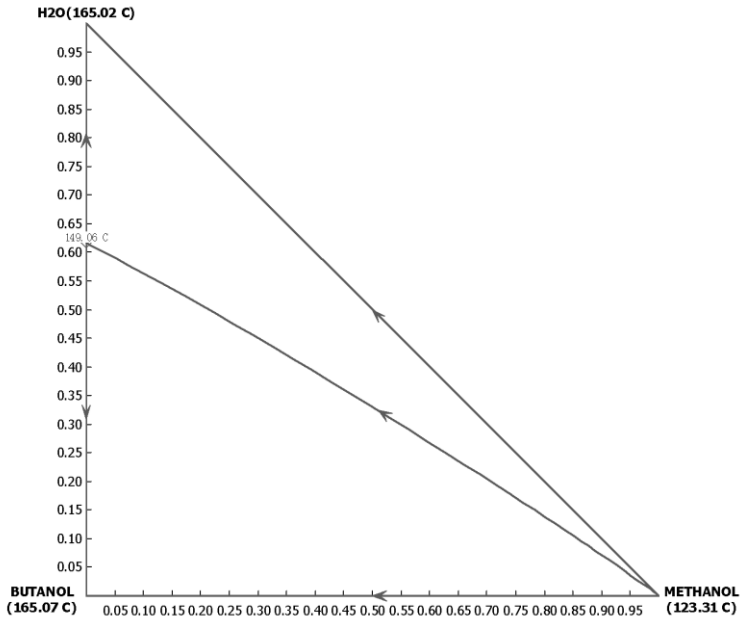


*Figure 36 Trinary distillation diagram*

Thus, in the first column, methanol is separated along with unreacted gas. Methanol is recovered as a product while the gas is led to a purge line. The remaining butanol and water are separated by azeotropic distillation in further processing.

### *3.3.3.1 Methanol distillation column (C–02)*

In the first column, methanol is removed due to azeotrope. A purge line is set on the top of the column to discharge the remaining gas. In Aspen Plus, the DSTWU model cannot be used since it cannot calculate azeotrope, therefore only the RadFrac model is used. Two distillates are set in to column top, the liquid distillate is the methanol product, and the vapor distillate is purged.

*Table 35 Feed information*

| Component | Flow rate (kmol/h) |
|---|---|
| $H_2$ | 0.069 |
| $CO_2$ | 0.002 |
| $H_2O$ | 19.93 |
| METHANOL | 19.82 |
| BUTANOL | 12 |
| Temperature | 40 ℃ |
| Pressure | 7 bars |

*Table 36 Column setting*

| | |
|---|---|
| Reflux ratio | 5 |
| Distillate to feed ratio | 0.384 |
| Stage number | 32 |
| Feed stage | 15 |
| Condenser temperature | 87 ℃ |
| Condenser pressure | 6.5 bars |

*Table 37 Stream result*

| | Feed | Bottom | Methanol | Purge |
|---|---|---|---|---|
| Mole Flow kmol/hr | | | | |
| $H_2$ | 0.069 | 0 | 0.0058 | 0.063 |
| $CO_2$ | 0.00018 | 1.32E–23 | 0.0002 | 2.49E–05 |
| $H_2O$ | 19.93 | 19.91 | 0.0162 | 1.32E–05 |
| METHANOL | 19.82 | 0.0068 | 19.78 | 0.035 |
| BUTANOL | 12 | 12 | 6.35E–08 | 1.77E–11 |
| Total Flow kmol/hr | 51.82 | 31.92 | 19.80 | 0.098 |
| Total Flow kg/hr | 1883.74 | 1248.45 | 634.06 | 1.240 |
| Total Flow l/min | 39.95 | 28.84 | 14.80 | 7.522 |
| Temperature ℃ | 40 | 152.36 | 87 | 87 |
| Pressure bars | 7 | 7 | 6.5 | 6.5 |
| Vapor Frac | 0.0007 | 0 | 0 | 1 |
| Liquid Frac | 0.9993 | 1 | 1 | 0 |

The result shows that most of $H_2$ is removed from the methanol, but $CO_2$ remains in the methanol due to its solubility in methanol. Moreover, there are some methanol losses in the vapor distillate, which can be optimized.

The methanol loss in the vapor distillate is determined by condenser temperature. Moreover, the feed stage and the RR (reflux ratio) are also key factors for the column operation. Thus, three parameters are optimized to improve methanol yield and to decrease energy costs.

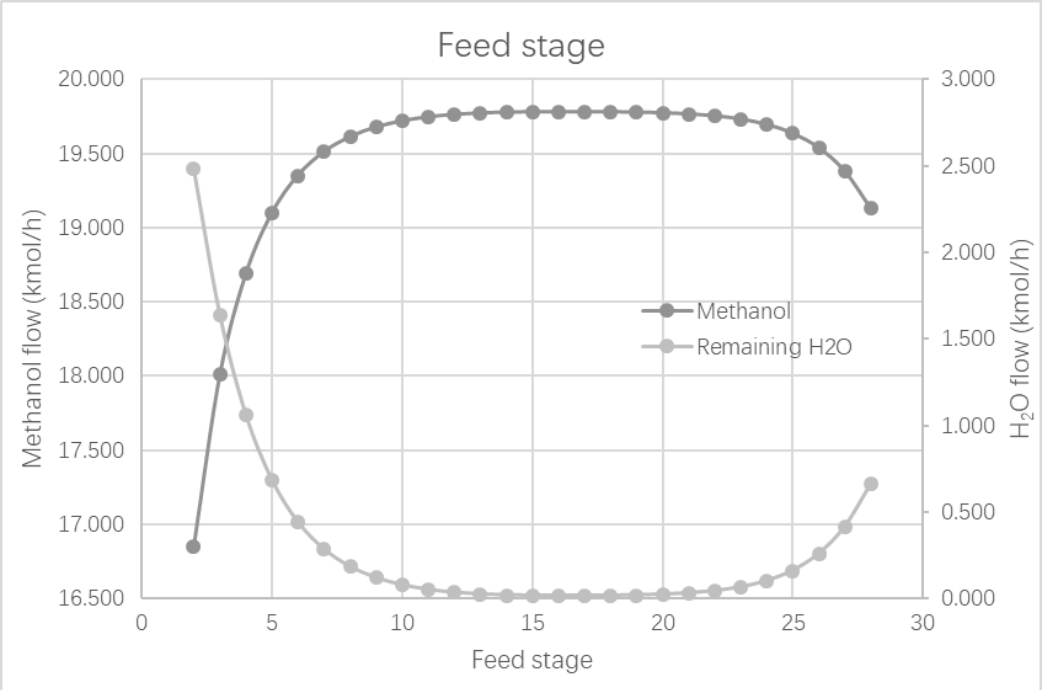


*Figure 37 Feed stage location*

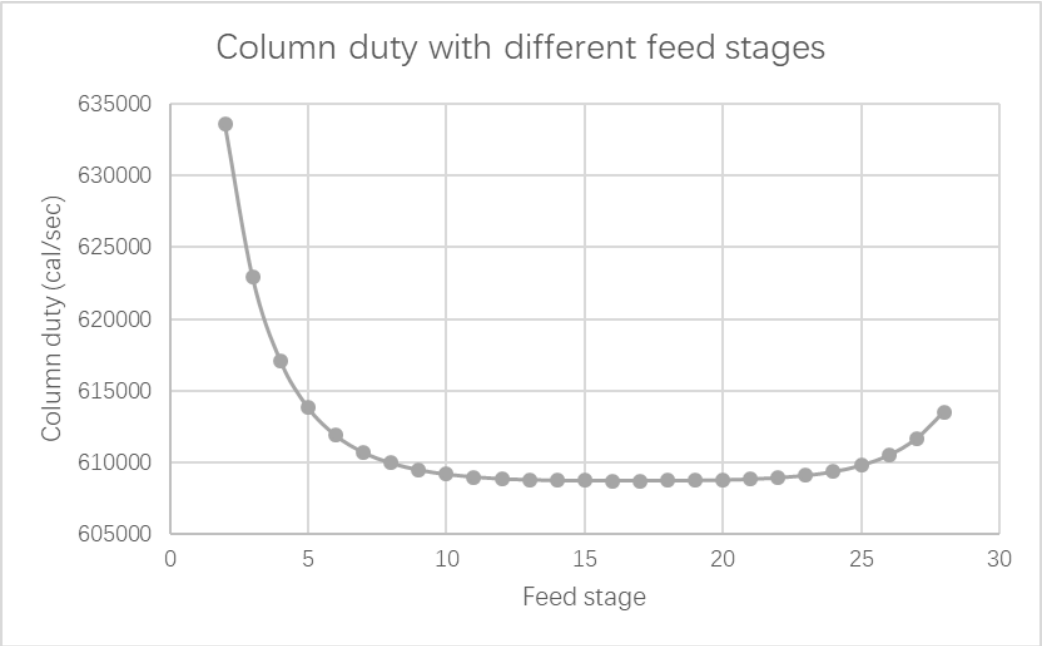


*Figure 38 Energy cost on different feed stages*

Figure 37 and 38 indicate that when the feed stage is at 16$^{th}$ stage, methanol yield, remaining water in distillate and energy costs are the best.

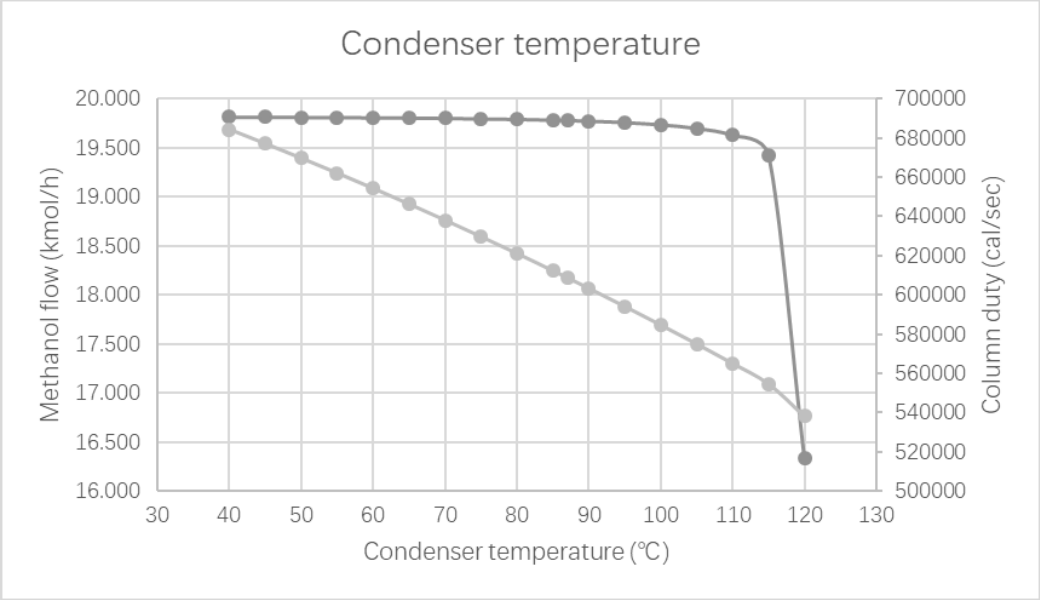


*Figure 39 Condenser temperature*

The condenser temperature shows that lower temperatures bring higher methanol yield but higher energy costs. But Figure 39 shows that when the condenser temperature is between 40 to 55 ℃, methanol yield does not decrease much and, therefore, it is better to choose a condenser temperature with a higher value. 55 ℃ is the optimal value.

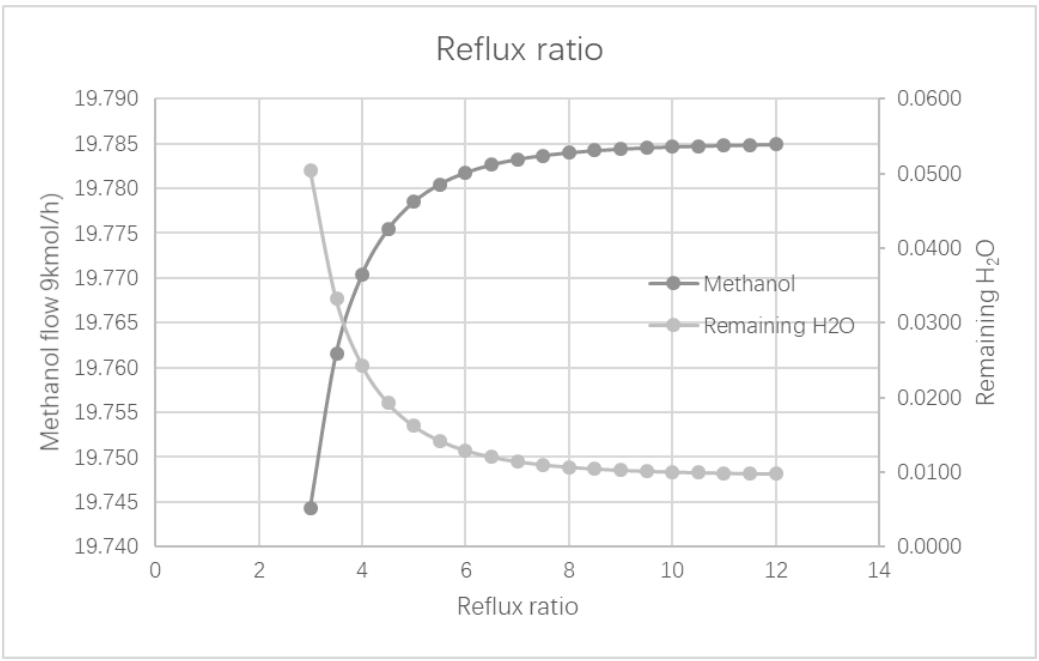


*Figure 40 Reflux ratio*

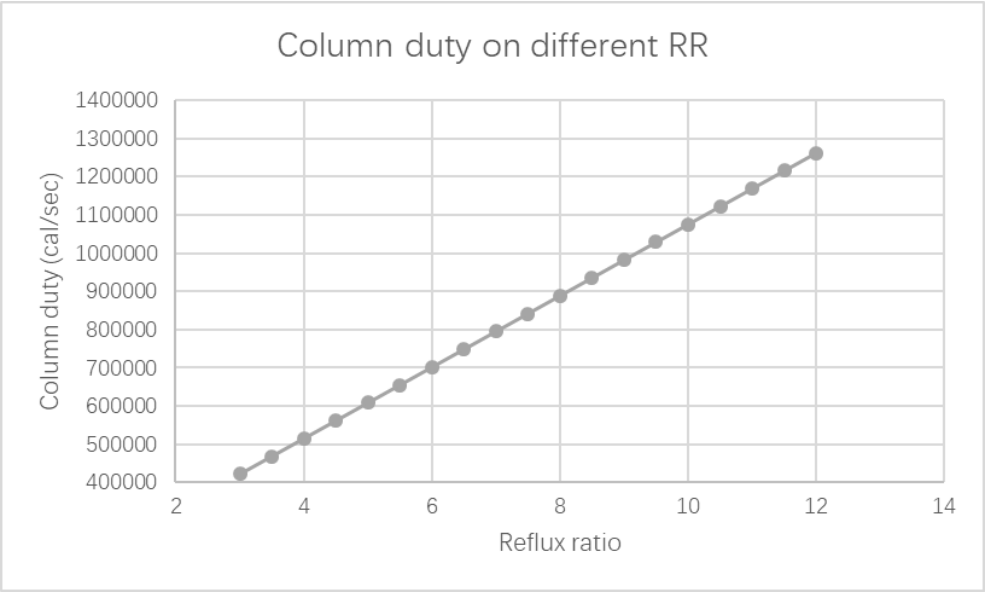


*Figure 41 Column duty on different reflux ratio*

High reflux ratio brings higher methanol yield, but the increasing trend vanishes when the reflux ratio is higher than 7. Besides, the column duty increases while reflux ratio increases. So, the optimal reflux ratio should be chosen as 7 to balance the methanol yield and column duty.

The optimal settings are listed in Table 38.

*Table 38 Optimal column setting*

| | |
|---|---|
| Reflux ratio | 7 |
| Distillate to feed ratio | 0.384 |
| Stage number | 32 |
| Feed stage | 17 |
| Condenser temperature | 55℃ |
| Condenser pressure | 6.5 bar |

*Table 39 Optimal distillation result*

| | Feed | Bottom | Methanol | Purge gas |
|---|---|---|---|---|
| Mole Flow kmol/hr | | | | |
| $H_2$ | 0.069 | 3.19E–32 | 0.0080 | 0.061 |
| $CO_2$ | 0.00018 | 4.22E–32 | 0.0002 | 1.08E–05 |
| $H_2O$ | 19.93 | 19.92 | 0.0109 | 1.49E–06 |
| METHANOL | 19.82 | 0.0015 | 19.81 | 0.01 |
| BUTANOL | 12 | 12 | 4.09E–08 | 1.63E–12 |
| Total Flow kmol/hr | 51.82 | 31.92 | 19.83 | 0.07 |
| Total Flow kg/hr | 1883.74 | 1248.37 | 635.02 | 0.35 |
| Total Flow l/min | 39.95 | 28.83 | 14.00 | 4.77 |
| Temperature ℃ | 40 | 152.36 | 55 | 55 |
| Pressure bar | 7 | 7 | 6.5 | 6.5 |
| Vapor Frac | 0.0007 | 0 | 0 | 1 |
| Liquid Frac | 0.9993 | 1 | 1 | 0 |

*3.3.3.2 Butanol azeotropic distillation columns*

Since butanol cannot be separated from water by simple distillation process due to azeotrope, and any water in recycling butanol can affect the reaction, it is necessary to find a proper way to separate butanol and water as pure streams as possible.

There are several different methods in industry to purify butanol from its water solution. The most common way is azeotropic distillation. A typical alcohol azeotropic process is shown un Figure 42. Which can be used in butanol separation.

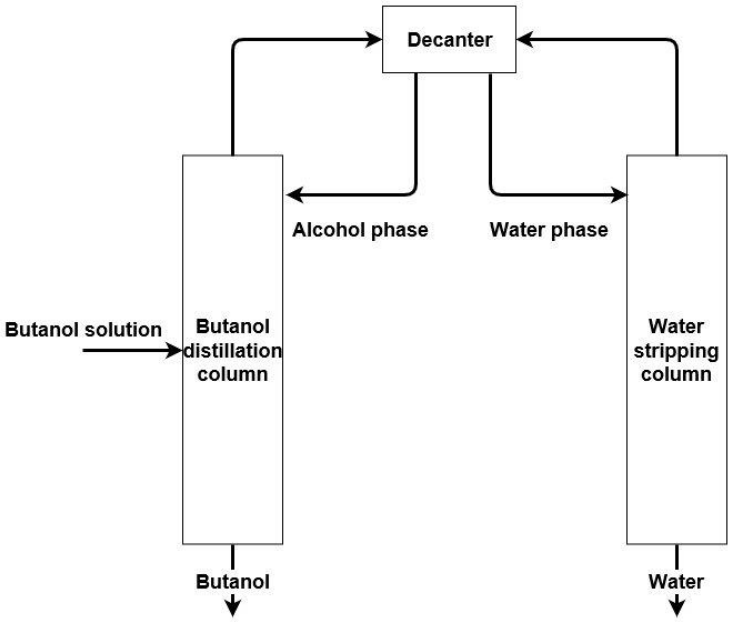


*Figure 42 Butanol azeotropic distillation process*

The butanol–water solution first enters the butanol distillation column, butanol is the heavy key component, and pure butanol is obtained from the bottom. The mix distillate goes to the decanter to liquify and stratification. The alcohol phase goes back to the distillation column as a reflux and the water phase goes to the water stripping column. In the stripping column, the azeotrope is broken by evaporating. From the column bottom, the waste water is discharged.

In Aspen Plus, only the RadFrac model can be used to simulate the process due to rge azeotrope. In the specifications, no condensers are set for both of the columns. Since the requirement of the process is to recycle the butanol, the bottom rate of the distillation column is determined. In the stripping column, any components except water should return to the decanter, thus the distillate to feed ratio is determined. Before the decanter, two heat exchangers are used to condense the streams.

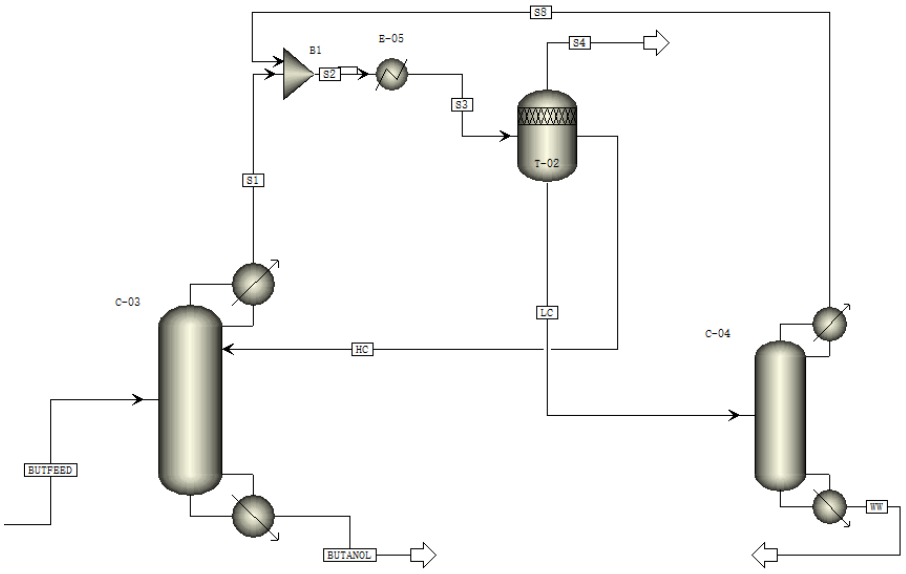


*Figure 43 Azeotropic distillation flowsheet*

The simulation settings are listed below in Table 40.

*Table 40 Column setting*

| | C–03 | C–04 |
|---|---|---|
| Stage number | 20 | 10 |
| Feed stage | 10 | 1 |
| Condenser | none | None |
| Bottom rate (kmol/h) | 12 | |
| Distillate to feed ratio (D/F ratio) | | 0.028 |
| Column pressure drop (bar) | 0.5 | 0.5 |

*Table 41 Decanter and heat exchanger setting*

| | Decanter (T–02) | E–05 | E–06 |
|---|---|---|---|
| Pressure (bar) | 1 | 1 | 1 |
| Outlet temperature (°C) | - | 45 | 45 |
| Vapor fraction | 0 | - | - |

And the simulation results are:

*Table 42 Stream results*

| | Recycling butanol | Waste water |
|---|---|---|
| Mole Flow kmol/hr | | |
| $H_2$ | 0 | 0 |
| $CO_2$ | 0 | 0 |
| $H_2O$ | 0.85 | 19.07 |
| METHANOL | 6.65E–07 | 0.0015 |
| BUTANOL | 11.15 | 0.85 |
| Total Flow kmol/hr | 12 | 19.92 |
| Total Flow kg/hr | 841.78 | 406.29 |
| Total Flow l/min | 21.86 | 9.65 |
| Temperature ℃ | 109.42 | 93.55 |
| Pressure bar | 1 | 1 |
| Vapor Frac | 0 | 0 |
| Liquid Frac | 1 | 1 |

*Table 43 Equipment result*

| | C–03 | C–04 | E–05 |
|---|---|---|---|
| Duty (cal/sec) | 134250 | 3061.6 | 157220 |

The simulation shows that most of the butanol can be recycled in the process, the yield is 96%. Purity is not yet very satisfying but can be improved in optimization. Since both columns do not have condensers, the top products go to the decanter to be separated and returned as reflux. C–04 is the stripping column and there is no reflux. The aim of E–05 is to condense both top products. Thus, only a few parameters can be optimized. They are the feed stage of C–03, the bottom product rate of C–03 and the D/F ratio in C–04. The bottom product of C–03 is determined by the butanol amount in feed, so a larger bottom rate mean that more water is to be separated from the C–03 bottom, which is bad for butanol recycling. Thus, only the feed stage of C–03 and the D/F ratio in C–04 can be optimized.

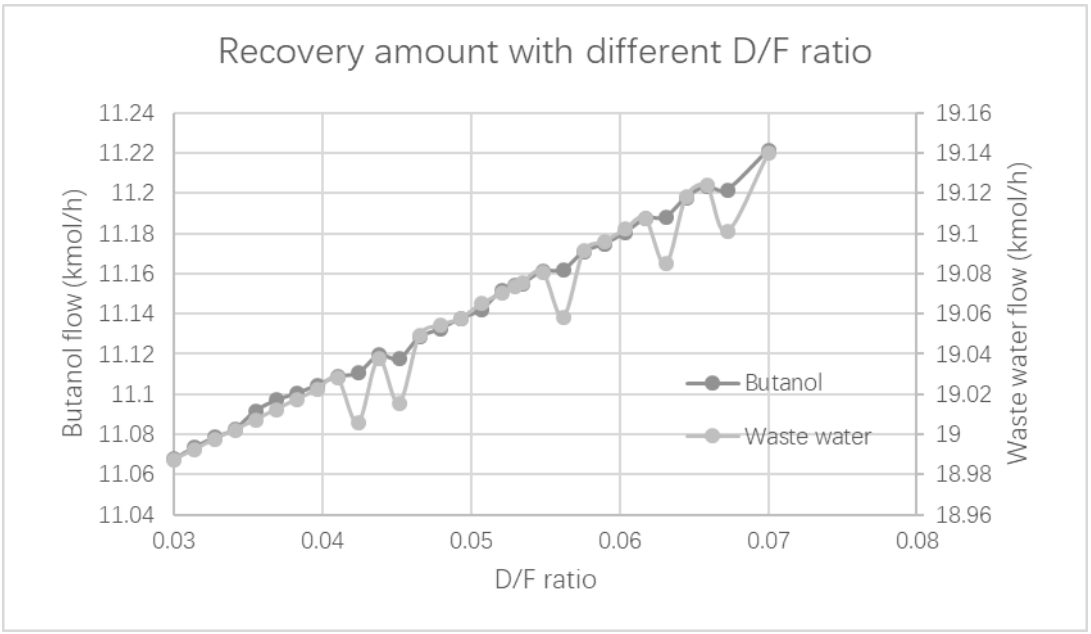


*Figure 44 Recovery amount with different D/F ratio*

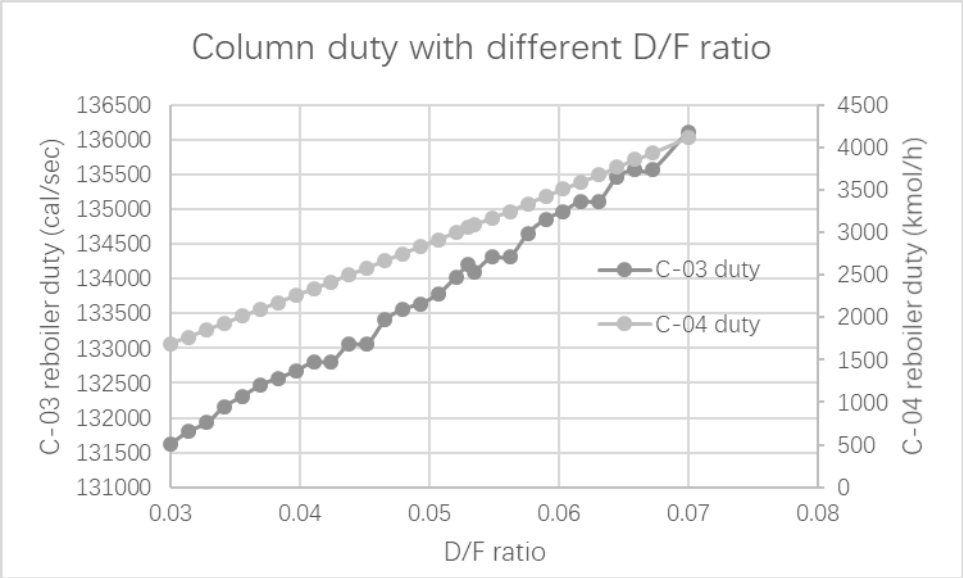


*Figure 45 Column duty with different D/F ratio*

The increasing D/F ratio brings higher butanol recovery rates along with higher column duty. Since the increasing rate of column duty is not very obvious, a larger D/F ratio is chosen as the optimal parameter.

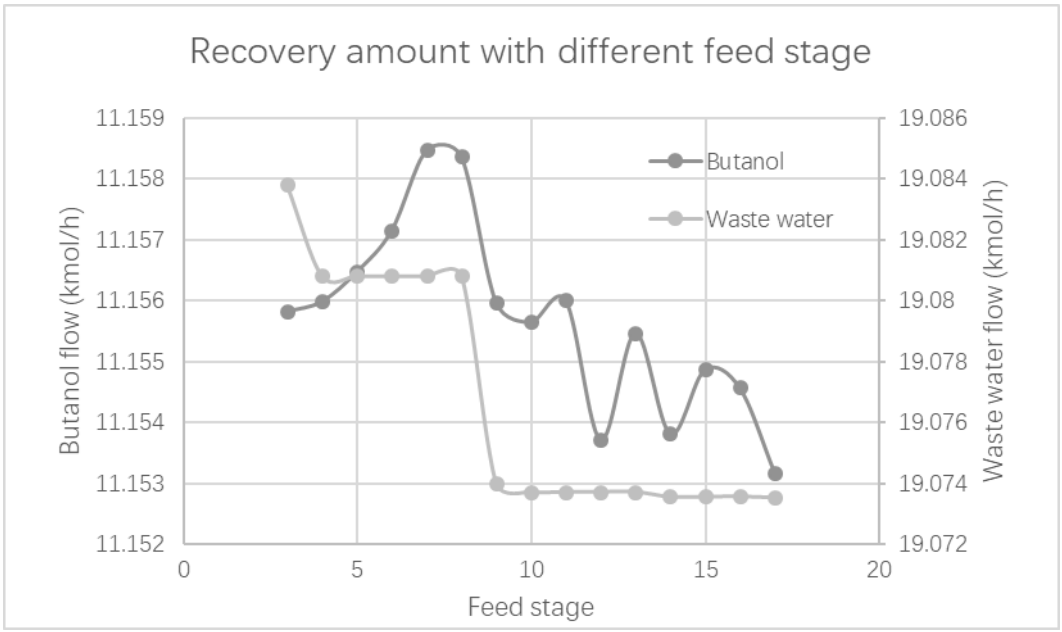


*Figure 46 Recovery amount with different feed stage*

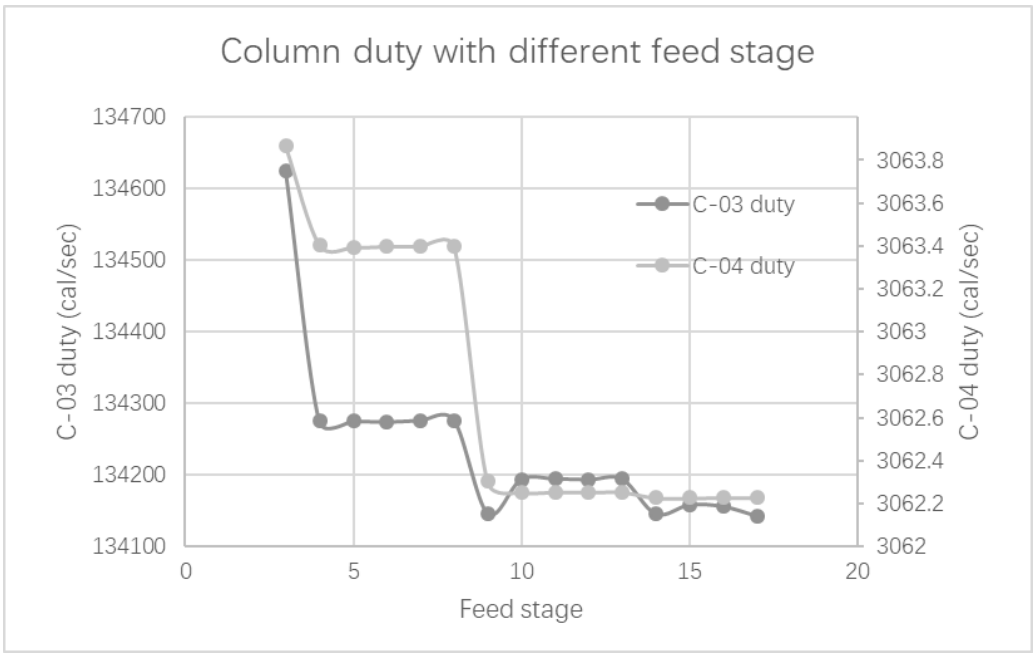


*Figure 47 Column duty with different feed stage*

The sensitivity analysis indicates that butanol recovery reaches the highest value when the feed stage is at 8$^{th}$. The column duties also stay at reasonable levels. Therefore, it is concluded that the best feed stage is the 8$^{th}$.

### *3.3.4 Full process simulation*

Based on all the chapters above, an optimal process is designed. Comparing with the initial process, the separating sequences have changed, the product methanol is separated in the first distillation column, and an azeotropic distillation system is added to obtain pure butanol.

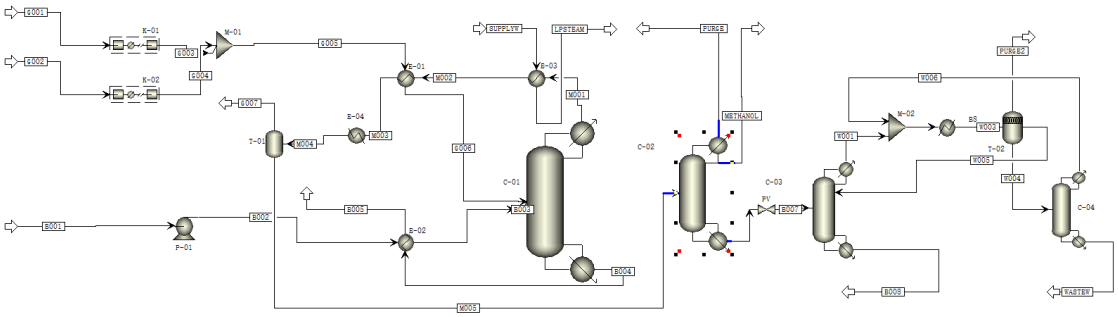

*Figure 48 Process flowsheet (without recycling line)*

The process can be roughly divided into several parts. The compressing unit, which includes two compressors and connected heat exchangers. The aim is to provide the feed enough pressure for the reactions. The reaction unit, which includes the reactive distillation column and the related reboiler and condenser, the feed heat exchanger and the distillate coolers. This the main part of the process, and the crude methanol product is obtained from this unit. The separation unit, which contains two subunits, the initial distillation unit and the azeotropic distillation column. In the first subunit, the product methanol and excess gases are separated. In the second subunit, water and butanol azeotrope is broken to recover the butanol back to process.

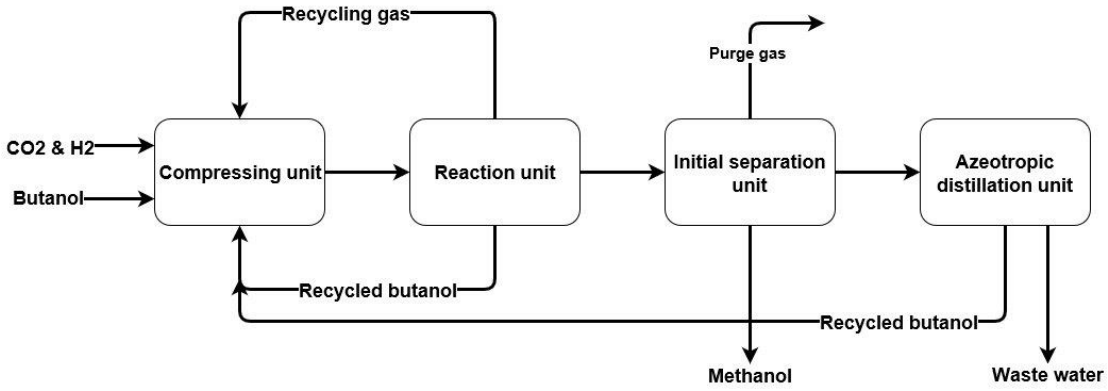


*Figure 49 Block diagram of the complete methanol process.*

The simulation results are shown in Appendix. The methanol production is 19.8 kmol/h, that is 5071 tons annually. The waste–water amount is 19.92 kmol/h, which contains 19.07 kmol/h of water, 0.85 kmol/h of butanol and 0.0015 kmol/h of methanol. Therefore, the annual supplement of butanol is 490 tons. If no azeotropic distillation exists, then 12 kmol/h of butanol would be lost, which is 6912 tons per year. Therefore, azeotropic distillation unit is very necessary to reduce butanol losses.

*Table 44 optimal equipment checklist*

| **Equipment number** | **Description** |
|---|---|
| K–01 | $H_2$ compressor |
| K–02 | $CO_2$ compressor |
| P–01 | Butanol feed pump |
| M–01 | Gas mixer |
| M–02 | Azeotropic mixer |
| E–01 | Gas feed heat exchanger |
| E–02 | Butanol feed heat exchanger |
| E–03 | Low pressure steam generator |
| E–04 | Distillate air–cooler |
| E–05 | Azeotropic heat exchanger |
| C–01 | Reactive distillation column |
| C–02 | Methanol distillation column |
| C–03 | Butanol distillation column |
| C–04 | Stripping column |
| T–01 | Flash tank |
| T–02 | Azeotrope decanter |

*Table 45 Optimal process specification*

| Equipment | Specification |
|---|---|
| K–01 | Outlet pressure: 25 bars |
| | Outlet temperature: 40℃ |
| K–02 | Outlet pressure: 25 bar |
| | Outlet temperature: 40℃ |
| P–01 | Outlet pressure: 25 bars |
| | Outlet temperature: 40℃ |
| E–01 | Gas feed outlet temperature: 120℃ |
| E–02 | Butanol feed outlet temperature: 80℃ |
| E–03 | Outlet steam vapor fraction: 1 |
| E–04 | Product outlet temperature: 40℃ |
| E–05 | Vapor fraction: 0 |
| | Pressure: 1 bar |
| T–01 | Operating temperature: 40℃ |
| | Operating pressure: 7 bars |
| T–02 | Vapor fraction: 0 |
| | Pressure: 0 |
| C–02 | Reflux ratio: 7 |
| | Distillate to feed ratio: 0.384 |
| | Reboiler: 7 bars |
| | Condenser temperature: 55 ℃ |
| | Number of stages: 38 |
| | Feed stages: 16 |
| C–03 | Distillate rate: 12kmol/h |
| | Reboiler: 1 bar |
| | Number of stages: 20 |
| | Feed stages: 10 |
| C–04 | Distillate to feed ratio: 0.053 |
| | Reboiler: 1 bar |
| | Number of stages: 10 |

In the simulations, only the azeotrope circulation is considered, because the feed circulation from butanol refinery unit to RD unit may dramatically increase the computations and may also bring some unexpected situations and results.

### 3.4. Reactive distillation column design

Based on the reactive distillation column and process simulations, optimal specifications of the column are determined. Therefore, a brief column design

calculation has been done in this chapter.

### *3.4.1 Column size and height*

The reactive distillation column is divided into three sections, the reaction section, the upper distillation section and the lower distillation section. In the reaction section, catalytic structured packing is selected to provide the reaction and separation needs. The upper and lower distillation sections use floating valves due to their high separating efficiency. The specific structured packing is Sulzer Mellapak$^{TM}$, because it can be used as a supporter, especially in reactive distillation process. Also, in the Aspen Plus, the detailed parameters of these packings are available. The design results are listed in Table 46 below.

*Table 46 Tray size result*

| | Upper distillation section | Lower distillation section |
|---|---|---|
| Starting stage | 2 | 29 |
| Ending stage | 11 | 39 |
| Traying type | Float valve | Float valve |
| Column diameter (m) | 1.43 | 2.2 |
| Number of passes | 2 | 2 |
| Flow path length (m) | 0.41 | 0.62 |
| Side downcomer width (m) | 0.2 | 0.33 |
| Side weir length (m) | 1 | 1.58 |
| Center downcomer width (m) | 0.2 | 0.32 |
| Center weir length | 1.42 | 2.2 |

*Table 47 Packing size result*

| | |
|---|---|
| Starting stage | 12 |
| Ending stage | 28 |
| Traying type | Mellapak |
| Size | 350Y |
| HETP (m) | 0.4 |
| Column diameter | 2.8 |
| Surface area ($m^2/m^3$) | 3.53 |
| Void fraction | 0.982 |

When calculating the height of the column, the tray space is usually estimated as 61 cm, the column top space is usually set as 213 cm, and the bottom space can carry at least

5 min of holdup, which considering 723.4 L/min, should be 3.6 $m^3$. Assuming that the shape of the bottom is a cylinder combining with a half sphere, the height of the bottom is 130 cm.

*Table 48 Column height estimation*

| **Section** | **Height (cm)** |
|---|---|
| Top | 213 |
| Upper section | 549 |
| Reaction section | 640 |
| Lower section | 610 |
| Bottom | 130 |
| Total | 2142 |

Therefore, approximate column height is 21.42 m. The column can be assembled as one unity or divided into two sections considering since different column sections have different size respectively.

### *3.4.2 Column pressure drop calibration*

From the packing and tray calculations, the total column pressure drop is obtained. The updated column pressure drop is 0.07 bar.

*Table 49 Column pressure drop calibration*

| Section (bar) | Pressure drop |
|---|---|
| Upper section | 0.0302572 |
| Reaction section | 0.00367 |
| Lower section | 0.0371266 |
| Total | 0.0710538 |

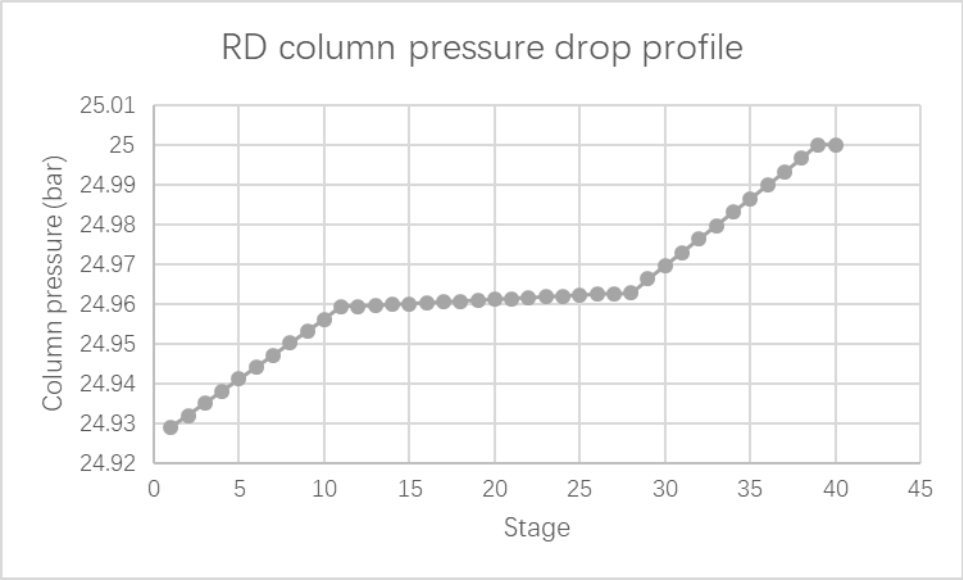


*Figure 50 RD column pressure drop profile*

## 4. Conclusions

The reuse of $CO_2$ has certain limits due its chemical stability, though there are lot of researches, most of them remain in laboratory scale. The RD technology combines reaction and separation at one equipment, which intensifies both processes simultaneously. But whenever using RD technology into some new process, there are always some uncertainties. Thus, application of CAD can avoid such risks by simulating the whole process with computer. The results then can be used to develop further the process or even design a pilot factory.

**Reactive distillation column**

Based on kinetic studies of butanol promoted $CO_2$ hydrogenation experiments, a reactive distillation column was designed with Aspen plus. The physical properties of the simulation use the PSRK model and the reaction in the column uses kinetic parameters. The result indicates that methanol yield is beyond 99.5% due to successful separation of water from the system.

*Table 50 RD column specification*

| Parameters | Value |
|---|---|
| Columns pressure (bar) | 25 |
| Butanol feed temperature (℃) | 80 |
| Gas feed temperature (℃) | 120 |
| Butanol to feed ratio | 3.125 |
| Number of column stages (without condenser and reboiler) | 38 |
| Number of reaction stages | 17 |
| Reaction stage location | 12–28 |
| Reaction stages liquid holdup (kmol) | 9 |
| Butanol feed stage | 12 |
| Gas feed stage | 28 |
| Reflux ratio | 8 |
| Condenser temperature (℃) | 186 |
| Reboiler temperature (℃) | 228 |

**Process simulation and design**

When considering industrial application, it is not enough to consider only the RD column, but also the whole process, since further process units may affect the RD column itself. Thus, several conclusions can be obtained:

1) Most heterogeneous reactions use column type reactors; therefore, RD column can be easily used in CO2 hydrogenation.

2) The RD column can maintain the water fraction at a relative low level at every stage, which is good for both methanol conversion and catalyst.

3) Comparing to conventional gas phase $CO_2$ hydrogenation process, the $CO_2$ hydrogenation RD process does not need set loop for reaction. Thus, the whole process is simpler with less equipment and pipeline.

4) The stoichiometry of $H_2/CO_2$ is 3, but both increasing and reducing the ratio can improve methanol yield. Since $CO_2$ has a relative high solubility in methanol, it is better to consume most of $CO_2$ so that no further $CO_2$ desorption process is needed.

The optimal $H_2/CO_2$ ratio is 3.45.

5) Due to physical limitation, the distillate of the RD column contains both products and unreacted syngas, and they cannot be directly separated at the column top. Thus, a flash tank is set to separate and recover the remaining gases from the crude product. It is possible to set a purge line to the column top to recover the $H_2$.

6) Water and butanol form an azeotrope. Therefore, it is impossible to gain methanol and water mixture from the RD column condenser. A further distillation column was implemented where methanol product is obtained from the condenser and the remaining water and butanol are led to further processing from the bottom. Also, a purge line is set at the column top to discharge non–condensable gases.

7) According to the reasons mentioned above, an azeotropic distillation system, including one distillation column, one stripping column, one decanter, one heat exchanger and related pumps, is needed to separate butanol and water and to maximize butanol recovery and minimize the waste–water amount. After azeotrope distillation system, 99% of butanol is recovered.

8) The RD column needs a certain amount of liquid holdup to maintain the reaction. There are a lot of RD internals available which can be used to satisfy the liquid holdup and catalyst requirement. The column is easy to scale up.

9) The major cost of the new process is in the RD unit, the capital cost of RD column may be high due to its complexity, and utility cost in heating and pressurizing. For further study, cost optimization can be an important factor.

10) The Aspen Plus simulations carried out are static simulations, which can only reflect the process when it is at steady state. Even though the conversion in the simulations is very satisfying, it is not known how long it can be maintained. Thus, improving the reaction rate by modifying the catalyst is a key factor for further studies.

# Appendix

*Table 51 Stream result*

| | Units | B001 | B002 | B003 | B004 | B005 | B006 | B007 | B008 | G001 | G002 | G003 |
|---|---|---|---|---|---|---|---|---|---|---|---|---|
| From | | | P–01 | E–02 | C–01 | E–02 | C–02 | PV | C–03 | | | K–01 |
| To | | P–01 | E–02 | C–01 | E–02 | | PV | C–03 | | K–01 | K–02 | M–01 |
| Substream: MIXED | | | | | | | | | | | | |
| Phase: | | Liquid | Liquid | Liquid | Liquid | Liquid | Liquid | Mixed | Liquid | Vapor | Vapor | Vapor |
| Component Mole Flow | | | | | | | | | | | | |
| $H_2$ | KMOL/HR | 0 | 0 | 0 | 9.60E–16 | 9.60E–16 | 0.00E+00 | 0.00E+00 | 0 | 69 | 0 | 69 |
| $H_2O$ | KMOL/HR | 0 | 0 | 0 | 0.0048 | 0.0048 | 1.47E–25 | 1.47E–25 | 0 | 0 | 0 | 0 |
| $CO_2$ | KMOL/HR | 0 | 0 | 0 | 7.35E–11 | 7.35E–11 | 19.92 | 19.92 | 0.85 | 0 | 20 | 0 |
| METHANOL | KMOL/HR | 0 | 0 | 0 | 0.0055 | 0.005482 | 0.0015 | 0.0015 | 6.65E–07 | 0 | 0 | 0 |
| BUTANOL | KMOL/HR | 250 | 250 | 250 | 237.97 | 237.97 | 12.00 | 12.00 | 11.15 | 0 | 0 | 0 |
| Mole Flow | KMOL/HR | 250 | 250 | 250 | 237.98 | 237.98 | 31.92 | 31.92 | 12 | 69 | 20 | 69 |
| Mass Flow | KG/HR | 18530.70 | 18530.70 | 18530.70 | 17639.46 | 17639.46 | 1248.03 | 1248.03 | 841.78 | 139.10 | 880.20 | 139.10 |
| Volume Flow | L/MIN | 442.10 | 441.69 | 471.41 | 723.29 | 571.05 | 28.83 | 4051.47 | 21.86 | 23774.00 | 8222.11 | 1215.89 |
| Temperature | ℃ | 25 | 26.23379 | 80 | 227.92 | 185.74 | 152.36 | 93.67 | 109.42 | 25 | 25 | 40 |
| Pressure | BAR | 1 | 25 | 25 | 24.5 | 24.5 | 7 | 1 | 1 | 1.2 | 1 | 25 |
| Vapor Fraction | | 0 | 0 | 0 | 0 | 0 | 0 | 0.25 | 0 | 1 | 1 | 1 |
| Liquid Fraction | | 1 | 1 | 1 | 1 | 1 | 1 | 0.75 | 1 | 0 | 0 | 0 |

*Table 51: (continued)*

| | Units | G004 | G005 | G006 | G007 | LPSTEAM | M001 | M002 | M003 | M004 | M005 | METHANOL |
|---|---|---|---|---|---|---|---|---|---|---|---|---|
| From | | K–02 | M–01 | E–01 | T–01 | E–03 | C–01 | E–03 | E–01 | E–04 | | C–02 |
| To | | M–01 | E–01 | C–01 | | | E–03 | E–01 | E–04 | T–01 | C–02 | |
| Substream: MIXED | | | | | | | | | | | | |
| Phase: | | Vapor | Vapor | Vapor | Vapor | Vapor | Vapor | Mixed | Mixed | Mixed | Mixed | Liquid |
| Component Mole Flow | | | | | | | | | | | | |
| $H_2$ | KMOL/HR | 0 | 69 | 69 | 8.94 | 0 | 9.00 | 9.00 | 9.01 | 9.01 | 0.069 | 0.008 |
| $H_2O$ | KMOL/HR | 0 | 0 | 0 | 0.061 | 41.08 | 19.99 | 19.99 | 19.99 | 19.99 | 0.00045 | 0.00042 |
| $CO_2$ | KMOL/HR | 20 | 20 | 20 | 0.003 | 0 | 0.0015 | 0.0015 | 0.0037 | 0.0037 | 19.93 | 0.011 |
| METHANOL | KMOL/HR | 0 | 0 | 0 | 0.18 | 0 | 19.99 | 19.99 | 19.99 | 19.99 | 19.82 | 19.80 |
| BUTANOL | KMOL/HR | 0 | 0 | 0 | 0.024 | 0 | 12.03 | 12.03 | 12.02 | 12.02 | 12.00 | 4.59E–08 |
| Mole Flow | KMOL/HR | 20 | 89 | 89 | 9.21 | 41.08 | 61.02 | 61.02 | 61.02 | 61.02 | 51.81 | 19.83 |
| Mass Flow | KG/HR | 880.20 | 1019.29 | 1019.29 | 26.70 | 740.00 | 1910.53 | 1910.53 | 1910.04 | 1910.04 | 1883.34 | 634.95 |
| Volume Flow | L/MIN | 308.31 | 1509.08 | 1934.01 | 572.64 | 5181.82 | 1354.96 | 408.22 | 325.75 | 206.83 | 39.92 | 14.00 |
| Temperature | ℃ | 40 | 32.59748 | 120 | 40 | 147.95 | 186.69 | 152.32 | 134.4698 | 40 | 40 | 55 |
| Pressure | BAR | 25 | 25 | 25 | 7 | 4.5 | 24.5 | 24.5 | 24.5 | 24.5 | 7 | 6.5 |
| Vapor Fraction | | 1 | 1 | 1 | 1 | 1 | 1 | 0.25 | 0.20 | 0.14 | 0.00 | 0 |
| Liquid Fraction | | 0 | 0 | 0 | 0 | 0 | 0 | 0.75 | 0.80 | 0.86 | 1.00 | 1 |

*Table 51: (continued)*

| | Units | PURGE | PURGE2 | SUPPLYW | W001 | W002 | W003 | W004 | W005 | W006 | WASTEW |
|---|---|---|---|---|---|---|---|---|---|---|---|
| From | | C–02 | T–02 | | C–03 | B1 | E–05 | T–02 | T–02 | C–04 | C–04 |
| To | | | | E–03 | B1 | E–05 | T–02 | C–04 | C–03 | B1 | |
| Substream: MIXED | | | | | | | | | | | |
| Phase: | | Vapor | Missing | Liquid | Vapor | Mixed | Liquid | Liquid | Liquid | Vapor | Liquid |
| Component Mole Flow | | | | | | | | | | | |
| $H_2$ | KMOL/HR | 0.061 | 0 | 0 | 0 | 0 | 0 | 0 | 0 | 0 | 0 |
| $H_2O$ | KMOL/HR | 2.71E–05 | 0 | 41.08 | 0 | 0 | 0 | 0 | 0 | 0 | 0 |
| $CO_2$ | KMOL/HR | 1.54E–06 | 0 | 0 | 43.40 | 44.26 | 44.26 | 19.93 | 24.33 | 0.863 | 19.07 |
| METHANOL | KMOL/HR | 0.0072 | 0 | 0 | 0.0086 | 0.0090 | 0.0090 | 0.0019 | 0.0071 | 0.00042 | 0.0015 |
| BUTANOL | KMOL/HR | 1.82E–12 | 0 | 0 | 12.62 | 12.87 | 12.87 | 1.10 | 11.78 | 0.25 | 0.85 |
| Mole Flow | KMOL/HR | 0.068 | 0 | 41.08 | 56.03 | 57.14 | 57.14 | 21.03 | 36.11 | 1.11 | 19.92 |
| Mass Flow | KG/HR | 0.35 | 0 | 740 | 1717.68 | 1751.85 | 1751.85 | 440.46 | 1311.43 | 34.17 | 406.29 |
| Volume Flow | L/MIN | 4.75 | 0 | 18.32 | 28062.99 | 28621.27 | 43.27 | 10.49 | 32.78 | 558.29 | 9.65 |
| Temperature | ℃ | 55 | | 147.95 | 93.30 | 93.30 | 93.23 | 93.30 | 93.30 | 93.30 | 93.55 |
| Pressure | BAR | 6.5 | 1 | 4.5 | 1 | 1 | 1 | 1 | 1 | 1 | 1 |
| Vapor Fraction | | 1 | | 0 | 1 | 1 | 0 | 0 | 0 | 1 | 0 |
| Liquid Fraction | | 0 | | 1 | 0 | 7.74E–09 | 1 | 1 | 1 | 0 | 1 |

## References

[1] Pbl.nl. (2018). Trends in global CO2 and total greenhouse gas emissions: 2017 report – PBL Netherlands Environmental Assessment Agency.

[2] US EPA. (2018). Sources of Greenhouse Gas Emissions | US EPA.

[3] Globalccsinstitute.com. (2018). Accelerating the uptake of CCS: industrial use of captured carbon dioxide | Global Carbon Capture and Storage Institute.

[4] Alvarado, M. (2018). Methanol Industry Overview.

[5] Zhang et al. (2016). Comparative studies on carbon dioxide emissions of typical modern coal. CHEMICAL INDUSTRY AND ENGINEERING PROGRESS, 35(12), 4060–4064.

[6] Qi et al. Thermodynamics Research of Methanol to Olefins (MTO). CHEMICAL ENGINEERING OF OIL & GAS 34.5(2005):349–353.

[7] Feng et al. Study on thermodynamics of methanol to aromatic reaction. Petrochemical Technology & Application. 35.2(2017):101–105.

[8] Ilias, Samia, and Aditya Bhan. "Mechanism of the catalytic conversion of methanol to hydrocarbons." ACS Catalysis 3.1 (2012): 18–31.

[9] Gu Daobin. The development on MTO process and catalyst. PETROCHEMICAL INDUSTRY TECHNOLOGY 4 (2013): 39–45.

[10] Li Changyan et al. Methanol to Olefins Technology VS Traditional Petroleum Hydrocarbons Cracking to Olefins Technology [J]. Coal Chemical Industry, 2011, 39(6): 41–44

[11] Wen Qian. The technological and economic analysis of MTA[J]. Coal Chemical Industry, 2012,40(02):1–4.

[12] Delledonne, Daniele, Franco Rivetti, and Ugo Romano. "Developments in the production and application of dimethylcarbonate." Applied Catalysis A: General 221.1–2 (2001): 241–251.

[13] Qi Zengzhong. Study on Dimethyl Carbonate Prepared from Urea and Methanol. Diss. Sichuan University, 2006.

[14] Li, Huaju, et al. "Designed SO42−/Fe2O3–SiO2 solid acids for

polyoxymethylene dimethyl ethers synthesis: The acid sites control and reaction pathways." Applied Catalysis B: Environmental 165 (2015): 466–476.

[15] Gao Xiaochen et al. New method of DMMn preparation, CN104276932A. 2015.

[16] Chen Jing et al. New method of DMMn preparation, CN 101182367 A. 2008.

[17] Słoczyński J, et al. Catalytic activity of the M/(3ZnO·ZrO2) system (M=Cu, Ag, Au) in the hydrogenation of CO2 to methanol [J]. *Applied Catalysis A*：*General*, 2004, 278：11–23.

[18] Toyir J, et al. Highly effective conversion of CO2 to methanol over supported and promoted copper–based catalysts ： Influence of support and promoter [J]. *Applied Catalysis B*：*Environmental*, 2001, 29：207–215.

[19] Toyir J, et al. Catalytic performance for CO2 conversion to methanol of gallium–promoted copper–based catalysts：Influence of metallic precursors [J]. *Applied Catalysis B*：*Environmental*, 2001, 34：255–266.

[20] Saito M, et al. Development of copper/zinc oxide–based multicomponent catalysts for methanol synthesis from carbon dioxide and hydrogen [J]. *Applied Catalysis A*：*General*, 1996, 138：311–318.

[21] Xu et al. The active center of CO2/H2 synthesis based on CuO–ZnO catalyst [J]. Chinese Journal of Catalysis, 1994, 15(2)：97–102.

[22] Zhang et al. Low–pressure CO2/H2 methanol synthesis based on CuO–ZnO and CuO–ZnO–ZrO2 catalyst [J]. Chinese Journal of Catalysis, 1989, 10(1)：22–28.

[23] Fierro G, et al. Study of the reducibility of copper in CuO–ZnO catalysts by temperature–programmed reduction [J]. *Applied Catalysis A*：*General*, 1996, 137：327–348.

[24] Liu et al. *In situ* EXAFS studies of copper on ZrO2 during catalytic hydrogenation of CO2 [J]. *Journal of Electron Spectronscopy and Related Phenomena*, 2005, 144–147：373–376.

[25] Arena F, et al. Solid–state interactions, adsorption sites and functionality of Cu–ZnO/ZrO2 catalysts in the CO2 hydrogenation to CH3OH [J]. *Applied Catalysis A*：*General*, 2008, 350：16–23.

[26] Kakumoto T, Watanabe T. A theoretical study for methanol synthesis by CO2 hydrogenation [J]. *Catalysis Today*, 1997, 36：39–44.

[27] Wang G C, Zhao Y Z, Cai Z S, et al. Investigation of the active sites of CO2 hydrogenation to methanol over a Cu–based catalyst by the UBI–QEP approach [J]. *Surface Science*, 2000, 465：51–58.

[28] Wang G C et al. Investigation of the active sites of CO2 hydrogenation to methanol over a Cu–based catalyst by the UBI–QEP approach [J]. Surface Science, 2000, 465: 51–58.

[29] Clausen B S, et al. *In situ* cell for combined XRD and on–line catalysis tests：Studies of Cu–based water gas shift and methanol catalysts [J]. *Journal of Catalysis*, 1991, 132：524–535.

[30] Xu et al. The surface composition of CO2 methanol synthesis copper–basd catalyst [J]. Journal of Fuel Chemistry and Technology, 1994, 22(2)：176–181.

[31] Yoshihara J, et al. Methanol synthesis and reverse water–gas shift kinetics over clean polycrystalline copper [J]. *Catalysis Letters*, 1995, 31：313–324.

[32] Yoshihara J, Campbell C T. Methanol synthesis and reverse water–gas shift kinetics over Cu (110) model catalysts：Structural sensitivity [J]. *Journal of Catalysis*, 1996, 161：776–782.

[33] Rasmussen P B, et al. Methanol synthesis on Cu (100) from a binary gas mixture of CO2 and H2 [J]. *Catalysis Letters*, 1994, 26：373–381.

[34] Chinchen G C, et al. The activity and state of the copper surface in methanol synthesis catalysts [J]. *Applied Catalysis*, 1986, 25：101–107.

[35] Pan, et al. Methanol synthesis activity of Cu/ZnO catalysts [J]. *Journal of Catalysis*, 1988, 114：440–446.

[36] Arena F, et al. Synthesis, characterization and activity pattern of Cu–ZnO/ZrO2 catalysts in the hydrogenation of carbon dioxide to methanol [J]. *Journal of Catalysis*, 2007, 249：185–194.

[37] Sun et al. A novel process for preparation of Cu/ZnO and Cu/ZnO/Al2O3 ultrafine catalyst：Structure, surface properties, and activity for methanol

synthesis from CO2 + H2 [J]. *Journal of Catalysis*, 1997, 167：92–105.

[38] Słoczyński J, et al. Effect of Mg and Mn oxide additions on structural and adsorptive properties of Cu/ZnO/ZrO2 catalysts for the methanol synthesis from CO2 [J]. *Applied Catalysis A*：*General*, 2003, 249：129–138.

[39] Zhang et al. Methanol synthesis from CO2 hydrogenation over Cu based catalyst supported on zirconia modified γ–Al2O3 [J]. *Energy Conversion and Management*, 2006, 47：3360–3367.

[40] Liu et al. Role of nanosized zirconia on the properties of Cu/Ga2O3/ZrO2 catalysts for methanol synthesis [J]. *Chinese Journal of Chemistry*, 2006, 24：172–176.

[41] Liu et al. Nanocrystalline zirconia as catalyst support in methanol synthesis [J]. *Applied Catalysis A*：*General*, 2005, 279：241–245.

[42] Wang et al. Synergistic catalysis of carbon dioxide hydrogenation into methanol by yttria–doped ceria/–alumina–supported copper oxide catalyst：Effect of promotor and dopant [J]. *Catalysis Letters*, 2002, 83：79–86.

[43] Zhong et al. Catalytic Performance of ZrO2–SiO2 Supported Ni–Cu Alloy Catalysts for CO2 Hydrogenation [J]. Journal of Fuel Chemistry and Technology, 2001, 29(2)：154–158.

[44] Cong et al. Characterization of Ultrafine Cu–ZnO–ZrO2 Catalysts for Methanol Synthesis via CO2 Hydrogenation [J]. CHINESE JOURNAL OF CATALYSIS, 2000, 21(4)：314–318.

[45] Shao et al. Selective methanol synthesis from CO2/H2 on new SiO2–supported PtW and PtCr bimetallic catalysts [J]. *Applied Catalysis A*：*General*, 1995, 128：L1–L6.

[46] Shao et al. *In–situ* FT–IR studies on the CO2 hydrogenation over the SiO2–supported RhM (M=Cr, Mo, W) complex catalysts [J]. *Journal of Molecular Catalysis A*：*Chemical*, 2001, 166：331–335.

[47] Inoue T, et al. Hydrogenation of carbon dioxide and carbon monoxide over supported rhodium catalysts under 10 bar pressures [J]. *Applied Catalysis*, 1989,

46：1–9.

[48] Solymosi F, et al. Surface interaction between H2 and CO2 over palladium on various supports [J]. *Journal of Catalysis*, 1985, 95：567–577.

[49] Shen W J, et al. Effect of reduction temperature on structural properties and CO/CO2 hydrogenation characteristics of a Pd–CeO2 catalyst [J]. *Applied Catalysis A*：*General*, 2001, 217：231–239.

[50] Köppel R A, et al. Copper– and silver–Zirconia aerogels：Preparation, structural properties and catalytic behavior in methanol synthesis from carbon dioxide [J]. *Journal of Catalysis*, 1998, 179：515–527.

[51] Melián–Cabrera I, et al. Reverse topotactic transformation of a Cu–Zn–Al catalyst during wet Pd impregnation：Relevance for the performance in methanol synthesis from CO2/H2 mixtures [J] *Journal of Catalysis*, 2002, 210：273–284.

[52] Melián–Cabrera I, et al. Pd–Modified Cu–Zn catalysts for methanol synthesis from CO2/H2 mixtures：Catalytic structures and performance [J]. *Journal of Catalysis*, 2002, 210：285–294.

[53] Calafatat A, et al. Effects of phase composition and of potassium promotion on cobalt molybdate catalysts for the synthesis of alcohols from CO2 and H2 [J]. *Applied Catalysis A*：*General*, 1998, 172：217–224.

[54] Tagawa T, et al. Effect of supports on copper catalysts for methanol synthesis from CO2+H2 [J]. *Research on Chemical Intermediates*, 1995, 21：193–202.

[55] Nomura N, et al. Effect of acid–base properties on copper catalysts for hydrogenation of carbon dioxide [J]. *Reaction Kinetics Catalysis Letters*, 1998, 63：21–25.

[56] Guo et al. The influence of La doping on the catalytic behavior of Cu/ZrO2 for methanol synthesis from CO2 hydrogenation [J]. *Journal of Molecular Catalysis A*：*Chemical*, 2011, 345：60–68.

[57] Jung et al. Effects of zirconia phase on the synthesis of methanol over zirconia–supported copper [J]. *Catalysis Letters*, 2002, 80：63–68.

[58] Xu et al. CO2/H2 methanol catalytic synthesis performance under low–pressure

[J]. Petrochemical Technology, 1993, 22(10)：655–660.

[59] Xu et al. ZrO2 promotion on CuO–ZnO–ZrO2 catalyst of low pressure methanol synthesis [J]. Chemical Journal of Chinese Universities, 1991, 12(6)：825–826.

[60] Li et al. function of CO2 methanol synthesis catalyst [J]. Natural Gas Chemical Industry, 1997, 22(5)：13–16.

[61] Nomura N, el al. Titania supported copper catalysts for methanol synthesis from carbon dioxide[J]. *Reaction Kinetics Catalysis Letters*, 1998, 63：9–13.

[62] Ma et al. A practical approach for the preparation of high activity Cu/ZnO/ZrO2 catalyst for methanol synthesis from CO2 hydrogenation[J]. *Applied Catalysis A*：*General*, 1998, 171：45–55.

[63] Qi et al. Hydrogenation of Carbon Dioxide on Cu–MnOx/Al2O3 Catalysts [J]. PETROCHEMICAL TECHNOLOGY, 1999, 28(10)：660–662.

[64] Zhu et al. Characterization and catalytic activity evaluation of ultrafine Cu/ZnO/TiO2–SiO2 catalysts for CO2 hydrogenation to methanol [J]. JOURNAL OF FUEL CHEMISTRY AND TECHNOLOGY, 2004, 32(4)：486–491.

[65] Fisher I A, el al. Effects of zirconia promotion on the activity of Cu/SiO2 for methanol synthesis from CO/H2 and CO2/H2 [J]. *Catalysis Letters*, 1997, 44：11–17.

[66] Bianchi D, et al. Intermediate species on zirconia supported methanol aerogel catalysts V. Adsorption of methanol [J]. *Applied Catalysis A*：*General*, 1995, 123：89–110.

[67] Chi et al. Assistant effect to ultra–fine catalyst of CO2 hydrogenation [J]. Journal of Molecular Catalysis, 1996, 10(6)：430–434.

[68] Liu et al. EFFECT OF LA2O3 ON THE CATALYTIC PERFORMANCE AND PROPERTIES OF CU/ZNO CATALYST FOR HYDROGENATION OF CO2 [J]. CHEMICAL ENGINEERING OF OIL AND GAS, 2001, 30(2)：55–57.

[69] Huang et al. Effect of Promoter on Performance of CuO–ZnO–Al2O3 Catalyst for CO2 Hydrogenation to Methanol [J]. PETROCHEMICAL TECHNOLOGY, 2009, 38(5)：482–485.

[70] Zhang et al. Study of CO2 hydrogenation to methanol over Cu–V/γ–Al2O3

catalyst [J]. *Journal of Natural Gas Chemistry*, 2007, 16：12–15.

[71] Wang et al. Promotion effect of V on CuO/Al2O3 catalyst for methanol synthesis from CO2 hydrogenation [J]. NATURAL GAS CHEMICAL INDUSTRY, 1999, 24(6)：12–16.

[72] Yin et al. Methanol synthesis from CO/CO2 hydrogenation over Cu/Zn/Al/Mn catalyst [J]. JOURNAL OF FUEL CHEMISTRY AND TECHNOLOGY, 2004, 32(4)：492–497.

[73] Lachowska M, et al. Methanol synthesis from carbon dioxide and hydrogen over Mn–promoted copper/zinc/zirconia catalysts [J]. *Reaction Kinetics Catalysis Letters*, 2004, 83：269–273.

[74] Inui T, et al. Structure and function of Cu–based composite catalysts for highly effective synthesis of methanol by hydrogenation of CO2 and CO [J]. *Catalysis Today*, 1997, 36：25–32.

[75] Słoczyński J, et al. Effect of metal oxide additives on the activity and stability of Cu/ZnO/ZrO2 catalysts in the synthesis of methanol from CO2 and H2 [J]. *Applied Catalysis A*：*General*, 2006, 310：127–137.

[76] Yang et al. Studies on the Dispersion Structure of Co–precipitated CuO–ZrO2 Mixed Oxides [J]. ACTA PHYSICO–CHIMICA SINICA, 2003, 19(8)：714–717.

[77] Nitta Y, et al. Effect of starting salt on catalytic behaviour of Cu–ZrO2 catalysts in methanol synthesis from carbon dioxide [J]. *Catalysis Letters*, 1993, 17：157–165.

[78] Deng J F, et al. A novel process for preparation of a Cu/ZnO/A12O3 ultrafine catalyst for methanol synthesis from CO2+H2：Comparison of various preparation methods [J]. *Applied Catalysis A*：*General*, 1996, 139：75–85.

[79] Ning et al. Study of the effect of preparation method on CuO–ZnO–Al2O3 catalyst [J]. *Applied Catalysis A*：*General*, 2001, 211：153–157.

[80] Liu et al. PREPARATION OF CuO/ZnO CATALYST FOR METHANOL SYNTHESIS BY CARBON DIOXIDE HYDROGENATION [J]. PETROLEUM

PROCESSING AND PETROCHEMICALS, 2000, 31(9)：58–61.

[81] Zhao et al. Study on the synthesis of methanol by low pressure hydrogenation of carbon dioxide over CuO–ZnO–Al_2O_3 catalyst [J]. NATURAL GAS CHEMICAL INDUSTRY, 2009, 34(6)：4–10.

[82] Fujita S I, et al. Methanol synthesis from CO2 over Cu/ZnO catalysts prepared from various coprecipitated precursors [J]. *Catalysis Today*, 1998, 45：241–244.

[83] Raudaskoski R, et al. The effect of ageing time on co–precipitated Cu/ZnO/ZrO2 catalysts used in methanol synthesis from CO2 and H2 [J]. *Topics in Catalysis*, 2007, 45：57–60.

[84] Hong et al. CO2 hydrogenation to methanol over Cu/ZnO/Al2O3 catalysts by a novel gel–network–coprecipitation method[J]. *Catalysis Letters*, 2002, 82：37–44.

[85] Shi et al. PREPARATION AND CHARACTERIZATION OF ULTRAFINE PARTICLE CUO/ZRO2 CATALYSTS Ⅰ. EFFECT OF HYDROGEL PH VALUE ON THE MORPHOLOGY OF THE CATALYSTS [J]. CHINESE JOURNAL OF CATALYSIS, 1996, 17(4)：277–280.

[86] Guo et al. Cu/Zn/Al xerogels and aerogels prepared by a sol–gel reaction as catalysts for methanol synthesis[J]. *European Journal of Inorganic Chemistry*, 2006, 2006 (23)：4774–4781.

[87] Su et al. Recent Developments of Low–Temperature Combustion Synthesis of Ultrafine Ceramic Powder [J]. PROGRESS IN CHEMISTRY, 2005, 17(3)：430–436.

[88] Patil K C, et al. Combustion synthesis：An update [J]. *Current Opinion in Solid State and Materials Science*, 2002, 6：507–512.

[89] Guo, et al. Combustion synthesis of CuO–ZnO–ZrO2 catalysts for the hydrogenation of carbon dioxide to methanol [J]. *Catalysis Communications*, 2009, 10：1661–1664.

[90] Guo, et al. Glycine–nitrate combustion synthesis of CuO–ZnO–ZrO2 catalysts for methanol synthesis from CO2 hydrogenation [J]. *Journal of Catalysis*, 2010,

271：178–185.

[91] Ye, et al. One–step solid–state reactions at ambient temperatures—A novel approach to nanocrystal synthesis [J]. *Advanced Materials*, 1999, 11：941–942.

[92] Wang, et al. Production of hydrogen by steam reforming of methanol over Cu/ZnO catalysts prepared *via* a practical soft reactive grinding route based on dry oxalate–precursor synthesis[J]. *Journal of Catalysis*, 2007, 246：193–204.

[93] Guo, et al. CO2 hydrogenation to methanol over Cu/ZnO/ZrO2 catalysts prepared *via* a route of solid state reaction [J]. *Catalysis Communications*, 2011, 12：1095–1098.

[94] Chi, et al. FFECT OF PRETREATMENT CONDITIONS ON THE PROPERTIES AND ACTIVITIES OF ULTRAFINE CUO ZNO SIO 2 CATALYSTS FOR HYDROGENATION OF CARBON DIOXIDE [J]. JOURNAL OF MOLECULAR CATALYSIS, 1996, 10(6)：423–429.

[95] Fujita S, et al. Preparation of a coprecipitated Cu/ZnO catalyst for the methanol synthesis from CO2—Effects of the calcination and reduction conditions on the catalytic performance [J]. *Applied Catalysis A*：*General*, 2001, 207：121–128.

[96] Cao, et al. Preparation of High Performance Cu/ZnO/Al2O3 Catalyst for Methanol Synthesis from CO2 Hydrogenation by Coprecipitation–reduction [J]. CHEMICAL JOURNAL OF CHINESE UNIVERSITIES, 2003, 24(7)：1296–1298.

[97] Weigel J, et al. Surface species in CO and CO2 hydrogenation over copper/zirconia：On the methanol synthesis mechanism [J]. *Langmuir*, 1996, 12：5319–5329.

[98] Klier K. Methanol synthesis [J]. *Advances in Catalysis*, 1982, 31：243–313.

[99] Chinchen G C, et al. Mechanism of methanol synthesis from CO2/CO/H2 mixtures over copper/zinc oxide/alumina catalysts：Use of 14C–labelled reactants [J]. *Applied Catalysis*, 1987, 30：333–338.

[100] Sun, et al. In situ IR studies on the mechanism of methanol synthesis over an ultrafine Cu/ZnO/Al2O3 catalyst [J]. Applied Catalysis A：General, 1998, 171：301–308.

[101] Mao, et al. STUDY ON THE REACTION MECHANISM OF CO2 HYDROGENATION OVER CUO/ZNO/ZRO2 CATALYST [J]. CHINESE JOURNAL OF CATALYSIS, 1992, 13(3)：187–191.

[102] Clarke D B, Bell A T. An infrared study of methanol synthesis from CO2 on clean and potassium–promoted Cu/SiO2[J]. *Journal of Catalysis*, 1995, 154：314–328.

[103] Cong, et al. TPSR AND TPD STUDIES OF ULTRAFINE Cu–ZnO–ZrO2 CATALYSTS FOR METHANOL SYNTHESIS [J]. JOURNAL OF FUEL CHEMISTRY AND TECHNOLOGY, 2000, 28(3)： 238–243.

[104] Jung K D, Bell A T. Role of hydrogen spillover in methanol synthesis over Cu/ZrO2 [J]. *Journal of Catalysis*, 2000, 193：207–223.

[105] Fujita S I, et al. Mechanisms of methanol synthesis from carbon dioxide and from carbon monoxide at atmospheric pressure over Cu/ZnO [J]. *Journal of Catalysis*, 1995, 157：403–413.

[106] Fisher I A, Bell A T. *In–situ* infrared study of methanol synthesis from H2/CO2 over Cu/SiO2 and Cu/ZrO2/SiO2 [J]. *Journal of Catalysis*, 1997, 172：222–237.

[107] Hong, et al, Mechanism of CO2 hydrogenation over Cu/ZrO2 ( –212) interface from first–principles kinetics Monte Carlo simulations [J]. *Surface Science*, 2010, 604：1869–1876.

[108] Fujitani T, et al. Scanning tunneling microscopy study of formate species synthesized from CO2 hydrogenation and prepared by adsorption of formic acid over Cu (111) [J]. *Journal of Physical Chemistry B*, 2000, 104：1235–1240.

[109] Yang R. A new method of low–temperature methanol synthesis on Cu/ZnO/Al2O3 catalysts from CO/CO2/H2 [J]. Fuel, 2008,87(4–5): 443–450.

[110] Chu et al. Investigation on the Catalysts and Reaction Process for the Methanol Synthesis at Lower–Temperature in Liquid Phase [J]. Progress in chemistry, 2001, 13(2): 128–134.

[111] Zeng et al.The promoting effect of alcohols in a new process of low–temperature synthesis of methanol from CO/CO2/H2[J].Fuel, 2002, 81:125–127.

[112] Yang et al. Spectroscopic and kinetic analysis of a new low–temperature methanol synthesis reaction[J]. Catal Lett, 2006,106(3–4): 153–159.

[113] Yang et al.Rideal–type reaction of formate species with alcohol: A key step in new low temperature methanol synthesis method[J]. Catal Commun, 2007, 8: 1829–1833.

[114] Yang R. Mechanistic study of a new low–temperature methanol synthesis on Cu/MgO catalysts[J]. Appl Catal A, 2005, 288(1–2): 126–133.

[115] Yang R. In situ DRIFT study of low–temperature methanol synthesis mechanism on Cu/ZnO catalysts from COcontaining syngas using ethanol promoter[J]. J Catal, 2004, 228(1): 23–35.

[116] Zhang et al. A new low–temperature methanol synthesis method: Mechanistic and kinetics study of catalytic process[J]. Catal Today, 2008, 132(1–4): 93–100.

[117] Reubroycharoen P. Continuous low–temperature methanol synthesis from CO/CO2/H2[J]. Energy Fuels, 2003, 17: 817–821.

[118] Reubroycharoen P. Development of a new low–temperature methanol synthesis process[J]. Catal Today, 2004, 89(4): 447–454.

[119] Bao J. Preparation of mesoporous Cu/ZnO catalyst and its application in low–temperature methanol synthesis [J]. Catal Commun, 2008,9(5): 913–918.

[120] Zhao T. Promotional effect of potassium salt in low temperature formate and methanol synthesis from CO/CO2/H2 on copper catalyst[J]. Chem Lett, 2007, 36(6):734–735.

[121] Xu B. A new method of low temperature methanol synthesis[J]. Catal Surv Asia, 2009, 13(3): 147–163.

[122] Filonenko, Georgy A., et al. "On the activity of supported Au catalysts in the liquid phase hydrogenation of CO2 to formates." Journal of Catalysis 343 (2016): 97–105.

[123] Liu, Qinggang, et al. "Direct catalytic hydrogenation of CO 2 to formate over a Schiff–base–mediated gold nanocatalyst." Nature communications 8.1 (2017): 1407.

[124] Ganguly, Gaurab, Munia Sultana, and Ankan Paul. "Photochemical Hydrogenation of CO2 to CH3OH and Pyridine to 1, 2–Dihydropyridine Using Plasmon–Facilitated Chemisorbed Hydrogen on Au Surface: Theoretical Perspective." The Journal of Physical Chemistry C 121.28 (2017): 15326–15332.

[125] Zhan, Guowu, and Hua Chun Zeng. "ZIF–67–Derived Nanoreactors for Controlling Product Selectivity in CO2 Hydrogenation." ACS Catalysis 7.11 (2017): 7509–7519.

[126] Vourros, A., et al. "Carbon dioxide hydrogenation over supported Au nanoparticles: Effect of the support." Journal of CO2 Utilization 19 (2017): 247–256.

[127] Willauer, Heather D., et al. "Modeling and kinetic analysis of CO2 hydrogenation using a Mn and K–promoted Fe catalyst in a fixed–bed reactor." Journal of CO2 Utilization 3 (2013): 56–64.

[128] Gesmanee, Sumpan, and Wanida Koo–Amornpattana. "Catalytic hydrogenation of CO 2 for methanol production in fixed–bed reactor using Cu–Zn supported on gamma–Al 2 O 3." Energy Procedia 138 (2017): 739–744.

[129] Guo, Xiaoming, et al. "Glycine–nitrate combustion synthesis of CuO–ZnO–ZrO2 catalysts for methanol synthesis from CO2 hydrogenation." Journal of Catalysis 271.2 (2010): 178–185.

[130] Bahruji, Hasliza, et al. "Pd/ZnO catalysts for direct CO2 hydrogenation to methanol." Journal of Catalysis 343 (2016): 133–146.

[131] Yan, Shi–Run, et al. "Promotion effect of Fe–Cu catalyst for the hydrogenation of CO2 and application to slurry reactor." Applied Catalysis A: General 194 (2000): 63–70.

[132] Zhang, Yanfei, et al. "Catalytic performance of spray–dried Cu/ZnO/Al2O3/ZrO2 catalysts for slurry methanol synthesis from CO2 hydrogenation." Journal of CO2 Utilization 15 (2016): 72–82.

[133] Shaharun, Salina, et al. "Catalytic Performance of Cu/ZnO/Al2O3/ZrO2 for Slurry Methanol Synthesis from CO2 Hydrogenation: Effect of Cu/Zn Molar Ratio." SAINS MALAYSIANA 47.1 (2018): 207–214.

[134] Kim, Jun Sik, et al. "Characteristics of carbon dioxide hydrogenation in a fluidized bed reactor." Korean Journal of Chemical Engineering 18.4 (2001): 463–467.

[135] Gallucci, Fausto, Luca Paturzo, and Angelo Basile. "An experimental study of CO2 hydrogenation into methanol involving a zeolite membrane reactor." Chemical Engineering and Processing: Process Intensification 43.8 (2004): 1029–1036.

[136] Chen, Guangwen, and Quan Yuan. "Methanol synthesis from CO2 using a silicone rubber/ceramic composite membrane reactor." Separation and purification technology 34.1–3 (2004): 227–237.

[137] ALMEIDA–RIVERA C P, et al. Designing reactive distillation processes: present and future[J]. Computers and Chemical Engineering, 2004, **28**(10): 1997–2020.

[138] Babcock P.D. Clump PD. Recent development in separation science. Vol (IV): 149.166. Ed. by Norman (1978)

[139] GAO X et al. " Review of basic and application investigation of reactive distillation technology for process intensification." *CIESC Jorunal.* 69.1(2017).

[140] ZENG Y R. Study on feasibility for reactive distillation using graphical method[D]. Fuzhou: Fuzhou University, 2014.

[141] LI H, MA X H, LI X G, *et al.* Research progress of reactive distillation process design[J]. Modern Chemical Industry, 2016,**36**(12): 132–135.

[142] VENIMADHAVAN G, BUZAD G, DOHERTY M F, *et al.* Effect of kinetics on residue curve maps for reactive distillation[J]. AIChE Journal, 1994, **40**(11): 1814–1824.

[143] VENIMADHAVAN G, MALONE M F, DOHERTY M F. Bifurcation study of kinetic effects in reactive distillation[J]. AIChE Journal, 1999, **45**(3): 546–556.

[144] UNG S, DOHERTY M F. Calculation of residue curve maps for mixtures with multiple equilibrium chemical reactions[J]. Ind. Eng. Chem. Res., 1995, **34**(10): 3195–3202.

[145] UNG S, DOHERTY M F. Synthesis of reactive distillation systems with

multiple equilibrium chemical reactions[J]. Ind. Eng. Chem. Res., 1995, **34**(8): 2555–2565.

[146] CHIPLUNKAR M, HONG M, MALONE M F, *et al.* Experimental study of feasibility in kinetically–controlled reactive distillation[J]. AIChE Journal, 2005, **51**(2): 464–479.

[147] GIESSLER S, DANILOV R Y, PISARENKO R Y, *et al.* Feasibility study of reactive distillation using the analysis of the statics[J]. Ind. Eng. Chem. Res., 1998, **37**(11): 4375–4382.

[148] GIESSLER S, DANILOV R Y, PISARENKO R Y, *et al.* Feasible separation modes for various reactive distillation systems[J]. Ind. Eng. Chem. Res, 1999, **38**(10): 4060–4067.

[149] SERAFIMOV L A, PISARENKO Y A, KULOV N N. Coupling chemical reaction with distillation: thermodynamic analysis and practical applications[J]. Chemical Engineering Science, 1999, **54**(10): 1383–1388.

[150] GIESSLER S, DANILOV R Y, PISARENKO R Y, *et al.* Design and synthesis of feasible reactive distillation processes[J]. Computers and Chemical Engineering Supplement, 1999, **23**: S811–S814.

[151] OKASINSKI M J, DOHERTY M F. Design method for kinetically controlled, staged reactive distillation columns[J]. Ind. Eng. Chem. Res., 1998, **37**(7): 2821–2834.

[152] HUSS R S, CHEN F, MALONE M F, *et al.* Computer–aided tools for the design of reactive distillation systems[J]. Computers and Chemical Engineering Supplement, 1999, **23**: S955–S962.

[153] HUSS R S, CHEN F, MALONE M F, *et al.* Reactive distillation for methyl acetate production[J]. Computers and Chemical Engineering, 2003, **27**(12): 1855–1866.

[154] GADEWAR S B, MALONE M F, DOHERTY M F. Feasible region for a countercurrent cascade of vapor–liquid CSTRS[J]. AIChE Journal, 2002, **48**(4): 800–814.

[155] GADEWAR S B, TAO L, MALONE M F, *et al.* Process alternatives for

coupling reaction and distillation[J]. Chemical Engineering Research and Design, 2006, **82**(A2): 140–147.

[156] JANTHARASUK A, GANI R, GÓRAK A, *et al.* Methodology for design and analysis of reactive distillation involving multielement systems[J]. Chemical Engineering Research and Design, 2011, **89**(8): 1295–1307.

[157] CHADDA N, MALONE M F, DOHERTY M F. Effect of chemical kinetics on feasible splits for reactive distillation[J]. AIChE Journal, 2001, **47**(3): 590–601.

[158] CHADDA N, MALONE M F, DOHERTY M F. Feasibility and synthesis of hybrid reactive distillation systems[J]. AIChE Journal, 2002, **48**(12): 2754–2768.

[159] ZHOU C G, GAO J, ZHAO W. Research progress of graphical design for reactive distillation process[J]. Chemical Engineering, 2002, **30**(4): 63–67.

[160] SHAH M, KISS A A, ZONDERVAN E, *et al.* A systematic framework for the feasibility and technical evaluation of reactive distillation processes[J]. Chemical Engineering and Processing, 2012, **60**: 55–64.

[161] MALONE M F, DOHERTY M F. Reactive distillation[J]. Ind. Eng. Chem. Res., 2000, **39**(11): 3953–3957.

[162] KELLER T, DREISEWERD B, GÓRAK A. Reactive distillation for multiple–reaction systems: optimization study using an evolutionary algorithm[J]. Chemical and Process Engineering, 2013, **34**(1): 17–38.

[163] KELLER T, DREISEWERD B, GÓRAK A. Reactive distillation for multiple–reaction systems: optimization study using an evolutionary algorithm[J]. Chemical and Process Engineering, 2013, **34**(1): 17–38.

[164] SEGOVIA–HERNÁNDEZ J G, HERNANDEZ S, PETRICIOLET A B. Reactive distillation: a review of optimal design using deterministic and stochastic techniques[J]. Chemical Engineering and Processing, 2015, **97**: 134–143.

[165] NIESBACH A, KUHLMANN H, KELLER T, *et al.* Optimization of industrial–scale *n*–butyl acrylate production using reactive distillation[J]. Chemical Engineering Science, 2013, **100**: 360–372.

[166] GONZÁLEZ–RUGERIO C A, FUHRMEISTER R, SUDHOFF D, *et al.* Optimal design of catalytic distillation columns: a case study on synthesis of TAEE[J]. Chemical Engineering Research and Design, 2014, **92**(3): 391–404.

[167] SEFERLIS P, GRIEVINK J. Optimal design and sensitivity analysis of reactive distillation units using collocation models[J]. Industrial & Engineering Chemistry Research, 2001, **40**(7): 1673–1685.

[168] YUAN Z H, CHEN B Z, SIN G, *et al.* State–of–the–art and progress in the optimization–based simultaneous design and control for chemical processes[J]. AIChE Journal, 2012, **58**(6): 1640–1659.

[169] FERNHOLZ G, ENGELL S, KREUL L U, *et al.* Optimal operation of a semi–batch reactive distillation column[J]. Computers and Chemical Engineering, 2000, **24**(2): 1569–1575.

[170] KENIG E, JAKOBSSON K, BANIK P, *et al.* An integrated tool for synthesis and design of reactive distillation[J]. Chemical Engineering Science, 1999, **54**(10): 1347–1352.

[171] KENIG E Y, DER H B, GÓRAK A, *et al.* Investigation of ethyl acetate reactive distillation process[J]. Chemical Engineering Science, 2001, **56**(21): 6185–6193.

[172] KENIG E Y, GÓRAK A, LAHTI A P, *et al.* Advanced rate–based simulation tool for reactive distillation[J]. AIChE Journal, 2004, **50**(2): 322–342.

[173] QI Y J, WENG H X. Progress in steady–state models for simulation of catalytic distillation process[J]. Chemical Industry and Engineering Progress, 2010, **29**(4): 600–605.

[174] LUO S J, LI D F. Recent progress of catalytic distillation[J]. Petrochemical Technology, 2011, **40**(1): 1–11.

[175] KELLER T, GÓRAK A. Modelling of homogeneously catalyzed reactive distillation processes in packed columns: Experimental model validation[J]. Computers & Chemical Engineering, 2013, **48**: 74–88.

[176] JIAO Z H, ZHOU C G, ZHAO W. Progress on mathematic models and algorithms for the steady–state reactive distillation process[J]. Chemical Industry

and Engineering, 2004, **21**(4): 308–313.

[177] XU X E, ZHU B F, CHEN H F, *et al.* Reactive distillation(Ⅱ)[J]. Petrochemical Technology, 1985, **14**(9): 550–555.

[178] XU X E, CHEN H F. Simulation of distillation processes with reactions in series[J]. Journal of Chemical Industry and Engineering(China), 1987, **38**(2): 165–175.

[179] KUANG G, ZHAO Z S, WANG L E, *et al.* The simulation of MeOAc hydrolysis prosis in catalytic distillation[J]. Journal of Fuzhou University (Natural Science), 1998, **26**(2): 92–96.

[180] WU Y X, WANG L E, QIU T. Bidiagonal matrix method and its application in simulation of catalytic distillation[J]. Journal of Fuzhou University (Natural Science), 2000, **28**(1): 82–86.

[181] QI Z W, SUN H J, SHI J M, *et al.* Simulation of distillation process with chemical reactions[J]. Journal of Chemical Industry and Engineering (China), 1999, **50**(4): 563–567.

[182] YUAN H, YANG B L. Mathematical simulation for the synthesis process of ethyl *tert*–butyl ether by means of reactive distillation[J]. Journal of South China University of Technology (Natural Science Edition), 2004, **32**(10): 85–89.

[183] LEI Z G, LI C Y, CHEN B H. Catalytic distillation of simultaneous alkylation and transalkylation for producing cumene[J]. Modern Chemical Industry, 2001, **21**(12): 41–43.

[184] KREUL L U, GÓRAK A, BARTON P I. Modeling of homogeneous reactive separation processes in packed columns[J]. Chemical Engineering Science, 1999, **54**(1): 19–34.

[185] NOERES C, KENIG E Y, GÓRAK A. Modelling of reactive separation processes: reactive absorption and reactive distillation[J]. Chemical Engineering and Processing, 2003, **42**(3): 157–178.

[186] HOLTBRUEGGE J, HEILE S, LUTZE P, *et al.* Synthesis of dimethyl carbonate and propylene glycol in a pilot–scale reactive distillation column: experimental investigation, modeling and process analysis[J]. Chemical

Engineering Journal, 2013, **234**: 448–463.

[187] CHEN F, HUSS R S, MALONE M F, *et al.* Simulation of kinetic effects in reactive distillation[J]. Computers and Chemical Engineering, 2000, **24**(11): 2457–2472.

[188] KELLER T, MUENDGES J, JANTHARASUK A, *et al.* Experimental model validation for *n*–propyl propionate synthesis in a reactive distillation column coupled with a liquid–liquid phase separator[J]. Chemical Engineering Science, 2011, **66**(20): 4889–4900.

[189] NIESBACH A, FUHRMEISTER R, KELLER T, *et al.* Esterification of acrylic acid and *n*–butanol in a pilot–scale reactive distillation column—experimental investigation, model validation, and process analysis[J]. Industrial & Engineering Chemistry Research, 2012, **51**(50): 16444–16456.

[190] CRUZ–DÍAZ M, BUCHALY C, KREIS P, *et al.* Synthesis of *n*–propyl propionate in a pilot–plant reactive distillation column: experimental study and simulation[J]. Computers & Chemical Engineering, 2012, **39**: 118–128.

[191] GONZÁLEZ–RUGERIO C A, KELLER T, PILARCZYK J, *et al.* TAEE synthesis from isoamylenes and ethanol by catalytic distillation: pilot plant experiments and model validation[J]. Fuel Processing Technology, 2012, **102**: 1–10.

[192] WANG E Q, LEI Z G, ZHANG J C, *et al.* Non–equilbrium model of suspension catalytic distillation for alkylation of benzene and C12 olefin[J]. Journal of Chemical Industry and Engineering (China), 2003, **54**(10): 1470–1473.

[193] GÓRAK A, HOFFMANN A. Catalytic distillation in structured packings: methyl acetate synthesis[J]. AIChE Journal, 2001, **47**(5): 1067–1076.

[194] ODZIEJ A K, JAROSZYŃSKI M, HOFFMANN A, *et al.* Determination of catalytic packing characteristics for reactive distillation[J]. Catalysis Today, 2001, **69**(1): 75–85.

[195] NOERES C A H M, GORAK A. Reactive distillation: non–ideal flow behaviour of the liquid phase in structured catalytic packings[J]. Chemical Engineering Science, 2002, **57**(9): 1545–1549.

[196] HOFFMANN A, NOERES C, GÓRAK A. Scale–up of reactive distillation columns with catalytic packings[J]. Chemical Engineering and Processing, 2004, **43**(3): 383–395.

[197] KLÖKER M, KENIG E Y, GÓRAK A, *et al.* Investigation of different column configurations for the ethyl acetate synthesis *via* reactive distillation[J]. Chemical Engineering and Processing: Process Intensification, 2004, **43**(6): 791–801.

[198] TAYLOR R, KRISHNA R. Modelling reactive distillation[J]. Chemical Engineering Science, 2000, **55**(22): 5183–5229.

[199] ZHANG R S, HAN Y, HOFFMANN U. Simulation procedure for distillation with heterogeneous catalytic reaction[J]. Journal of Chemical Industry and Engineering (China), 1989, **40**(6): 693–703.

[200] QI Z W, ZHANG R S, YU Z H. Simulation of heterogeneous catalytic distillation process[J]. Journal of East China University of Science and Technology, 1998, **24**(3): 38–44.

[201] ZHAO Z S, KUANG G, WANG L E, *et al.* Improvement of BP algorithm on network training and application of ANN in catalytic distillation column simulation[J]. Chemical Engineering, 1998, **26**(6): 46–48.

[202] HU H, WU H X, XU S M, *et al.* Predictions catalytic distillation column start–up processes *via* artificial neural network[J]. Journal of Molecular Catalysis, 2006, **20**(4): 360–362.

[203] NIKAČEVIĆ N M, HUESMAN A E M, VAN DEN HOF P M J, *et al.* Opportunities and challenges for process control in process intensification[J]. Chemical Engineering and Processing: Process Intensification, 2012, **52**: 1–15.

[204] SNEESBY M G, TADE M O, SMITH T N. Two–point control of a reactive distillation column for composition and conversion[J]. Journal of Process Control, 1999, **9**(1): 19–31.

[205] AL–ARFAJ M, LUYBEN W L. Comparison of alternative control structures for an ideal two–product reactive distillation column[J]. Ind. Eng. Chem. Res., 2000, **39**: 3298–3307.

[206] FERNBOIZ G, FRIEDRICB. M, GRONER S, *et al.* Linear MIMO controller design for an industrial reactive distillation column[C]//IFAC Symposium on Dynamics and Control of Process Systems. Jejudo Island, Korea, 2001.

[207] GRÜNER S, MOHL K D, KIENLE A, *et al.* Nonlinear control of a reactive distillation column[J]. Control Engineering Practice, 2003, **11**(8): 915–925.

[208] VORA N, DAOUTIDIS P. Dynamics and control of an ethyl acetate reactive distillation column[J]. Ind. Eng. Chem. Res., 2001, **40**(3): 833–849.

[209] CHEN M Q, YU N, LIU Y L, *et al.* Optimization and control of reactive dividing wall column for production of *n*–butylacetate[J]. CIESC Journal, 2016, **67**(12): 5066–5081.

[210] KHALEDI R, YOUNG B R. Modeling and model predictive control of composition and conversion in an ETBE reactive distillation column[J]. Ind. Eng. Chem. Res., 2005, **44**(9): 3134–3145.

[211] SEBAN L, KIRUBAKARAN V, ROY B K, *et al.* GOBF–ARMA based model predictive control for an ideal reactive distillation column[J]. Ecotoxicology and Environmental Safety, 2015, **121**: 110–115.

[212] KAWATHEKAR R, RIGGS J B. Nonlinear model predictive control of a reactive distillation column[J]. Control Engineering Practice, 2007, **15**(2): 231–239.

[213] HUANG Q Q, BO Y N, BO C M, *et al.* MPC of distillation column with side reactors for methyl acetate production [J]. Modern Chemical Industry, 2015, **35**(9): 159–164.

[214] YUAN Z H, CHEN B Z, ZHAO J S. An overview on controllability analysis of chemical processes[J]. AIChE Journal, 2011, **57**(5): 1185–1201.

[215] GEORGIADIS M C, SCHENK M, PISTIKOPOULOS E N, *et al.* The interactions of design control and operability in reactive distillation systems[J]. Computers & Chemical Engineering, 2002, **26**(4): 735–746.

[216] MIRANDA M, RENEAUME J M, MEYER X, *et al.* Integrating process design and control: an application of optimal control to chemical processes[J]. Chemical Engineering and Processing: Process Intensification, 2008, **47**(11):

2004–2018.

[217] YU S B, LI Y H, CHEN H F. Application of a novel structured catalyst packing[J]. Petrochemical Technology, 2003, **32**(5): 45–48.

[218] DU C H. Study on the preparation of structured solid acid catalyst packing for catalytic distillation[D]. Tianjin: Tianjin University, 2004

[219] SUN W, YANG H J, HOU K H. A study on hydrodynamic of a novel structured catalyst parking[J]. Journal of Hebei University of Technology, 2008, **37**(6): 31–36.

[220] GAO X R, CHANG H H, WEI W L, *et al.* Advance in catalytic distillation technique and its application[J]. Modern Chemical Industry, 2008, **28**(S1): 136–140.

[221] WU W, SUI H, LI Y H, *et al.* Simulation of methyl acetate synthesis in distillation column with external side reactors[J]. Chemical Engineering, 2012, **40**(4): 14–18.

[222] ZHENG H D, ZHAO S Y, ZENG Y R, *et al.* Catalytic distillation coupled with a side reactor for methyl acetate hydrolysis[J]. Chemical Industry and Engineering Progress, 2012, **31**(9): 2102–2106.

[223] LI X G, ZHANG R, GAO X, *et al.* Simulation of reactive distillation etherification process of light gasoline[J]. Chemical Industry and Engineering Progress, 2009, **28**(z2): 364–367.

[224] LU S Q, YANG B L, LEI Z, *et al.* Simulation study of FCC light gasoline etherification using a combined method[J]. Chemical Reaction Engineering and Technology, 2008, **24**(3): 246–251.

[225] ZHU E J, HUANG K J. A reactive distillation system with double reactive sections for the esterification of ethylene glycol with acetic acid[J]. Journal of Beijing University of Chemical Technology (Natural Science), 2015, **42**(1): 26–33.

[226] WEI N N, WANG S F, HUANG K J. Control of reactive distillation columns with single and double reactive sections for esterification of ethylene glycol with acetic acid[J]. Journal of Beijing University of Chemical Technology (Natural

Science), 2015, **42**(4): 34–39.

[227] XIA C Y, HUANG K J, WANG S F. Control of a novel reactive distillation column for the two–stage consecutive reversible reactions[J]. Modern Chemical Industry, 2015, **35**(8): 173–176.

[228] WANG K, HUANG K J, WANG S F, *et al.* Design and evaluation of reactive distillation column with three reactive sections: disproportionation of trichlorosilane to silane[J]. Modern Chemical Industry, 2015, **35**(6): 172–175.

[229] BAO C Y, LIN M H, CAI X, *et al.* Simulation and energy efficiency analysis of the synthesis of isopropanol by reactive dividing–wall–column[J]. Computers and Applied Chemistry, 2016, **33**(3): 325–329.

[230] LI W Y, HUANG K J, WU C L. Design of reactive dividing–wall distillation columns with two external recycles[J]. Modern Chemical Industry, 2016, **36**(9): 143–146.

[231] ZHAO G S, YANG B L. Dehydration of tert–butyl alcohol in reactive distillation adapted to chemical heat pump[J]. Journal of Chemical Industry and Engineering (China), 2004, 55(3): 384–389.

[232] LEE H Y, LEE Y C, CHIEN I, et al. Design and control of a heat–integrated reactive distillation system for the hydrolysis of methyl acetate[J]. Ind. Eng. Chem. Res., 2010, 49(16): 7398–7411.

[233] WU Y, LEE H, LEE C, *et al.* Design and control of thermally–coupled reactive distillation system for esterification of an alcohol mixture containing *n*–amyl alcohol and *n*–hexanol[J]. Industrial & Engineering Chemistry Research, 2013, **52**(48): 17184–17197.

[234] KLÖKER M, KENIG E Y, GÓRAK A. On the development of new column internals for reactive separations *via* integration of CFD and process simulation[J]. Catalysis Today, 2003, **79**: 479–485.

[235] WIERSCHEM M, BOLL S, LUTZE P, *et al.* Evaluation of the enzymatic reactive distillation for the production of chiral compounds[J]. Chem. Ing. Tech., 2016, **88**(1/2): 147–157.

[236] WIERSCHEM M, SKIBOROWSKI M, GÓRAK A, *et al.* Techno–economic

evaluation of an ultrasound–assisted enzymatic reactive distillation process[J]. Computers & Chemical Engineering, 2017, **105**:123–131.

[237] LI H, CUI J J, LI X G, *et al.* Recent developments in microwave–assisted chemical separation processes[J]. Chemical Industry and Engineering Progress, 2016, **35**(12): 3735–3745.

[238] ALTMAN E, STEFANIDIS G D, VAN GERVEN T, *et al.* Process intensification of reactive distillation for the synthesis of *n*–propyl propionate: the effects of microwave radiation on molecular separation and esterification reaction[J]. Industrial & Engineering Chemistry Research, 2010, **49**(21): 10287–10296.

[239] ALTMAN E, STEFANIDIS G D, GERVEN T V, *et al.* Microwave–promoted synthesis of *n*–propyl propionate using homogeneous zinc triflate catalyst[J]. Ind. Eng. Chem. Res., 2012, **51**(4): 1612–1619.

[240] GAO X, LI X G, ZHANG J, *et al.* Influence of a microwave irradiation field on vapor–liquid equilibrium[J]. Chemical Engineering Science, 2013, **90**: 213–220.

[241] GAO X. Study on catalytic reactive distillation process intensified by microwave irradiation[D]. Tianjin: Tianjin University, 2011.

[242] WERTH K, LUTZE P, KISS A A, *et al.* A systematic investigation of microwave–assisted reactive distillation: influence of microwaves on separation and reaction[J]. Chemical Engineering and Processing: Process Intensification, 2015, **93**: 87–97.

[243] LUTZE P, GORAK A. Reactive and membrane–assisted distillation: recent developments and perspective[J]. Chemical Engineering Research and Design, 2013, **91**(10): 1978–1997.

[244] YANG S B, YANG B L. Catalytic reactive distillation coupled with pervaporation for synthesizing ethyl *tert*–butyl ether[J]. Journal of Chemical Industry and Engineering (China), 2001, **52**(11): 950–956.

[245] YANG B L, YANG Z, YANG S B, *et al.* Preparation of gasoline blender of ethyl *tert*–butyl ether by a combined process[J]. Science & Technology in

Chemical Industry, 2001, **9**(1): 1–5.

[246] BUCHALY C, KREIS P, GÓRAK A. Hybrid separation processes—combination of reactive distillation with membrane separation[J]. Chemical Engineering and Processing, 2007, **46**(9): 790–799.

[247] MITKOWSKI P T, BUCHALY C, KREIS P, *et al*. Computer aided design, analysis and experimental investigation of membrane assisted batch reaction–separation systems[J]. Computers & Chemical Engineering, 2009, **33**(3): 551–574.

[248] NIESBACH A, FINK N, LUTZE P, *et al*. Design of reactive distillation processes for the production of butyl acrylate: impact of bio–based raw materials[J]. Chinese Journal of Chemical Engineering, 2015, **23**(11): 1840–1850.

[249] NEUMANN K, WERTH K, MARTÍN A, *et al*. Biodiesel production from waste cooking oils through esterification: catalyst screening, chemical equilibrium and reaction kinetics[J]. Chemical Engineering Research and Design, 2016, **107**: 52–62.

[250] STANKIEWICZ A. Reactive separations for process intensification: an industrial perspective[J]. Chemical Engineering and Processing: Process Intensification, 2003, **42**(3): 137–144.

[251] SMITH JR L A. Process for separating isobutene from C4 streams: US4242530[P]. 1980–12–30.

[252] CHEN W, YANG W S. Simulation of separating isobutene from C4 hydrocarbons by reactive distillation[J]. Computers and Applied Chemistry, 2016, **33**(8): 938–942.

[253] RILTERL D L, SYLVESTRE L F, DOHERTY M F. Separation of closely boiling mixtures by reactive distillation (I): Theory[J]. Industrial & Engineering Chemistry Process Design and Development, 1985, **24**(4): 1062–1071.

[254] CLEARY W, DOHERTY M F. Separation of closely boiling mixtures by reactive distillation(Ⅱ): Experiments[J]. Industrial & Engineering Chemistry Process Design and Development, 1985, **24**(4): 1071–1073.

[255] ZHOU J B, HUANG J F, REN H O, et al. Simulative study of water removal

from ethanol–water azeotropic mixture by catalytic distillation[J]. Modern Chemical Industry, 2008, 28(S1): 153–155.

[256] LIU J X. Research of reactive distillation in 2,3–butanediol separation[D]. Shanghai: East China University of Science and Technology, 2012.

[257] OKASINSKI M J, DOHERTY M F. Simultaneous kinetic resolution of chiral propylene oxide and propylene glycol in a continuous reactive distillation column[J]. Chemical Engineering Science, 2003, **58**: 1289–1300.

[258] ODZIEJ A K, JAROSZYŃSKI M, ACKI W S, *et al.* Catalytic distillation for TAME synthesis with structured catalytic packings[J]. Chemical Engineering Research and Design, 2004, **82**(A2): 175–184.

[259] NIESBACH A, DANIELS J, SCHRÖTER B, *et al.* The inhibition of acrylic acid and acrylate ester polymerization in a heterogeneously catalyzed pilot–scale reactive distillation column[J]. Chemical Engineering Science, 2013, **88**: 95–107.

[260] HOLTBRUEGGE J, LEIMBRINK M, LUTZE P, *et al.* Synthesis of dimethyl carbonate and propylene glycol by transesterification of propylene carbonate with methanol: catalyst screening, chemical equilibrium and reaction kinetics[J]. Chemical Engineering Science, 2013, **104**: 347–360.

[261] MA J H, LIU J Q, LI J T, *et al.* The progress in reactive distillation technology[J]. Chemical Reaction Engineering and Technology, 2003, **19**(1): 1–8.

[262] LI Z, WANG X, ZHENG H Y, *et al.* Process for preparing dimethyl carbonate by oxidative carbonylation of methanol: 104892423A[P]. 2015–09–09.

[263] ZHU Y F, TIAN H S. Synthesis of 3–amino–2–oxazolidone from dimethyl carbonate by carbonylation reaction[J]. Fine Chemical Intermediate, 2004, **34**(4): 23–25.

[264] GU Z G, MAO M F, LIN J, *et al.* Study on the synthesis of diethoxy methane using toluene–*p*–sulfonic acid as catalyst[J]. Chinese Journal of Applied Chemistry, 2005, **22**(12): 1366–1368.

[265] WANG Y Z, LUO Y Q, QIAN X, *et al.* Simulation of thermally coupled catalytic distillation flowsheets for C3 alkyne selective hydrogenation [J]. CIESC

Journal, 2016, **67**(2): 580–587.

[266] ZHANG X J, TONG Y N, GAO Z R, *et al.* Simulation analysis of diolefin hydrogenation of FCC gasoline in catalytic distillation[J]. Petroleum Processing and Petrochemicals, 2016, **47**(2): 89–92.

[267] YANG H J, LUO X, HOU K H. Simulation analysis of the hydrodesulfurization process of FCC gasoline heavy fraction *via* catalytic distillation[J]. Petroleum Processing and Petrochemicals, 2010, **41**(10): 47–51.

[268] WANG X Q. Production technology and application of methyl isobutyl ketone[J]. Petrochemical Technology, 2002, **31**(5): 393–400.

[269] LEI Z G, YANG Y, LI Q, *et al.* Catalytic distillation for the synthesis of *tert*–butyl alcohol with structured catalytic packing[J]. Catalysis Today, 2009, **147**: S352–S356

[270] HUANG Y, BO C M. Design of bi–objective control system for benzene chlorination distillation[J]. Modern Chemical Industry, 2016, **32**(10): 166–170.

[271] LIANG Z L, WU Y H, LIU J, *et al.* Advances of application of reactive distillation in aldol condensation[J]. Chemical Industry Times, 2010, **24**(1): 66–70.

[272] REN D M. Study of preparation of diacetone alcohol by condensation of acetone[J]. Applied Chemical Industry, 2005, **34**(6): 383–384.

[273] SONG L. New process development of methylal with reactive distillation technology[D]. Qingdao: Qingdao University of Science & Technology, 2009.

[274] ZHAO L. Progress in technology for isomerization of butenes[J]. Petrochemical Industry Technology, 2010, **17**(4): 39–42.

[275] Nieminen, Harri. "Liquid–phase alcohol promoted methanol synthesis from CO2 and H2." (2016).

[276] Yang, Sheng, Yu Qian, and Siyu Yang. "Development of a Full CO2 Capture process based on the rectisol wash technology." Industrial & Engineering Chemistry Research 55.21 (2016): 6186–6193.

[277] Qiangqiang An. “On Application of Computer Simulation Technology in Methanol Synthesis in the Coal Chemical Industry.” CHEMICAL

ENGINEERING TRANSACTIONS Vol. 59 (2017): 607–612

[278] Yue Fanghua，Liu Dongbin, Shen Yangming. “Dynamic Simulation of the Methanol Synthesis Reactor with the Aspen Dynamic Software.” Chemical Engineering Design Communications 40.05 (2014): 59–62

[279] Muzen, Alejandra, and Miryan C. Cassanello. "Liquid holdup in columns packed with structured packings: Countercurrent vs. cocurrent operation." Chemical engineering science 60.22 (2005): 6226–6234.

[280] Sun Baoquan, Lin Huadong，Wen Yaoshun.” Study on the formation and effect of $CO_2$ in the product gas of industrial methanol to olefins unit.” Petrochemical Industry Technology 23 (7) (2016) :52–54